IRON PHASE CONTROL DURING PRESSURE LEACHING AT ELEVATED TEMPERATURE

by

Camille Fleuriault

A thesis submitted to the Faculty and the Board of Trustees of the Colorado School of Mines in partial fulfillment of the requirements for the degree of Master of Science (Metallurgical and Materials Engineering).

Golden, Colorado

Date _____

Signed: _____

Camille Fleuriault

Signed: _____

Dr. Corby G. Anderson
Thesis Advisor

Golden, Colorado

Date _____

Signed: _____

Dr. Ivar Reimanis
Professor and Department Head
Department of Metallurgical and
Materials Engineering

ABSTRACT

Iron is a common contaminant encountered in most metal recovery operations, and particularly hydrometallurgical processes. For example, the Hematite Process uses autoclaves to precipitate iron oxide out of the leaching solution, while other metals are solubilized for further hydrometallurgical processing. In some cases, Basic Iron Sulfate (BIS) forms in place of hematite. The presence of BIS is unwanted in the autoclave discharge because it diminishes recovery and causes environmental matters. The focus of this master thesis is on the various iron phases forming during the pressure oxidation of sulfates. Artificial leaching solutions were produced from $CuSO_4$, $FeSO_4$ and H_2SO_4 in an attempt to recreate the matrix composition and conditions used for copper sulfides autoclaving. The following factors were investigated in order to determine which conditions hinder the formation of BIS: initial free acidity (5 – 98 g/L), initial copper concentration (12.7 – 63.5 g/L), initial iron concentration (16.7 - 30.7 g/L) and initial iron oxidation state.

There were three solid species formed in the autoclave: hematite, BIS and hydronium jarosite. The results show that free acid is the main factor influencing the composition of the residue. At an initial concentration of 22.3 g/L iron and no copper added, the upper limit for iron oxide formation is 41 g/L H_2SO_4. The increase of BIS content in the residue is not gradual and occurs over a change of a few grams per liter around the aforementioned limit. Increasing copper sulfate concentration in the solution hinders the formation of BIS. At 63.5g/L copper, the upper free acidity limit is increased to 61g/L. This effect seems to be related to the buffering action of copper sulfate, decreasing the overall acid concentration and thus extending the stability range of hematite. The effect of varying iron concentration on the precipitate chemistry is unclear. At high iron levels, the only noticeable effect was the inhibition of jarosite. The results were reported within a Cu-Fe-S ternary system and modeled. The modeling confirmed the experimental observations with the exception that increasing iron concentrations seem to promote BIS stability.

TABLE OF CONTENTS

INDEX OF FIGURES

INDEX OF TABLES

INDEX OF APPENDICES

ACKNOWLEDGMENTS

I would like to thank my advisor Dr. Corby Anderson for his tutoring during my graduate program. I also thank the members of my committee for their help: Dr. Scott Shuey, Erik Spiller and Dr. Patrick Taylor.

Special thanks are due to Newmont Mining Corporation for funding this research project, and Newmont's Metallurgical Services group for their precious support with analytical matters.

I want to thank my fellow Kroll students, Dr. Gerald Martins and Scott Pawelka for the brainstorming sessions and their assistance with practical and mechanical problems.

I would also like to express my gratitude to family and friends in France and Colorado. I am especially grateful to my parents for their support.

Finally, many thanks to my boyfriend Vincent for his infinite patience.

CHAPTER 1 INTRODUCTION

Iron is a common contaminant in hydrometallurgy. This first chapter presents general facts about iron contamination during extraction processes. The motivation for this thesis is also detailed.

1.1 Background

Iron is the 4th most abundant element in Earth's crust (5% by weight) and is present in many minerals forming the ores exploited for mining activities. Iron sulfides, especially, are a common component of base and precious metals deposits. Iron is readily solubilized and oxidized by most acid leach solutions. It interferes with the extraction process on many levels, thus it is paramount to achieve separation as early as possible in the metallurgical circuit.

Among the metallurgical processes used to treat sulfide ores, leaching methods are widely used to concentrate and recover metals. The last decades have witnessed an increasing complexity to efficiently process ore bodies. Because most high grade ore bodies have already been found, the mining industry has turned to lesser grade and more complex deposits. New leaching processes had to be developed to efficiently extract metals. For base and precious metals, the challenge consists in selectively solubilizing the wanted values, leaving as many contaminants as possible in the residue. It relies on the use of high pressure over a wide range of temperature to break down complex minerals, as well as overstep kinetic and thermodynamic barriers.

1.2 Motivation

The Hematite Process is used to precipitate iron from leach liquors as an oxide, hematite. The residues are washed and filtered while the leach solutions are further processed for metal recovery. Within some gold and/or copper pressure leaching operations, iron hydroxysulfates or Basic Iron Sulfate (BIS) appear to precipitate along with hematite. They are highly unwanted products in the autoclave discharge. BIS have been proven to form even when operating at conditions which would normally yield hematite. Because they are only forming under high pressure and very corrosive environments, BIS stability is not fully understood. By quantifying

the effect of leach solution composition on residue chemistry, this project aims at defining the conditions hindering BIS formation.

CHAPTER 2 LITERATURE REVIEW

The second chapter presents pressure leaching and how it is used to process complex ores and selectively precipitate iron.

2.1 Historical overview and development of high pressure leaching

Pressure leaching describes the use of high pressure to enhance the chemical break down of mineral particles. Because pressurization is coupled with heat, pressure leaching is often associated with higher temperatures than regular hydrometallurgical processes. This branch of metallurgy has been used for about 150 years but most advances were made over the last 30 years. Pressure metallurgy is a great application for "difficult" ores which cannot be treated by traditional techniques. As a result, it also represents a technical challenge.

2.1.1 Early work

The very first pressure hydrometallurgy experimentation was conducted in 1859 by Nikolai Nikolayevitch Beketoff, a Russian chemist [1]. He managed to precipitate silver by using overpressure of hydrogen gas in a sealed glass tube. The first major application was found by Karl Josef Bayer in 1885, in Saint Petersburg. Bayer used a pressurized autoclave operating at 170°C to enhance the crystallization process of aluminum hydroxide, known for its gelatinous structure. This was the beginnings of the Bayer Process for aluminum production from bauxite.

2.1.2 Developments made in the 20th century

The applications of pressure leaching for base metals such as copper, nickel and cobalt were discovered in 1903 when Malzac leached sulfides with ammonia [1]. This specific patent recommended the use of high pressure and temperature in pressure vessels. Leaching of zinc sulfide was later achieved by Fredrick A. Heinglein (1927), using pure oxygen at 290 psi and 180°C. He demonstrated that galena (which was normally insoluble even at very high temperatures) could be completely converted as lead sulfate in six hours (Equation 2.1).

$$MS + 2O_2 + nNH_3 \rightarrow [M(NH_3)_n]^{2+} + SO_4^{2-} \qquad \text{(Equation 2.1)}$$

About 40 years later, nickel sulfide leaching by ammonia in oxidative conditions prior reduction to nickel was developed by Sherritt Gordon Limited and the Chemical Construction Corporation. Next, Vladimir N. Mackiw discovered that copper could be taken out of the solution as a sulfide prior to reducing nickel, just by boiling treatment in presence of thiosulfate ions. Consecutively, all existing patents on ammonia leaching were used to obtain an efficient method for precipitating pure nickel in 1956 in Ottawa[1].

In the meantime, a Canadian team (Kenneth W. Downes and R.W. Bruce) succeeded in solubilizing nickel out of a pyrrhotite-pentlandite concentrate while hematite and sulfur remained in the residue. In 1953, the leaching of a Ni-Cu-Co concentrate started in Fort Saskatchewan, Canada, at the Sherritt-Gordon Plant which is still active today. The development of this process was the most important advance made in pressure leaching technology in the 20th century.

As presented above, most of the early significant developments at industrial scale were made for the aluminum and nickel industries. Pressure leaching is nowadays used for uranium, copper, gold, tungsten, zinc and titanium (Figure 2.1). Common leaching agents are ammonia, chloric or sulfuric acid, sodium hydroxide.

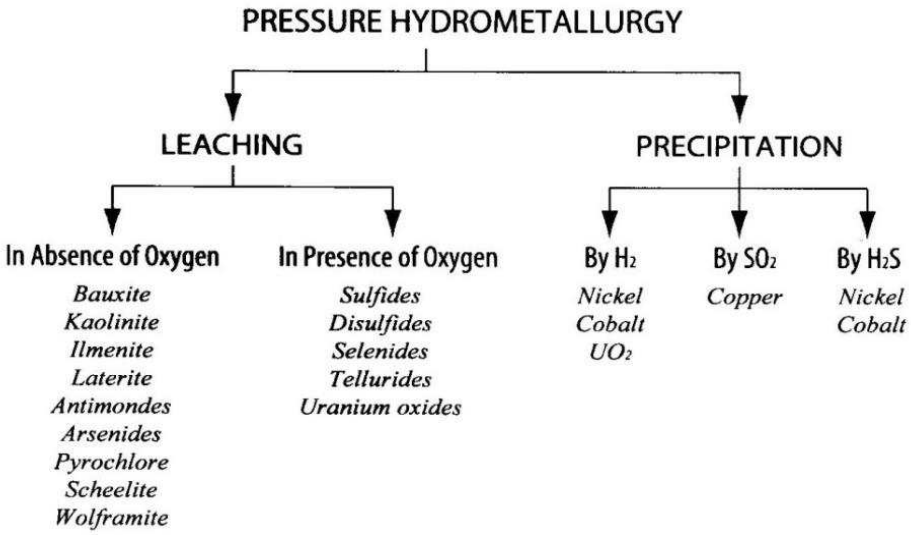

Figure 2.1: Summary of hydrometallurgical processes related to pressure leaching [1]

2.2 Recent advances in pressure leaching

Three applications have driven recent developments in high pressure technology: oxidation of refractory gold ores, leaching of base metals sulfide concentrates and leaching of aluminum-

rich laterites [2]. One of the reasons for development of high pressure leaching is the increasing complexity of the extracted ores, requiring stronger treatments for acceptable separation [3].

2.2.1 High pressure acid leaching for gold recovery

One of the methods used in gold recovery circuits is cyanidation followed by solid-liquid separation. The solution is then treated to extract the gold (Equation 2.2). This method becomes problematic when the ore has low-grade or a complex composition, referred as "refractory". The diversity and refractoriness of ores is explained by mineralogical, metallurgical and chemical properties. From a definition standpoint, refractoriness is due to:

- Physical encapsulation in an inert gangue preventing the precious metals to be leached and/or,
- Contamination by a constituent which interfere with the chemicals used.

Common gangue minerals are arsenopyrite, pyrite, pyrrhotite and realgar. Gold is usually found finely disseminated in these minerals [4].

$$4Au + 8[X]CN + H_2O + O_2 = 4NaOH + 4[X]KAu(CN)_2 \qquad [X]= K \text{ or } Na \qquad \text{(Equation 2.2)}$$

To liberate the gold, sulfides are oxidized prior to cyanidation. It can be achieved by roasting, pressure oxidation or bacterial leaching [5]. Up to 25 years ago, roasting with air was the main process used for oxidation. The switch to pressure leaching from roasting was made because of:

- environmental regulations on sulfur dioxide and arsenic trioxide release in the air
- higher gold recovery was achieved by pressure leaching

Autoclaving achieves better results because of the concentrate dissolution in the vessel, allowing the oxidation of all particles, even the finest, fully encapsulated in the gangue. Roasting products are porous, but not enough to ensure an optimum complexation of the gold with cyanide [4]. Bacterial leaching is a recent and promising technique, which development has been slowed down by technical issues. As of 2010, only 10 plants in the world were operating using bacterial leaching.

As an alternative, pressure leaching was developed in order to break down the sulfide matrix and convert sulfides to sulfates reporting to the aqueous phase (Figure 2.2). After leaching, the pregnant leach solution is neutralized and pumped to cyanidation tanks [3].

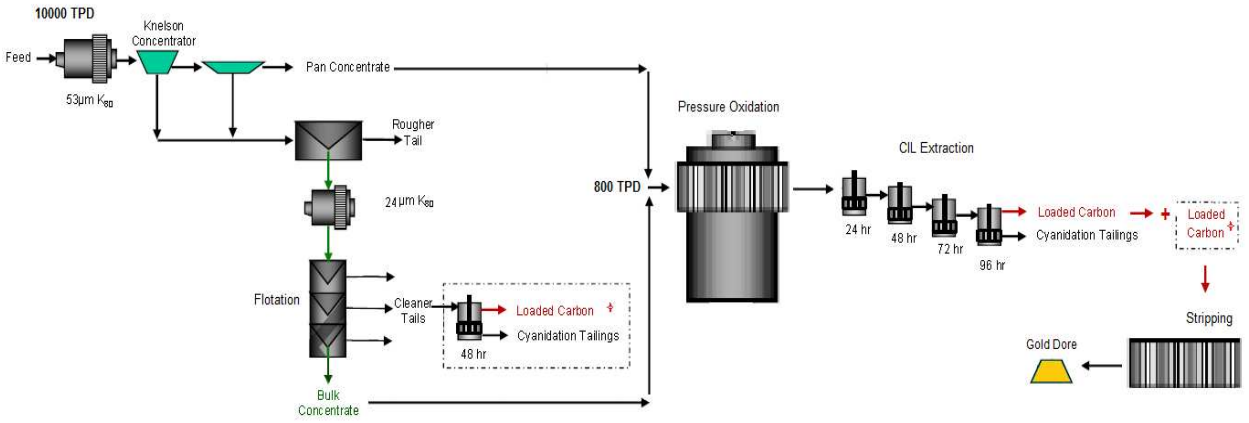

Figure 2.2: Gold extraction flowsheet by cyanidation including pressure oxidation [6]

When refractoriness is associated with contaminants, there are two common difficulties encountered to treat the ore:

- consumption of the leaching agent or oxygen by sulfides which react readily with cyanide (in this case, increasing the concentrations is not always economically viable)
- carbonaceous material in the ore responsible for the preg-robbing phenomenon: after being solubilized in cyanide, gold is readsorbed onto the carbon particles. Several options have been considered to overcome this issue: deactivate carbonaceous materials with chlorine or organic compounds, mineral processing, roasting or using Carbon In Leach (CIL) rather than Carbon In Pulp (CIP) with specific activated carbon. There is no universal solution to the carbonaceous matter problem and each of the previous techniques cited has its own disadvantages (kinetics, cost…). Pressure leaching in this specific case is not always adapted because it potentially activates the particles of carbonaceous material [4].

As aforementioned, refractory ores represent most of the new deposits found over the last decades. Besides ore diversity which prevents the use of a single process for all of them, refractoriness requires the development of new extraction schemes. As a result, it is more and more difficult to extract the precious values economically. When the contamination by carbonaceous material is minor, pressure leaching is extremely relevant and has been widely used for refractory ore treatment.

2.2.2 Extraction of zinc and copper from sulfide ores

Development of high pressure oxidation (HPOX) processes was also promoted by the necessity of finding alternatives to roasting of copper and zinc sulfide ores.

2.2.2.1 Pressure leaching of zinc sulfides

The Cominco Process developed in 1981 in British Columbia was the first zinc treatment plant by pressure leaching [1]. Sphalerite concentrates are oxidized in acidic environment at 150°C and 700kPa oxygen overpressure (Equation 2.3). After oxidation, the PLS is purified and zinc is recovered by electrolysis (Figure 2.3). In this specific process, sulfides are only oxidized to elemental sulfur because of the process temperature.

$$ZnS + 2H^+ + \tfrac{1}{2}O_2 \rightarrow Zn^{2+} + S + H_2O \qquad \text{(Equation 2.3)}$$

When it was first introduced, this process helped solving two major problems related to hydrometallurgical treatment of roasted ores. First, no sulfur dioxide was produced, thus reducing emissions or necessity for recycling as fertilizer. Then, this method prevented ferrites formation, increasing the ratio of zinc effectively recovered in solution.

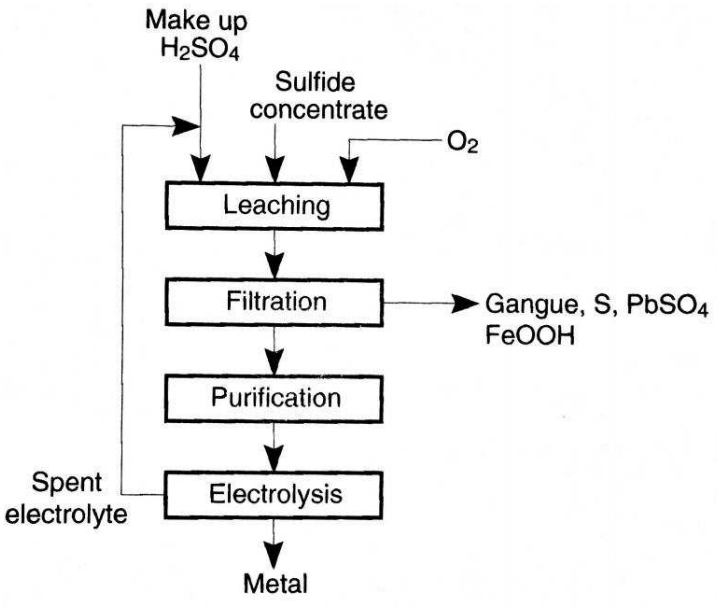

Figure 2.3: Flowsheet for the oxidation of sulfide concentrates in acid medium [7]

2.2.2.2 Pressure leaching of copper sulfides

The most common copper sulfides ore is chalcopyrite. The development of pressure leaching of copper sulfide concentrates was motivated by favorable thermodynamics at elevated pressure and technical improvements [8]. After pressure leaching, the pregnant leach solution (PLS) is suitable for traditional copper recovery techniques: solvent extraction and electrowinning. Depending on the conditions, two main HPOX processes were implemented:

- Partial oxidation process taking place at 150˚C, with formation of elemental sulfur (chalcopyrite acid leaching developed by Sherritt Gordon)
- Total oxidation process taking place at 220˚C, with formation of sulfate

Figure 2.4 illustrates the conditions of formation of sulfur vs. sulfate. Sulfate ion is stable over a wide range of pH, but mostly in oxidizing conditions (blue area). In acid medium, the stability domain of sulfate ions is adjacent to elemental sulfur (red area), which explains why S^0 can form at low to medium temperature. If the process temperature exceeds 150°C, elemental sulfur becomes unstable [1].

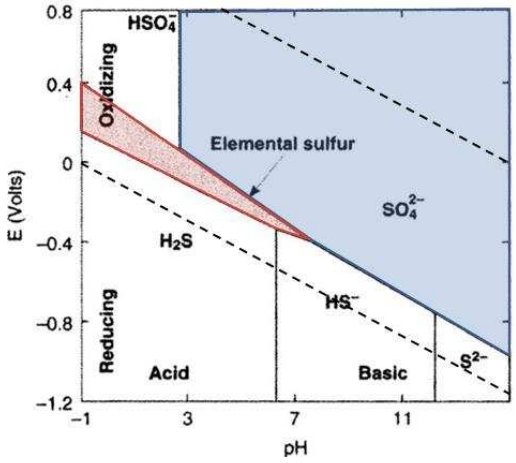

Figure 2.4: Eh-pH diagram for sulfides at 100°C [1]

Total oxidation suggests harsher conditions (higher temperature and oxygen partial pressure) and is more energy consuming. Sulfate formation is favored over elemental sulfur in many cases such as gold bearing copper deposits which are also treated by cyanidation. Elemental sulfur is hindered to avoid downstream cyanide consumption and thiocyanate formation [5]. Higher temperatures are also favored to produce hematite if there is a significant amount of iron in solution.

The world's first commercial application of high temperature pressure leaching of chalcopyrite was implemented by Phelps Dodge (now Freeport-McMoRan) in 2003 at Bagdad, AZ (Figure 2.5). The success of this process was due to:

- Possible recycling of sulfuric acid produced during the process for leaching of oxide ores and low grade materials. Generating and neutralizing acid is expensive and can represent a prohibitive cost.
- Possibility of also treating ores containing gold and silver along with copper. The principle connects to refractory ore processing techniques presented in section 2.2.1.
- Possible precipitation of iron as by-product hematite.

The Phelps Dodge process achieves excellent copper extraction (>97%) and operates at 475psi and 225˚C. Equation 2.4 presents the acid leaching of chalcopyrite reaction in oxidative conditions (oxygen overpressure).

$$4CuFeS_2 + 17\ O_2 + 2\ H_2SO_4 = 4CuSO_4 + 10\ H_2SO_4 + 2\ Fe_2(SO_4)_3 + 2\ H_2O \qquad \text{Equation (2.4)}$$

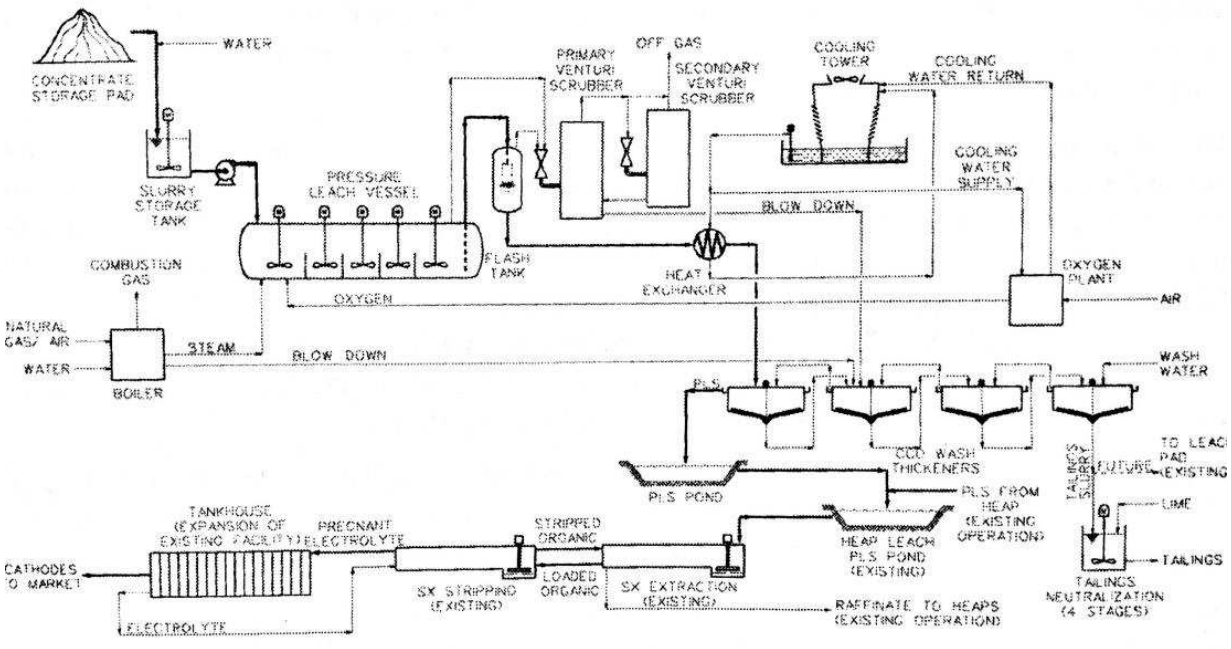

Figure 2.5: Process flowsheet for Phelps's Dodge's leaching facility at Bagdad, AZ [9]

2.2.3 Pressure leaching of bauxites

In terms of annual tonnage of ore processed, pressure leaching of bauxite or Bayer Process is the largest pressure leaching process (90 million tonnes/year) [1]. The patent for the Bayer Process was deposited in 1888; it is the oldest pressure leaching process in hydrometallurgy. A very few changes have been made to the Bayer Process over the years. For this specific leaching procedure, sodium hydroxide is used rather than sulfuric acid due to the presence of iron and titanium oxides in the ore. It would lead to acid consumption and contamination issues during the precipitation stage, especially since iron hydroxide is very difficult to filter. Moreover, aluminum hydroxide precipitated from acid solutions forms a gelatinous product that is difficult to treat.

The Bayer Process will not be further detailed in this thesis. But it is interesting to note that iron is also an important contamination issue during bauxite leaching. In this case, it does not report to the pregnant leach solution but to the residue as it is insoluble in alkaline media. The product of the process is called red mud, and causes pronounced disposal issues as BIS and jarosites.

2.3 Pressure leaching characteristics and control

This section describes pressure leaching fundamentals and operating parameters. Leaching takes place in high pressure vessels, also called autoclaves.

2.3.1 General design and operation facts

Autoclaves can measure up to 40m long and 7m diameter. They are cylinders, horizontal or vertical depending on the application. More rarely, spherical autoclaves or tubes are also used. Most autoclaves are static, but agitation is sometimes achieved by rotating the entire unit. In vertical autoclaves, agitation comes from steam injection, while horizontal vessels are partitioned and agitated with propellers [1]. If required, the injection of oxygen or air is usually performed from the bottom of the vessels for ideal dispersion (Figure 2.6).

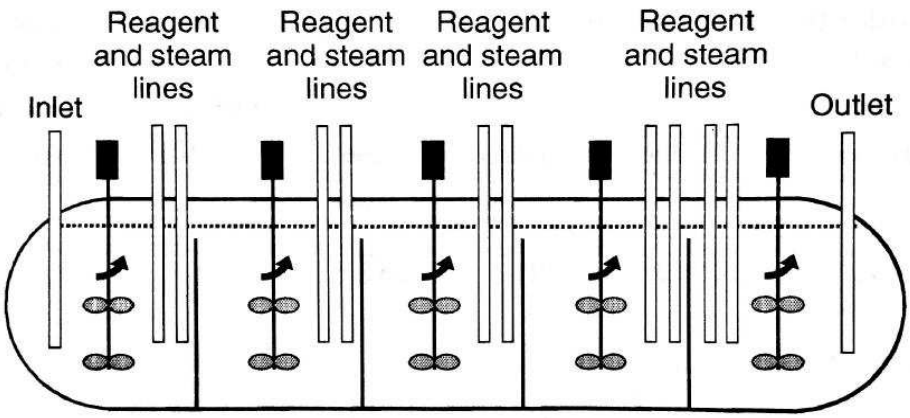

Figure 2.6: Schematic diagram of a horizontal autoclave [10]

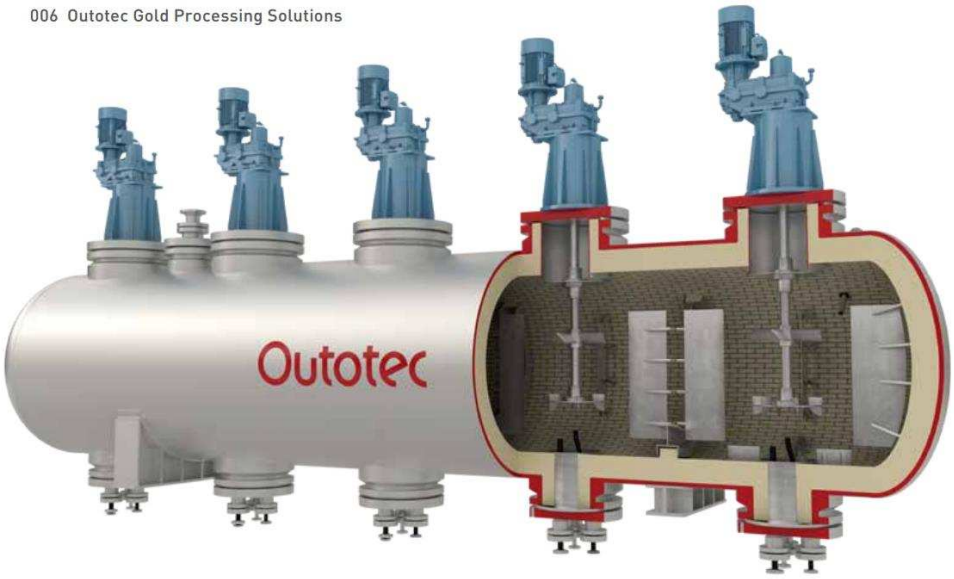

Figure 2.7: Outotec's OKTOP® pressure vessel [11]

At medium to high temperature and pressure, resistive lining is a very important feature. It is usually made of an acid-resistant brick protected from cracking by carbon or rubber. Metallic parts are stainless steel, steel alloys or lead for medium temperature processes. Titanium and its alloy are used when stronger conditions are required. In addition to the hazards implied by operating at high temperature and pressure, titanium must be handled with care due to the risk of ignition in presence of oxygen. Table 2.1 gives some operating values for high pressure vessels.

Table 2.1: Typical operating values for high pressure vessels [1], [9], [12], [13] and [14]

Parameters	**Refractory gold ores**	**Hematite Process**	**Copper sulfides**
Total pressure	400-500 psi	225-275 psi	470 psi
Oxygen overpressure	20 psi	15-60 psi	100 psi
Temperature	190-230°C	200°C	225˚C
Average residence time	1 to 2 hrs	2 hrs	1 hr

The main parameters conditioning process efficiency and oxidation rate are:

- temperature
- oxygen partial pressure
- acid concentration
- contamination (other metals, carbon, carbonates…)
- pulp density
- residence time

In the case of sulfide ores, the extend of oxidation can be monitored through redox potential. It is paramount to determine the maximum rate of oxidation as fast as possible in the process development. Indeed, the optimum residence time is directly related to the size of the vessel. Knowing this parameter helps with the estimation of capital cost and later condition the feasibility of the project [4].

2.3.2 Autoclave integration in the metallurgical circuit

Leaching circuits are usually also equipped with conditioning tanks (heating and homogenization) and flash tanks to release the pressure at the exit (Figure 2.8). Most commonly, several compartments are mounted in series in continuous systems [1].

The slurry pumped in the autoclave is usually preconditioned. Carbonates, which are common contaminants in refractory ores, are neutralized with sulfuric acid treatment. This prevents acid consumption as well as formation of carbon dioxide in the autoclave, and therefore helps keeping a high oxidation rate. When the ore carbonate content is too high, the process is changed and the autoclave is operated under alkaline conditions, like at Barrick's former Mercur

Gold Mine in Utah [15]. Alkaline conditions imply longer residence time and higher temperatures, but the operating costs are balanced by higher recovery.

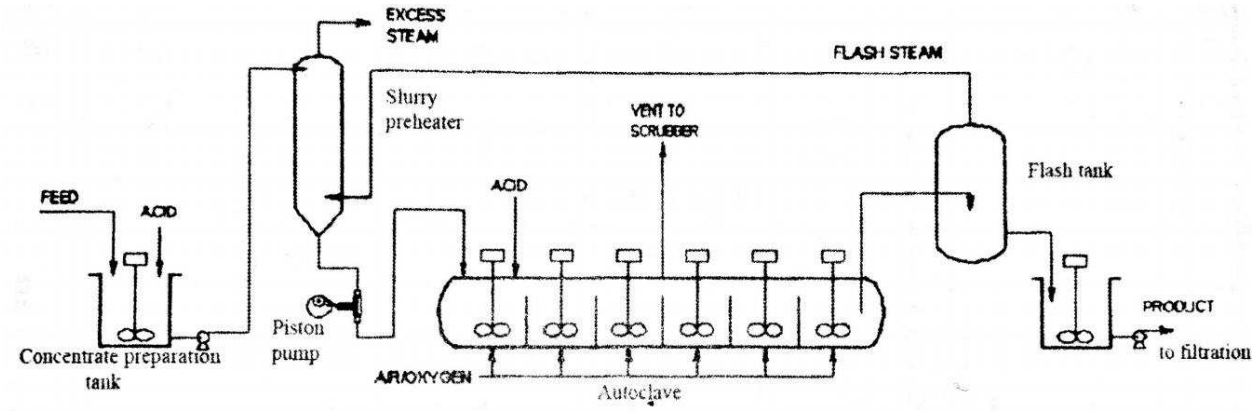

Figure 2.8: Typical HPOX leaching plant [1]

Preconditioning is also achieved by controlling the feed density. The solid:liquid ratio of the slurry is modified to its optimum where solids density and sulfide concentration will help decreasing heat and acid supply [4]. Because sulfide oxidation is exothermic, the heat balance can be controlled by adjusting the amount of sulfides to maintain the desired temperature in the autoclave. Even if it is more reasonable to plan the need for supplemental heating, sulfide content is a reliable parameter to use for plant design. Conway and Gale [16] formulated the optimum pulp density for a pyrite-containing feed (Equation 2.5):

$$\text{P.D.} = \frac{100}{\{0.3*[S^{2-}]+0.825\}} \qquad \text{(Equation 2.5)}$$

Although sulfide oxidation is exothermic, the slurry is often pre-heated to optimize the leaching stage for the treatment of low sulfide ores. Heat is recovered at the vessel discharge, and then transferred back ahead by counter current heat exchangers. When the sulfide ore is high grade, oxidation provides enough heat to maintain temperature in the autoclave, and excessing heat is usually discharged by releasing scrubbed steam in the atmosphere or adding cooling water. For the same reason, the vessels are usually equipped with cooling devices in order to control any runaway reaction. Cooling of the discharge is performed via a series of flash tanks heat exchangers.

Acid is recycled or neutralized depending on the leaching conditions. In the case of gold recovery, neutralization precedes cyanidation and CIP unit operations. If acid is recycled, the PLS is filtered or goes through Counter-Current Decantation (CCD) [4].

2.4 Iron removal using pressure leaching

Iron is often found in complex ores such as sulfides bearing formations. It represents an issue during leaching which is widely used for the treatment of this type of ore:

- Iron has the particularity of forming hydroxides when leached under certain conditions. Iron hydroxides form a viscous gel difficult to filter and trap some valuable elements such as silver.
- Iron is solubilized along with other metals and interferes with the following extraction steps.

As a result, purification of the pregnant leach solutions is required to achieve economical extraction. In the 1960s, metallurgists developed purification by precipitation [7]. Nowadays, precipitation of iron bearing species (goethite, hematite, jarosite) has become one of the most common methods used in the industry to purify leach liquors. To be suitable, the precipitate has to be readily filterable and have a minimum particle size. Precipitation takes place in autoclaves at medium to high temperatures, under oxygen or air overpressure [17]. It can also be cited that several achievements have been made using solvent extraction but no operating facility has successfully used this technology yet [18].

In the following paragraphs, three precipitation processes are detailed. Because most developments were achieved for the zinc industry, zinc hydrometallurgy is used to describe these processes named after the precipitate chemistry.

2.4.1 Goethite process

Goethite (FeO.OH) is a common iron hydroxide found in weathered iron-rich rocks. It is the most commonly mined iron ore because of its high iron content. Goethite can also be precipitated from leach solution, during a process occurring at 70-90°C and pH 2-3.5 (Equation 2.6).

$$Fe_2(SO_4)_3 + 4H_2O \leftrightarrow 2FeO.OH + 3H_2SO_4 \qquad \text{(Equation 2.6)}$$

The reaction produces sulfuric acid which has to be neutralized during the process (Figure 2.9). To precipitate iron as goethite from a sulfate solution, the concentration of ferric ion must be less than 1g/L. Two different processes have been developed: the Vieille Montagne and the Electrolytic Zinc processes [17].

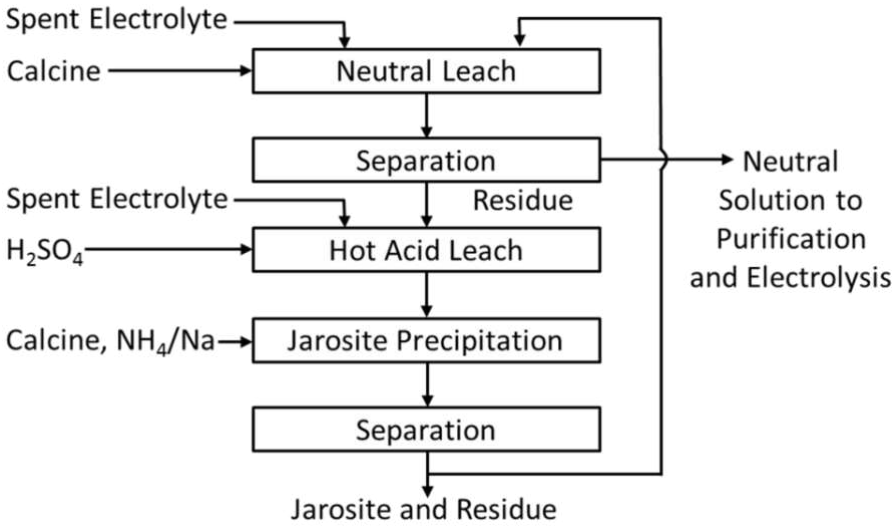

Figure 2.9: General flowsheet of the Goethite Process [17]

2.4.1.1 The Vieille Montagne process

The Vieille Montagne process (VM) was developed by at the Balen Plant in Belgium by, Vieille Montagne S.A. and described in 1973 by Andre and Masson [14]. After hot acid leaching, all ferric ions are reduced to homogenize the solution (Figure 2.10). Then, a slow oxidation by pressurized air is performed at controlled rate. Equation 2.7 presents the global reaction:

$$Fe_2(SO_4)_3 + ZnS + \tfrac{1}{2}O_2 + 3H_2O \rightarrow 2FeO.OH + ZnSO_4 + S + 2H_2SO_4 \qquad \text{(Equation 2.7)}$$

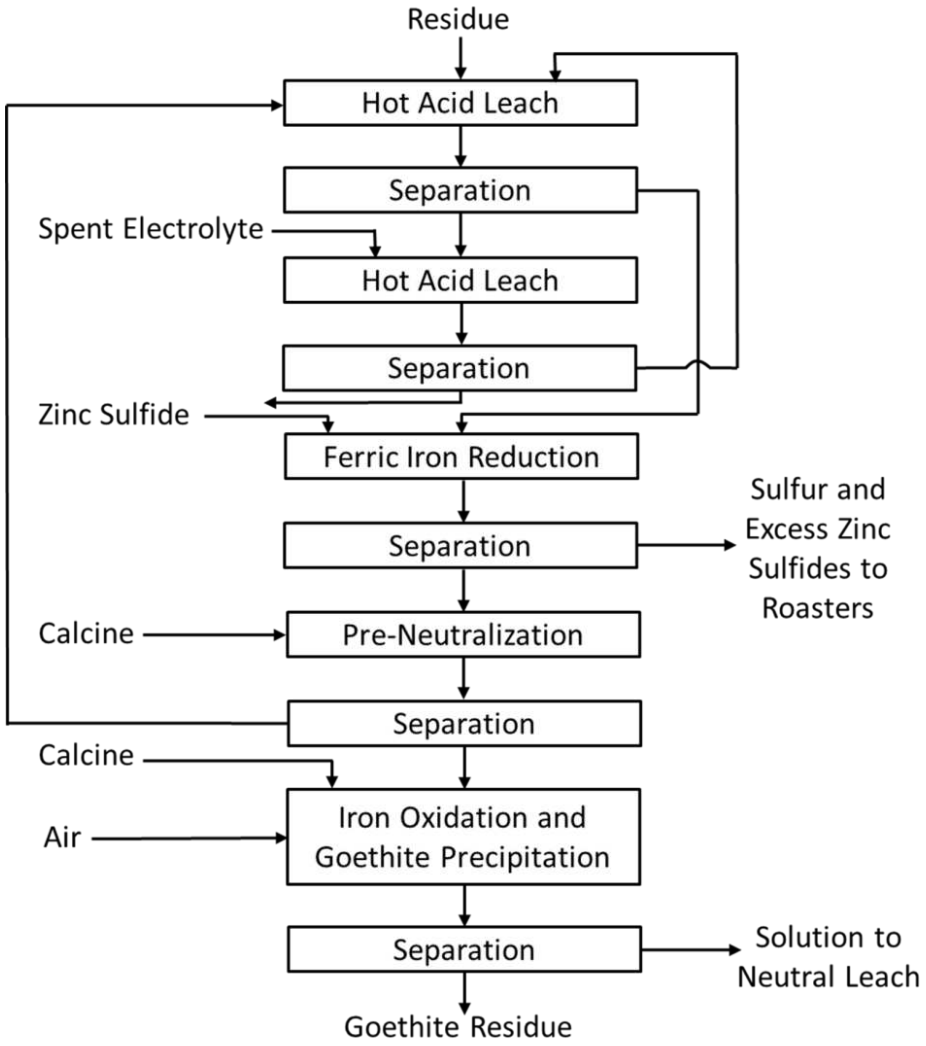

Figure 2.10: Vieille Montagne Process flowsheet [17]

2.4.1.2 The Electrolytic Zinc process

The second process (EZ) was presented by the Electrolytic Zinc Co. of Australasia Ltd and described by Allen et al. in 1970. The difference with the VM process relies on the oxidation of ferrous ions while the solution is flowing into a continuous reactor. Slow precipitation forms α FeO.OH, progressively removed from the vessel. At high rates, the specie forming is βFeO.OH or akagenite, a partially crystallized species which is more difficult to filter [19].

For both VM and EZ processes, pH and ferric ion concentration appear to be the main controlling factors. The advantages of the Goethite Process are that any acid leach liquor can be

used for the treatment, and the amount of solid produced is lesser than for jarosite process [14]. Some other benefits are high iron removal and no requirement for alkali components. The VM process has been shown to achieve better iron extraction, but the EZ process is easier to implement [17]. Contamination by zinc ferrite can occur with both methods, which means thorough washing is required. The main drawback of the goethite process is the presence of cations and anions in the precipitate, decreasing its purity and thus its quality as a by-product. Sulfate anions especially represent a problem. They are sorbed on the goethite particles and become difficult to extract down to an acceptable content.

2.4.2 The Jarosite Process

The Jarosite process is widely used in the zinc industry. It was developed by Asturiana de Zinc S.A. of Spain, Det Norske Zinc kompani A/S of Norway and the Electrolytic Zinc Co. of Australasia Ltd. in the mid-60s [13]. Jarosite describes a family of compounds of formula $MFe_3(SO_4)_2(OH)_6$, where M can be Na^+, NH_4^+, H_3O^+, Li^+, K^+, metals such as Pb, Ag, Zn, Hg, Rb [17]... The reaction equation is the following (Equation 2.8):

$$3Fe_2(SO_4)_3 + M_2SO_4 + 12H_2O \rightarrow 2MFe_3(SO_4)_2(OH)_6 + 6H_2SO_4 \qquad \text{(Equation 2.8)}$$

Zinc and iron are readily dissolved by sulfuric acid if the temperature has reached the boiling point. Iron sulfate is then precipitated as jarosite while zinc stays in solution. Influencing factors are:

- Temperature: jarosite precipitates over a wide range of temperatures (20 to 200°C). However, 90-100°C are the optimum values used in industry. Even if the rate of reaction increases with temperature, jarosite stability starts decreasing at 180°C.
- pH: precipitation occurs in acidic conditions, depending on the temperature ($0<pH<2$). Practical operation takes place at pH 1.5. Acid concentration also has an important effect on jarosite formation: the higher the initial H_2SO_4 concentration, the lower the precipitation.
- Alkali concentration: increasing the ratio of alkali ions to iron in solution enhance jarosite precipitation. Lower concentration limit for precipitation is 10^{-3}M [19]. Potassium-jarosite is the two most stable compound of the family.
- Contaminants: high iron concentrations inhibit co-precipitation.

- Seeding seems to enhance sharply the jarosite precipitation (both amount and rate). It also helps improving settling, filtering and washing.

The weakness of the process is the co-precipitation of other elements, which increases with pH of solution and concentration of contaminants (Cu, Zn, Co, Ni, Mn, In, Ga, Ge, Al and mostly Ag). Argento-jarosite precipitation is a real problem for industrial application. It is extremely difficult to recover the precious metal from the precipitate and subsequent silver losses can be encountered [17].

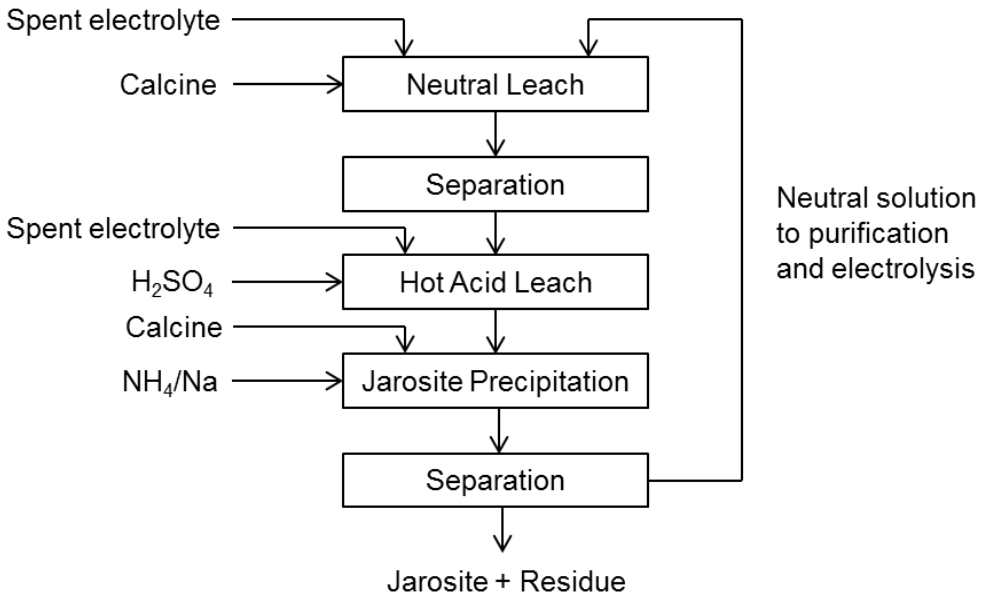

Figure 2.11: Simplified flowsheet of the Jarosite Process [17]

2.4.3 The Hematite Process

The Hematite Process principle is used for the experimental development of this thesis. It aims at removing soluble iron from zinc leach liquor solutions by precipitation.

2.4.3.1 General presentation

Hematite is one of the forms of ferric oxide, known for its ferromagnetic properties and widely used in the steel industry as a source of iron. The Hematite Process has been introduced by Akita Zinc Smelter of Japan in 1972 [20] and is currently used in several operations across the world. As a result of hot acid leaching of a ferrite residue, ferrous iron and zinc are solubilized in a sulfate solution, followed by selective precipitation of hematite (Equation 2.9). In

the autoclave, typical oxygen partial pressure ranges from 15-60 psi and temperature is over 185°C (usually 200°C) [12].

$$2FeSO_4 + ½O_2 + 2H_2O \rightarrow Fe_2O_3 + 2H_2SO_4 \qquad \text{(Equation 2.9)}$$

The presence of zinc sulfate has been shown to promote hematite precipitation at high temperatures and high acid content [18]. For instance at 200˚C and 72-75g/L $ZnSO_4$, the limit sulfuric acid concentration for hematite precipitation lies around 100g/L, against 65g/L when no zinc sulfate is present [21]. Disadvantages of the Hematite Process are high capital and operating costs due to the utilization of autoclaves. If pure enough, the hematite produced can be sold as a pigment or for the cement industry to balance these expenditures. As for today, a very few operations were able to produce marketable products.

2.4.3.2 The Akita Zinc Hematite Process

The Akita Zinc Process was developed by Dowa Mining Co., a Japanese nonferrous metals manufacturer. It has been operated at the Iijima Zinc Refinery since 1972 and uses the Hematite Process principle [20].

The ore treated at the Iijima Zinc Refinery contains Zn, Fe, Pb, Cu, Cd, Ag and Au along with alkali elements (K, Na). The process consists of first leaching the roasted ore with neutral solution and weak acid to eliminate the impurities (Figure 2.12). Then, the residue is leached with spent electrolyte and SO_2 at 105°C, in order to solubilize the metals. Copper is precipitated by H_2S reduction. Most lead, gold and silver also report to this residue. A two-stage neutralization with calcium carbonate eliminates free H_2SO_4, produces clean gypsum and Ga-In-Ge-enriched gypsum. The neutralized solution is finally heated up to 200°C with an oxygen overpressure of 15-45 psi to precipitate hematite. Contaminants include Zn, As, K and Na. Even though some of these contaminants represent an issue and Zn, Mg and Mn remain in solution, the Akita Zinc Process is successful extracting most of the iron out of the PLS.

Tables 2.2 and 2.3 compare the material balances for neutral leaching and hematite precipitation steps. They account for the separation of metals and contaminants during the process.

Table 2.2: Material balance based on operational results for neutral leaching [20]

	Au ($g t^{-1}$)	Ag ($g t^{-1}$)	Cu (%)	Pb (%)	Zn (%)	Fe (%)	Cd (%)
Calcine 18 727 tons per month	1.1	222	1.16	3.06	60.3	6.4	0.30
Residue 7050 tons per month	2.9	601	1.38	7.93	20.4	18.8	0.20
Distribution	99.2	100	44.8	97.6	12.7	110	25.0

Table 2.3 : Material balance based on the operational results for the Akita Zinc Process[20]

	Fe	Zn	Cd	K	Na
Neutralized solution ($g l^{-1}$) 36 386 m^3 per month	39.2	78.8	0.33	0.44	0.12
Hematite precipitate (%) 2396 tons per month	53.2	0.73	0.01	0.64	0.18
Distribution to hematite (%)	89.2	0.6	2.0	95.5	98.8
De-iron solution ($g l^{-1}$) 36 575 m^3 per month	4.2 +63.4 $g l^{-1}$ free acid	77.9			

Neutralized solution → Precipitate

Ratio > 80%:	Fe, As, K, Na, Sb, Ga
2% < Ratio < 80%:	In, Al, Ge
Ratio < 2%:	Cd, Zn, Mg, Mn, Ni, Co

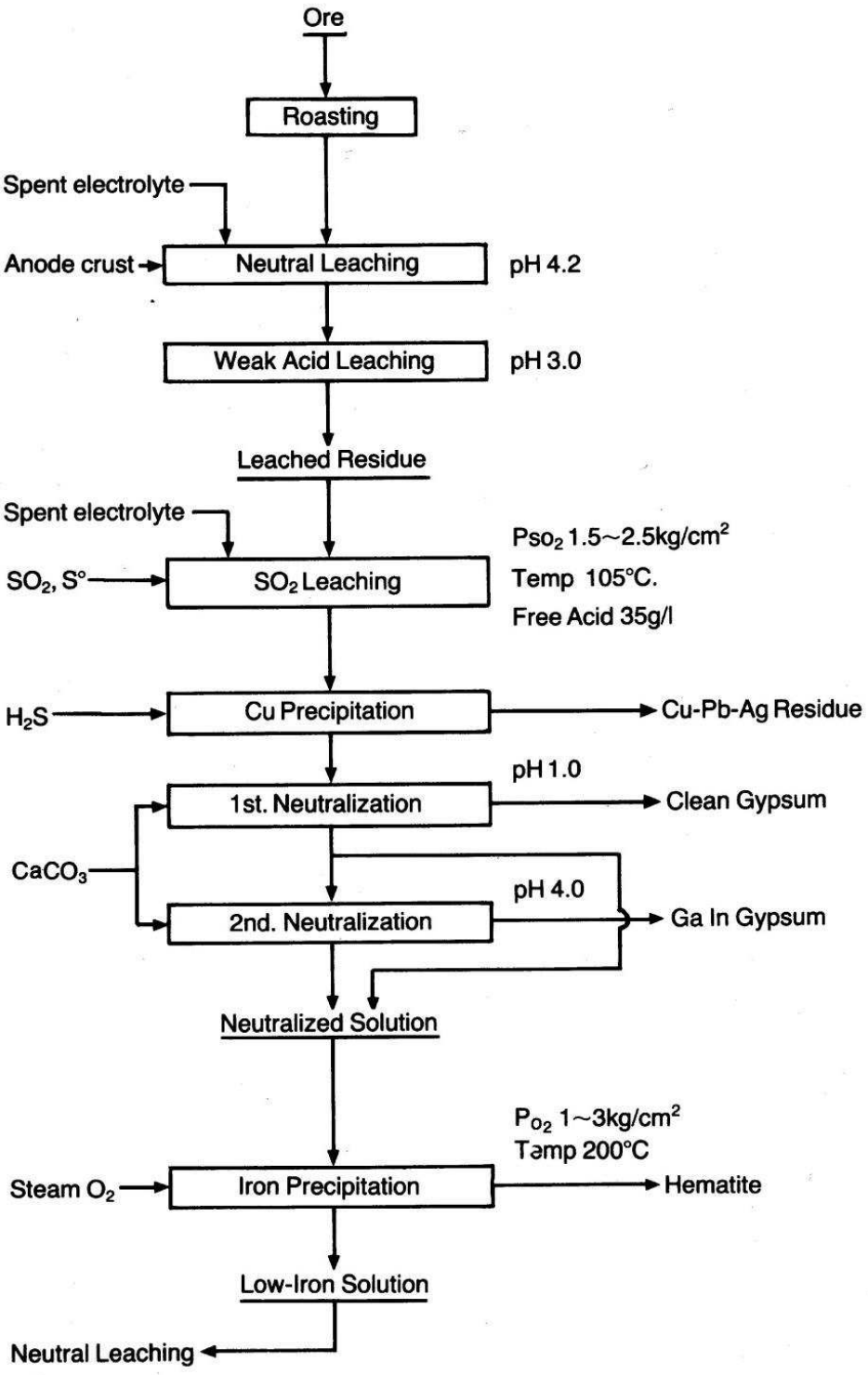

Figure 2.12: Flowsheet of the leaching and residue treatment operations in the Akita Zinc Process [20]

2.4.3.3 Factors influencing the precipitation of iron in the Akita Zinc hematite process

The following factors are influencing the process, and thus will be of great importance in this project:

- Acidity of the leach solution: as mentioned before, the acidity content controls the chemistry of the iron precipitate. At 185°C, hematite is stable up to a sulfuric concentration of 56g/L. At 200°C, the concentration increases up to 65g/L H_2SO_4. Above these boundaries, the stable species are BIS and jarosite.
- $CuSO_4$ and $ZnSO_4$: the presence of base metals as sulfates enhances hematite stability over a wide range of acidity and temperature. This aspect will be further developed in paragraph 3.4.
- Impurities: they usually prevent complete hematite precipitation. The elements which have the most impact on the process are: K>Mg>Sb>As>Zn.
    - K, Na, As and Sb most exclusively report to the precipitate. K and Na are part of jarosite crystals which compete with hematite formation and lower the iron concentration in the precipitate. As concentration in the precipitate increases along with moisture content and thus alters filterability.
    - Zn, Mg and Mn do not significantly report to the precipitate (less than 1%), but change the solution physical properties. These elements tend to decrease the particle size of the forming particles and consequently hematite has a tendency for redissolution. Mg and Zn sulfates have a positive effect on solution viscosity and density.
    - When present in high concentration in the PLS, Ca and Al can decrease the iron content in the precipitate by contamination (as an inclusion or nuclei).
    - Ge, Ga and In can report to the precipitate as high as 80% for the former and 30% for the latter, but their impact on hematite recovery is negligible. Elements such as Cd, Co and Ni have no effect on the process as they do not precipitate.
    - Lastly, high concentration of iron in the PLS tends to logically increase iron content in the precipitate. It must stay within a reasonable range, to avoid excessive iron content in the outlet solution.

2.4.4 Comparison of the Goethite, Jarosite and Hematite Processes

None of the precipitates of the Goethite and Jarosite Processes is suitable for direct commercialization as they are produced. Further refining is needed. In the production of hematite, ferrite materials can be considered as marketable products if they are pure enough.

The following table summarizes and compares the characteristics of the three precipitation processes (Table 2.4).

Table 2.4: Comparison of Goethite, Jarosite and Hematite Processes [14] and [22]

	Goethite	Jarosite	Hematite
Compound formed	FeO.OH	$MFe_3[(SO_4)_2(OH)_6]$ with Me=K, Na, NH_4	Fe_2O_3
Temperature (°C)	70-90	90-100	>185
pH	2-3.5	1.5	Up to 2% H_2SO_4
Anion present	Any	SO_4^{2-}	SO_4^{2-}
Cation added	None	Na^+, K^+, NH_4^+	None
Cationic impurities	Medium	Low	Low
Anionic impurities	Medium	High Medium	
Filterability	Very good	Very good	Very good
Fe left in solution (g/L)	<0.05	1-5	3
Metal recovery %	Zn 96 % Cu 90 % Ag 85 %	Zn 96 % Cu 90 % Ag 60-65%	Zn 98.2 % Cu 98.2 % Ag 98.2 %
Residue composition %	Fe 40-45 % Zn 5-10 % S 2.5-5 %	Fe 25-30 % Zn 4-6 % S 10-12 %	Fe 50-60 % Zn 0.5-1 % S 2-3%
Moisture	50	50	10
Amount produced/t ore	0.25	0.40	0.18
Zn loss in t/t slab	0.025	0.025	0.002

Until recently, the Jarosite Process was prevailing. But jarosite residues are not only more voluminous than hematite, but they also tend to host toxic metals such as Zn, Cd and Pb in their crystal structure. Their stability over time is poor and represents environmental concern. Additionally, zinc losses can be relatively high (Table 2.4). The Hematite Process has for long been considered too difficult and costly to implement. However, progresses in high pressure leaching technology as well as product quality appear to have addressed these issues. The Akita Zinc Hematite Process is economical, and its products are clean enough from S and Zn to be used in iron-steel making.

2.5 The iron hydroxysulfates problem

In numerous pressure leaching plants where the Hematite Process is used to purify the leach liquors, iron hydroxysulfates have been forming in place of hematite. They are described in this section.

2.5.1 Iron hydroxysulfates formation during iron precipitation processes

During HPOX processes, iron forms ferrous sulfate, which is then oxidized in ferric sulfate. Hydrolysis of ferric sulfate then forms an iron precipitate. At T>185˚C in oxidative environment, several iron species can form. Hematite is the desirable product as previously presented in paragraph 2.4.3. The conditions of hematite formation are stringent and sometimes difficult to control. It is likely that other iron solids (called iron hydroxysulfates) precipitate along with hematite [5].

Iron hydroxysulfates are unwanted constituents in the residue for several reasons:

- Poor settling and filtering properties
- Relatively unstable compounds which represent an environmental impact if stockpiled
- Trapping of precious values in their crystal structure and thus lower recovery
- In the case of gold cyanidation circuits, high concentration of iron hydroxysulfates in the autoclave residue means high lime consumption and difficulties to maintain pH > 10 during the cyanidation step. There is a risk of forming toxic HCN.

Several publications have shown that the total amount of free acid in solution determines which iron species preferentially forms [2], [5], [17], [21]. Depending on the leaching

conditions, the limit acid concentration for the formation of one or the other varies. Because hematite is preferred over iron hydroxysulfates in the final product, the acid quantity is closely monitored.

2.5.2 Iron hydroxysulfates characterization

The nomenclature of iron hydroxysulfate species vary depending on the authors. They can also be referred as ferric hydroxysulfate, basic ferric sulfate or iron hydroxyl sulfate.

Early work by Posnjak and Merwin showed that there is a large number of ferric sulfate salts but most of them are not actual crystalline species [23]. Our species of interest, the BIS, are amorphous, metastable and often composed of mixtures. As a result, they are quite difficult to characterize and very few data is available.

Posnjak and Merwin have identified three series of BIS. However, at the time, the authors did not exclude that other hydrated species also exist. The three series were subdivided and organized by the ratio Fe_2O_3 to SO_3. The following table presents the BIS already identified at the time of this study. Carphosiderite will later be identified as hydronium jarosite.

Table 2.5: BIS classified by $Fe2O_3$:SO_3 ratio as they were first identified in 1922 [23]

Fe_2O_3 : SO_3 ratio	Formula	Crystal	Color	Name
3:4	$3Fe_2O_3.4SO_3.9H_2O$	Rhombohedral	Light-deep yellow	Carphosiderite
	$Fe_2O_3.2SO_3.H_2O$	Orthorhombic	Orange-yellow	
	$Fe_2O_3.2SO_3.5H_2O$	Monoclinic	Light yellow	
1:2	$2Fe_2O_3.5SO_3.17H_2O$	Orthorhombic	Light-bright yellow	Copiapite
	$Fe_2O_3.2SO_3.7H_2O$		Yellowish	Amarantite
	$Fe_2O_3.2SO_3.8H_2O$		Yellowish	Castanite
2:5	$Fe_2O_3.2SO_3.10H_2O$		Yellowish	Fibroferrite

In the late 1970s, the iron hydroxysulfate minerals were divided in two series [24] and [25]:

- Elements with the general formula $Fe(OH)SO_4.nH_2O$, with the following members: basic iron sulfate $Fe(OH)SO_4$, butlerite/parabutlerite (they are polymorphs) $Fe(OH)SO_4.2H_2O$ and fibroferrite: $Fe(OH)SO_4.5H_2O$. According to several publications, the non-hydrated member of the BIS series is synthetic and has only been obtained in laboratory.
- Jarosites. The main jarosite species are presented in section 2.5.

In 1982, Lazaroff et al. also make the distinction between crystalline jarosites and amorphous ferric hydroxysulfates, but refers of this last category as BIS [26]. In order to simplify the nomenclature and avoid any confusions within the next sections, we will distinguish BIS (Fe(OH)SO4 and its hydrated species) from the jarosite compounds. We will consider BIS and jarosite as iron hydroxysulfates.

The following table presents the most common BIS encountered in high temperature systems, using the most recent nomenclature.

Table 2.6: Selected hydroxysulfates of Fe [27]

Name	Formula
Copiapite	$Fe^{II}Fe_4^{III}(SO_4)_6(OH)_2.2H_2O$
Fibroferrite	$Fe^{III}(SO_4)(OH).5H_2O$
Amarantite	$Fe^{III}(SO_4)(OH).3H_2O$
Butlerite	$Fe^{III}(SO_4)(OH).2H_2O$
-	$Fe^{III}(SO_4)(OH)$

2.5.3 Jarosite characterization

Jarosites are the compounds of formula: $MFe_3(SO_4)_2(OH)_6$, where M can be H_3O^+, Na, K, NH_4^+, Pb, Ag, Zn, Hg, Rb [17]. Silver-jarosite and potassium-jarosite are the two most stable compounds of the family. Other extensive substitutions occur for Fe^{3+}, SO_4^{2-}, OH^-.

As for BIS, not all jarosites are naturally occurring. Out of ten species synthetized, six of them only occur in minerals. The first mineral to be identified was potassium jarosite, in Andalusia, Spain in 1852 [28]. Table 2.7 lists all known types of jarosites.

Table 2.7: Chemical and mineral names of jarosites [29]

Formula	Chemical Name	Mineral Name
$H_3OFe_3(SO_4)_2(OH)_6$	Hydronium Jarosite	Carphosiderite
$NaFe_3(SO_4)_2(OH)_6$	Sodium Jarosite	Natrojarosite
$KFe_3(SO_4)_2(OH)_6$	Potassium Jarosite	Jarosite
$RbFe_3(SO_4)_2(OH)_6$	Rubidium Jarosite	None
$AgFe_3(SO_4)_2(OH)_6$	Silver Jarosite	Argentojarosite
$NH_4Fe_3(SO_4)_2(OH)_6$	Ammonium Jarosite	Ammoniojarosite
$TlFe_3(SO_4)_2(OH)_6$	Tallium Jarosite	None
$Pb_{1/2}Fe_3(SO_4)_2(OH)_6$	Lead Jarosite	Plumbojarosite
$Hg_{1/2}Fe_3(SO_4)_2(OH)_6$	Mercury Jarosite	None
$PbCuFe_3(SO_4)_2(OH)_6$	Lead-Copper Jarosite	Beaverite

2.5.4 Iron hydroxysulfates comparison

A spectroscopic analysis of the products of ferric sulfate hydrolysis was performed in 1996, with emphasis made on the amorphous species, which are compared to jarosite [30]. While jarosite is inert, BIS are reactive in water. This difference is explained by the atomic arrangement of each species: jarosites are trimers, and amorphous BIS are tetramers (Figure 2.13). The reactivity of BIS is believed to be caused by the small separation of neighboring irons, short Fe-O distance and strong hydrogen bonds (creating a large number of highly acid centers). This would promote the oxidation of H_2O in O_2 and thus explain BIS reactivity in water.

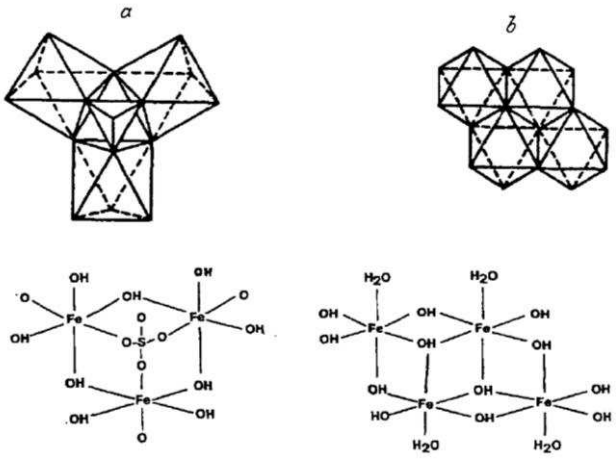

Figure 2.13: Molecular structures of jarosite (trimer) and BIS (tetramer) [30]

BIS are also reactive in the atmosphere [23], decomposing either in ferric hydroxide and gypsum (alkaline conditions) or ferric sulfate (acidic conditions). BIS can be formed by precipitation, hydrolysis or evaporation but none of these processes yielded a product that fully reaches equilibrium, producing mixtures.

In the case of pressure leaching, the main factors influencing BIS formation are acidity, temperature and iron concentration. BIS readily precipitate at high acidity (>20g/L) and lower temperatures (< 200˚C) [5]. As mentioned before, jarosite formation is favored by high acidity as well and presence of some cations in relatively high concentration (Na+, NH4+, K+, Ag+ or Pb+). Concerning the influence of initial ferric concentration, BIS seem to be promoted by increasing ferric concentration. At 225˚C, within the stability region of hematite, Dutrizac and Chen have observed that BIS becomes the predominant phase if the initial [Fe^{3+}] exceeds 22.3g/L [31]. A more specific presentation of the factors influencing BIS formation is made in section 3.3.

2.5.5 Methods to prevent BIS formation

Some attempts have been made to hinder the formation of BIS after autoclaving: the Lime Boil Process and the Hot Cure Process.

The Lime Boil Process was developed by Sherritt to avoid silver losses due to iron hydroxysulfate formation [32], [5]. It consists of treating the residue with lime to reach pH > 2. Above 100˚C, hematite readily forms; under 100˚C, goethite is forming (assuming relatively short residence time). Drawbacks of the process are related to consumption at industrial scale: up to 200kg of lime per ton has to be used during a process which can last up to 24hrs. Additionally, the slurry produced has many fines and represents handling issues.

The Hot Cure Process uses the acid and heat produced during the hydrolysis reaction to break down the BIS into ferric sulfate (Figure 2.14). Neutralization of the remaining acid and ferric sulfate formed can be achieved with limestone and not lime (Equation 2.10).

$$Fe_2(SO_4)_3 + 3CaCO_3 + 3H_2O = 2Fe(OH)_3 + 3CaSO_4 + 3CO_2 \qquad \text{(Equation 2.10)}$$

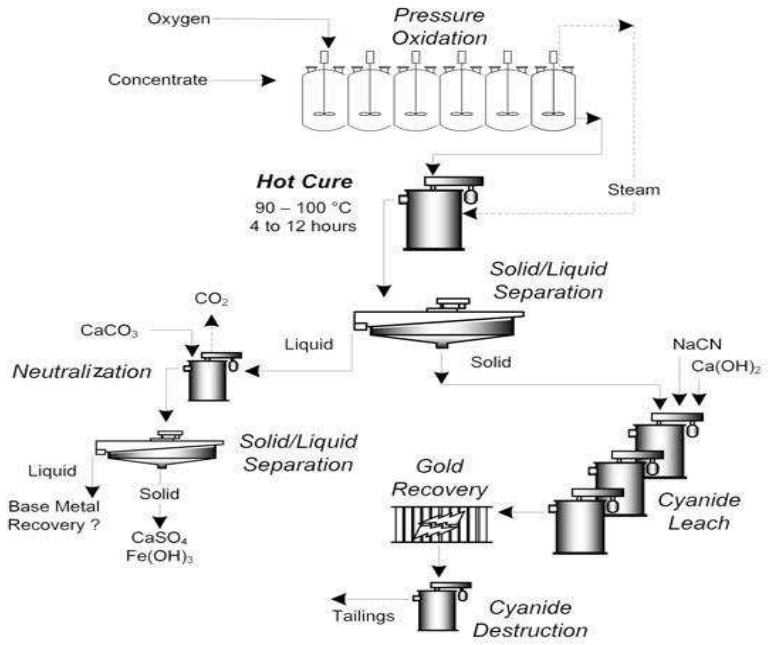

Figure 2.14: The Hot Cure Process [5]

Lime being more expensive than limestone, the Hot Cure Process can represent a rather economical option. It is a faster process and according to Equation 2.10, ferric hydroxide and gypsum are precipitated during this stage. This way, they are kept out of the pulp which is treated later by cyanidation, and do not interfere during the leaching step.

A major drawback of the Hot Cure is silver recovery losses after cyanidation, argentojarosite being one of the products of this process. For ores containing fair amounts of silver, the loss of revenue might not balance the operating costs savings. Additionally, capital costs associated with the Hot Cure Process reduce its economic interest.

CHAPTER 3 PROCESS DEVELOPMENT

In this section, chemical and thermodynamic data relative to iron hydroxysulfates precipitation is analyzed. The conditions of hydrolysis are used to best predict BIS formation.

3.1 Iron hydroxysulfates and hematite precipitation

This section details some of the chemical reactions and associated thermodynamics of iron precipitation.

3.1.1 Reactions Equations

The overall mechanism of iron phase precipitation from sulfate is described in this section. In sulfide ores, typical iron bearing species are chalcopyrite and pyrite. Chalcopyrite oxidation yields ferric ions, while pyrite forms ferrous ions. Thus, for this project, ferrous sulfate oxidation to ferric sulfate will be chosen as the starting species for the overall oxidation process. Dissolution of chalcopyrite in ferric sulfate media is one of the processes used in copper sulfide leaching operations (Equation 3.2). It will not be investigated in this thesis as no chalcopyrite will be used during the experiments.

Iron sulfide oxidation:

$2FeS_2 + 7O_2 + 2H_2O = 2FeSO_4 + 2H_2SO_4$ (Equation 3.1)

$4CuFeS_2 + 17\ O_2 + 12\ H_2SO_4 = 4CuSO_4 + 10\ H_2SO_4 + 2\ Fe_2(SO_4)_3 + 2\ H_2O$ (Equation 2.4)

$CuFeS_2 + 4Fe^{3+} = Cu^{2+} + 5Fe^{2+} + 2S$ (Equation 3.2)

Ferrous sulfate oxidation to ferric sulfate:

$2FeSO_4 + H_2SO_4 + ½O_2 = Fe_2(SO_4)_3 + H_2O$ (Equation 3.3)

Ferric sulfate hydrolysis to iron precipitates:

$2Fe_2(SO_4)_3 + 6H_2O = 2Fe_2O_3 + 6H_2SO_4$ (Equation 3.4)

$2Fe_2(SO_4)_3 + 4H_2O = 4Fe(OH)SO_4 + 2H_2SO_4$ (Equation 3.5)

$3Fe_2(SO_4)_3 + 14H_2O = 2H_3OFe_3(SO_4)_2(OH)_6 + 5H_2SO_4$ (Equation 3.6)

General equation for jarosite hydrolysis:

$3Fe_2(SO_4)_3 + M_2SO_4 + 12H_2O = 2MFe_3(SO_4)_2(OH)_6 + 6H_2SO_4$ (Equation 2.8)

($M = Ag^+, NH_4^+, K^+, 1/2Pb^{2+}$)

The following equations compare the sulfuric acid amount produced for each species. Ferrous sulfate oxidation consumes half a mole of sulfuric acid for each mole of ferrous sulfate produced. Hematite precipitation produces 1 mole of sulfuric acid for each mole of ferrous sulfate oxidized. Jarosite formation releases 0.33 mole of sulfuric acid, against 0 moles for BIS. The amount of sulfuric acid consumed or produced is paramount for this project as it allows understanding the residue chemistry.

Hematite precipitation:

$2FeSO_4 + H_2SO_4 + ½O_2 = Fe_2(SO_4)_3 + H_2O$ (Equation 3.3)

$\underline{Fe_2(SO_4)_3 + 3H_2O = Fe_2O_3 + 3H_2SO_4}$ (Equation 3.4)

$2FeSO_4 + ½O_2 + 2H_2O = Fe_2O_3 + 2H_2SO_4$ (Equation 2.9)

BIS precipitation:

$2FeSO_4 + H_2SO_4 + ½O_2 = Fe_2(SO_4)_3 + H_2O$ (Equation 3.3)

$\underline{Fe_2(SO_4)_3 + 2H_2O = 2Fe(OH)SO_4 + H_2SO_4}$ (Equation 3.5)

$2FeSO_4 + ½O_2 + H_2O = 2Fe(OH)SO_4 + 0H_2SO_4$ (Equation 3.7)

Hydronium jarosite precipitation:

$2FeSO_4 + H_2SO_4 + ½O_2 = Fe_2(SO_4)_3 + H_2O$ (Equation 3.3)

$\underline{Fe_2(SO_4)_3 + {}^{14}/_{3}H_2O = {}^{2}/_{3}H_3OFe_3(SO_4)_2(OH)_6 + {}^{5}/_{3}H_2SO_4}$ (Equation 3.8)

$2FeSO_4 + ½O_2 + {}^{11}/_{3}\ H_2O = {}^{2}/_{3}H_3OFe_3(SO_4)_2(OH)_6 + {}^{2}/_{3}H_2SO_4$ (Equation 3.9)

3.2 Thermodynamics

Thermodynamic evolution of the system was estimated using HSC Chemistry 7.1. Free energy and reaction constant were calculated in order to predict the Fe-O-S system evolution. Additionally, multi-components equilibrium compositions were calculated and plotted to estimate the species consumption and production in the leach solution.

3.2.1 Oxidation of ferrous sulfate

The thermodynamics of ferrous sulfate oxidation help determine if the reaction is complete at the conditions of leaching.

The oxidation of ferrous sulfate to ferric sulfate is highly favorable and spontaneous in weak acid conditions. Thus the first oxidation reaction will be considered as complete, and all iron is available for hydrolysis (Table 3.1).

Table 3.1: Thermodynamic data for oxidation of ferrous sulfate between 185 and 210˚C

2FeSO4 + H2SO4 + 0.5O2(g) = Fe2(SO4)3 + H2O					
T C	deltaH kcal	deltaS cal/K	deltaG kcal	K	Log(K)
185.000	-48.298	-31.823	-33.718	1.218E+016	16.086
190.000	-48.317	-31.864	-33.559	6.870E+015	15.837
195.000	-48.335	-31.904	-33.399	3.921E+015	15.593
200.000	-48.353	-31.942	-33.240	2.264E+015	15.355
205.000	-48.371	-31.979	-33.080	1.322E+015	15.121
210.000	-48.387	-32.014	-32.920	7.805E+014	14.892

3.2.2 Hematite precipitation

The following table presents thermodynamic data for the precipitation of hematite from ferrous sulfate between 185 and 200˚C. At atmospheric pressure, ΔG and K show that the reaction is not spontaneous.

Table 3.2: Thermodynamic data for overall hematite precipitation reaction between 185 and 210˚C

2FeSO4 + 0.5O2(g) + 2H2O = Fe2O3 + 2H2SO4					
T C	deltaH kcal	deltaS cal/K	deltaG kcal	K	Log(K)
185.000	-5.048	-17.538	2.987	3.759E-002	-1.425
190.000	-5.023	-17.482	3.074	3.541E-002	-1.451
195.000	-4.998	-17.430	3.162	3.341E-002	-1.476
200.000	-4.975	-17.380	3.249	3.157E-002	-1.501
205.000	-4.952	-17.333	3.335	2.988E-002	-1.525
210.000	-4.931	-17.289	3.422	2.831E-002	-1.548

The effect of pressure on precipitation thermodynamics was modelled using equilibrium compositions calculation (Figure 3.1). Chosen temperature is 195˚C, which is the running temperature for this project. The input is 3kmol of O_2(g), 2kmol of H_2O and $FeSO_4$.

Conversion factor for iron is only 16.1% (hematite produced). Conversion factor for sulfuric acid is 32.2%. Experimentally, some factors which can be expected to influence the mass balance are:

- Agitation which promotes the formation of hematite
- Oxygen overpressure which shifts Equation 2.9 to the left
- Excess sulfuric acid which shifts Equation 2.9 to the right

$2FeSO_4 + ½O_2 + 2H_2O \rightarrow Fe_2O_3 + 2H_2SO_4$ (Equation 2.9)

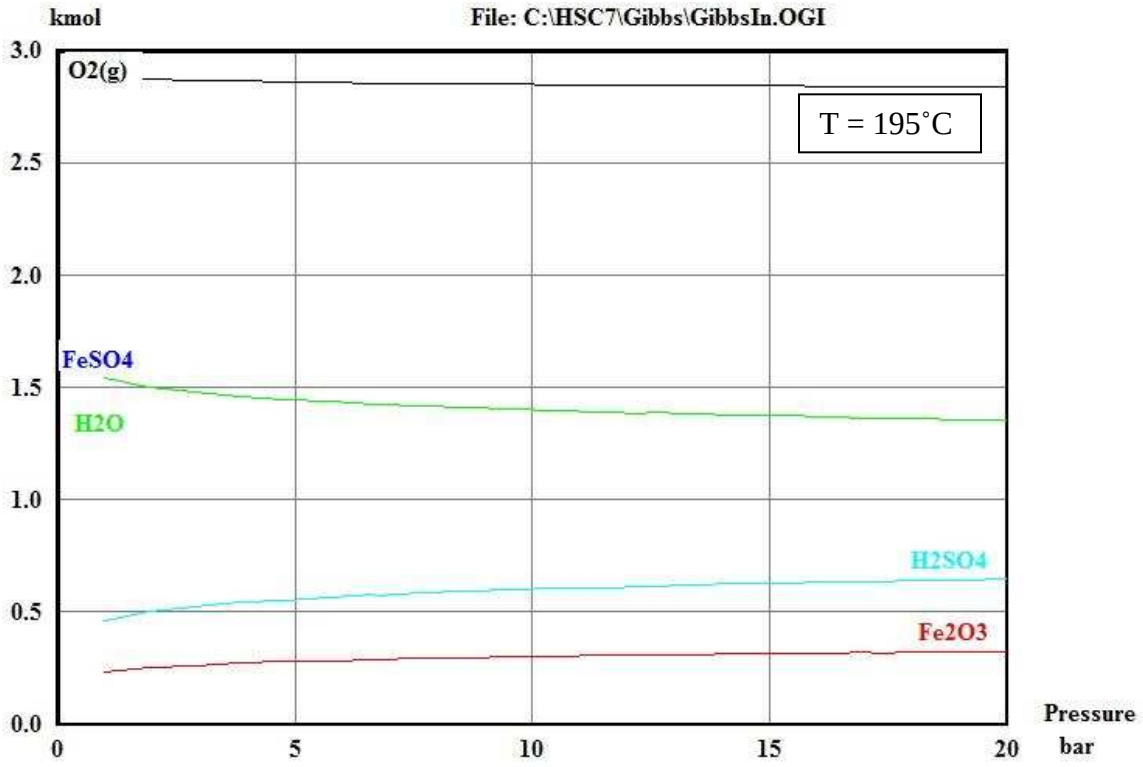

Figure 3.1: Equilibrium composition for the precipitation of hematite from ferrous sulfate at 195˚C

3.2.3 Iron hydroxysulfates precipitation

At the time of this study, thermodynamic data for BIS was not available for a thermodynamic estimation. Solid BIS does not form under ambient conditions and as a result it is extremely difficult to measure thermodynamic properties and attempt to develop a model.

Because BIS and jarosite both belong to the iron hydroxysulfates group, the thermodynamic study of hydronium jarosite will be used to try to understand BIS formation. Thermodynamic data for hydronium jarosite was collected in the literature and added to HSC database (Table 3.3) [33], [34].

Table 3.3: Thermodynamic data for Hydronium Jarosite [33], [34]

ΔG°_f (298K)	ΔH°_f (298K)	S° (298K)	a	b	c
-3,226.4	-3,770.2	448.2	287.2	0.6281	-3286000
kJ/mol	kJ/mol	J/mol.K	J/mol.K	$J/mol.K^{-1}$	J.K/mol

The heat capacity coefficients are given for the Maier Kelley polynomial (Equation 3.10):

$$C_p(T \text{ in } K) = a + bT + cT^{-2} \qquad \text{(Equation 3.10)}$$

Table 3.4: Thermodynamic data for overall hydronium jarosite precipitation reaction between 185 and 210˚C

6FeSO4 + 1.5O2(g) + 11H2O = 2(H3O)Fe3(SO4)2(OH)6 + 2H2SO4					
T C	deltaH kcal	deltaS cal/K	deltaG kcal	K	Log(K)
185.000	141.983	-169.332	219.563	1.795E-105	-104.746
190.000	141.706	-169.935	220.411	9.650E-105	-104.015
195.000	141.427	-170.532	221.262	4.989E-104	-103.302
200.000	141.148	-171.126	222.116	2.484E-103	-102.605
205.000	140.867	-171.716	222.973	1.192E-102	-101.924
210.000	140.585	-172.304	223.833	5.520E-102	-101.258

At the temperature range used for the Hematite Process, it can be seen from the thermodynamic data that formation of hydronium jarosite is neither spontaneous nor favorable. When modelling the system with the Equilibrium Composition function in HSC (Figure 3.2), the same observation can be made (no formation of hydronium jarosite but ferric sulfate). An input

of 3kmol O_2, 2kmol $FeSO_4$ and H_2O was used. Increasing the total pressure to 50 bar (725 psi), did not change the results. Some reasons for hydronium jarosite and BIS meta-stability are presented in section 3.3.2.

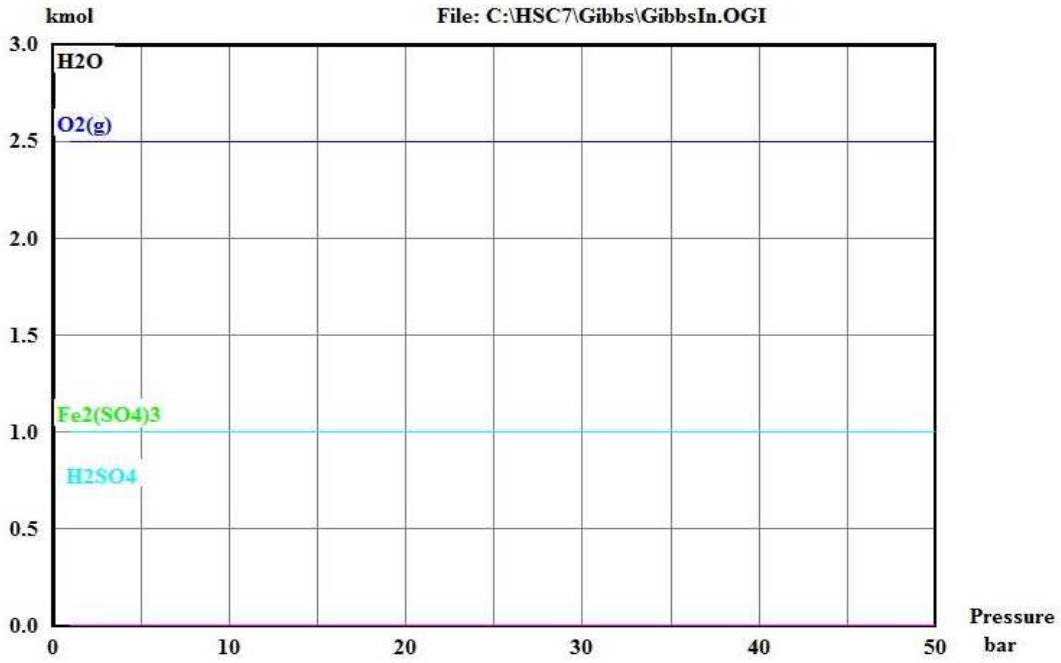

Figure 3.2: Equilibrium composition for the precipitation of hydronium jarosite from ferrous sulfate at 195˚C

3.3 Stability of iron hydroxysulfates

Because no data was available for modeling, experimental observations and models from the literature were used to identify the main factors controlling iron hydroxysulfate precipitation over hematite.

3.3.1 3D model of the $Fe_2(SO_4)_3$-H_2SO_4-H_2O system

Based on Posnjak and Merwin's work, Tourre [17] produced a 3D model of the hematite/sulfates system (see figures 3.3 and 3.4). According to this model:

- Hydronium jarosite is only stable up to 170˚C, i.e. below the operating temperature of this project. Above this point, the only stable phases are hematite and BIS. Thus this study should witness a simple system with only two coexisting species.
- Increasing sulfate content in the system favors the formation of BIS over jarosites.

- Two factors seem to control BIS stability over hematite: sulfate and ferric iron content.
- At 200˚C, the area of hematite stability progressively increases up to 22wt% sulfate where it reaches an optimum. At this point, the upper limit for hematite stability is 2.3wt% ferric in the system. Above 22wt% sulfate, the limit stabilizes around 1.9wt% ferric in the system.

These observations were confirmed by Lazaroff and al. [26]. In the simple Fe-O-S system, hydronium jarosite has a limited area of stability, because it is one of the least stable jarosite species. If additional ions such as Na^+, K^+ or $NH4^+$ were present in the system (which is extremely likely in a real industrial conditions), jarosites would certainly replace BIS.

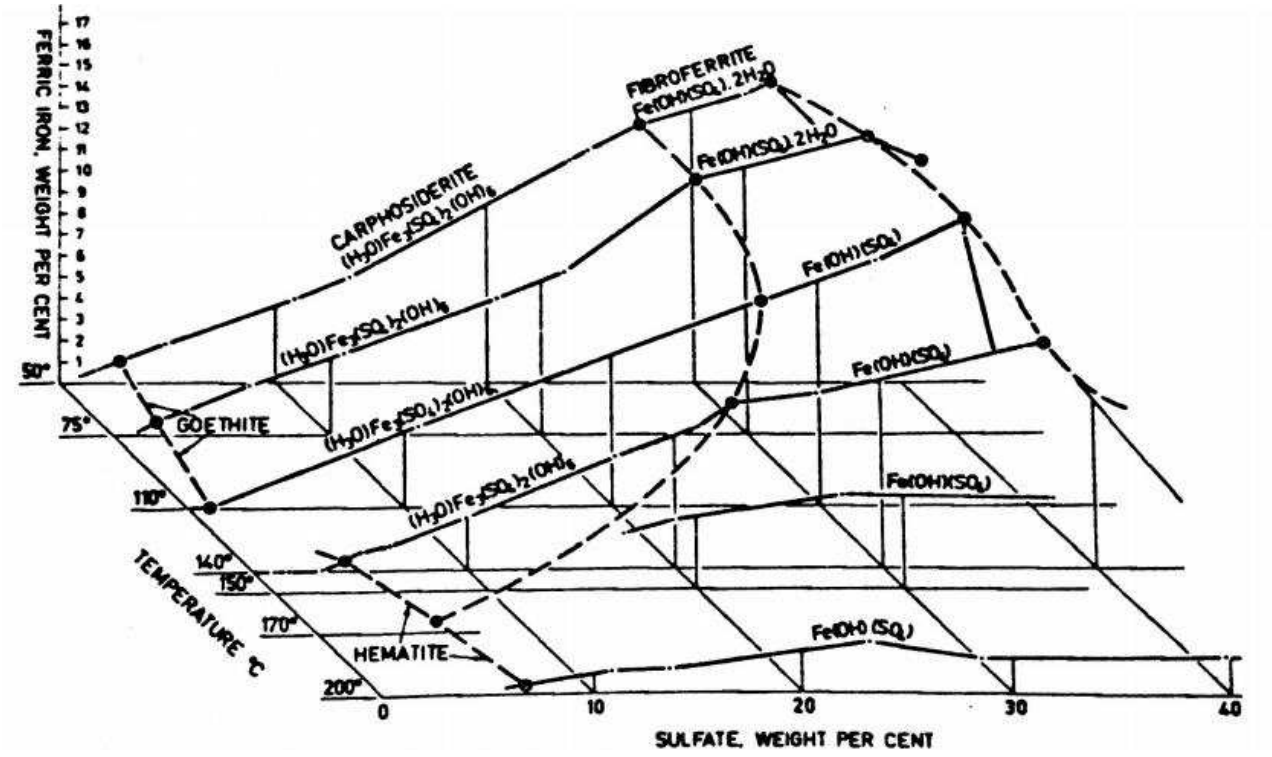

Figure 3.3: System $Fe_2(SO_4)_3$-H_2SO_4-H_2O; polytherm 50˚C to 200˚C, 0 to 40% SO_4 [17]

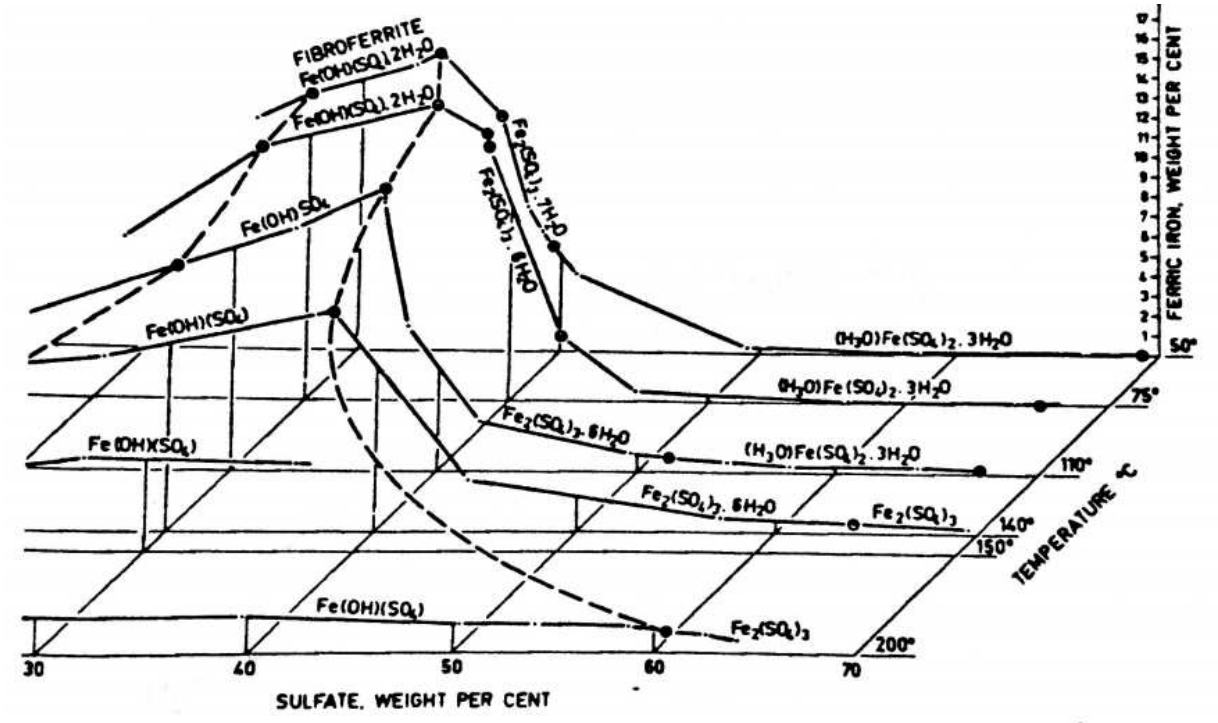

Figure 3.4: System $Fe_2(SO_4)_3$-H_2SO_4-H_2O; polytherm 50˚C to 200˚C, 30 to 70% SO_4 [17]

3.3.2 Experimental approach

In 1971, Babcan and al. defined the area of stability of iron hydroxysulfates in the Fe-O-S system (Figure 3.5) [35]. In more recent studies, BIS have been proven to be also stable at conditions which would normally lead to hematite formation [31], [36]. Cheng and al. refer to Stranski's rule, also called Ostwald's step rule to explain this phenomenon [2]:

"*If a reaction can result in several products, it is not the most stable state with the least amount of free energy that is initially obtained, but the least stable one, lying nearest to the original state in free energy*" [37].

In the present case, if the oxidation conditions were maintained for a longer time, the most stable phase would eventually form. As a result, from a thermodynamic point of view, iron hydroxysulfates are metastable.

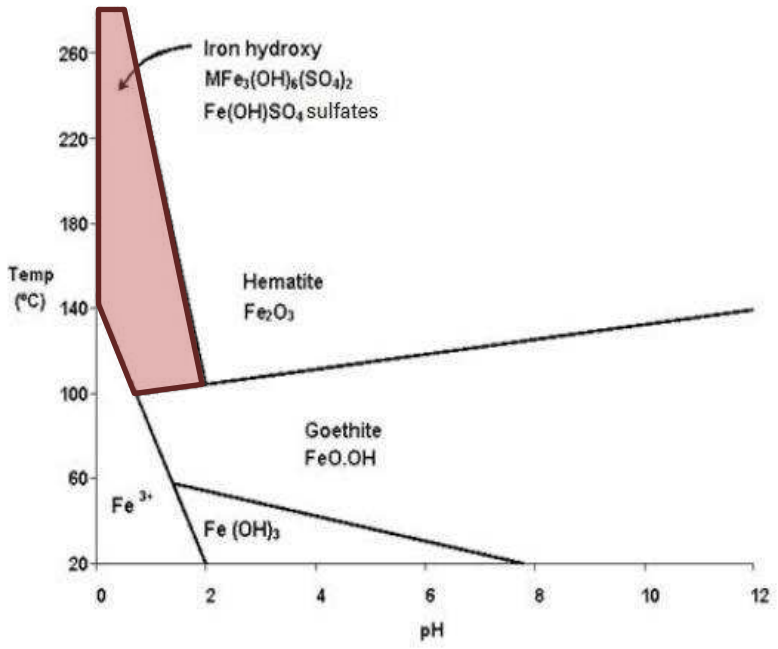

Figure 3.5: Areas of stability of various compounds in the Fe-S-O system (modified after Babcan [36])

Several hematite solubility studies have been conducted in order to identify the optimum conditions for iron oxide precipitation. At equilibrium and room temperature, Umetsu and al. proposed a linear relation between ferric concentration and free acidity (Equation 3.11) [21]:

$$Log[Fe(III)]_{total} = a*Log[H_2SO_4]_{free} - b \qquad \text{(Equation 3.11)}$$

Where a and b are coefficient which depend on temperature and the presence of other metal sulfates.

This linear model has been experimentally confirmed and modelled (Figure 3.6) [38]. The conditions used for this study were similar to the parameters used in the present thesis (170-200˚C, 30-100 g/L free acidity) except for the fact that no oxygen overpressure was added. Investigations on the hydrolysis of iron sulfate solution by the same authors highlighted the same linear relation between ferric ion and free acid concentrations, but up to a certain point. The solid phase equilibrium curve is actually made of two straight lines of different slopes (Figure 3.7). At lower free acidity, the curve describes hematite equilibrium, and at higher acidity, the curve describes BIS equilibrium.

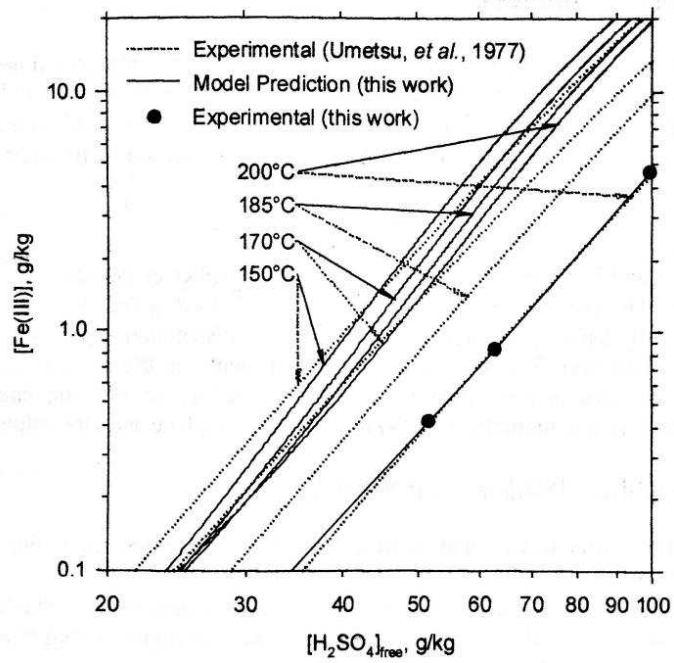

Figure 3.6: Hematite solubility – comparison between model prediction and experimental data [38]

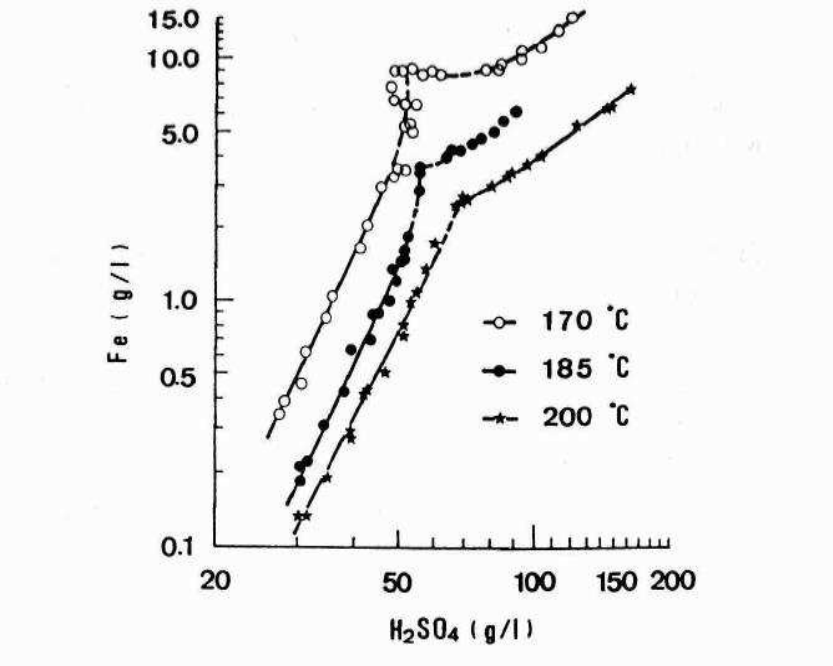

Figure 3.7: Relationship between concentrations of ferric ion and free sulfuric acid in the absence of other metal sulfates [39]

3.4 Effect of other sulfates on iron hydroxysulfates formation

This section details previous results obtained when leaching synthetic solutions prepared with several different sulfate salts.

3.4.1 Selective precipitation of iron

Sulfide ores bear many different metals which can be leached along with iron. Common sulfates in leaching solution are $CuSO_4$, $ZnSO_4$, Na_2SO_4. Assessing their impact on hematite or BIS precipitation is paramount.

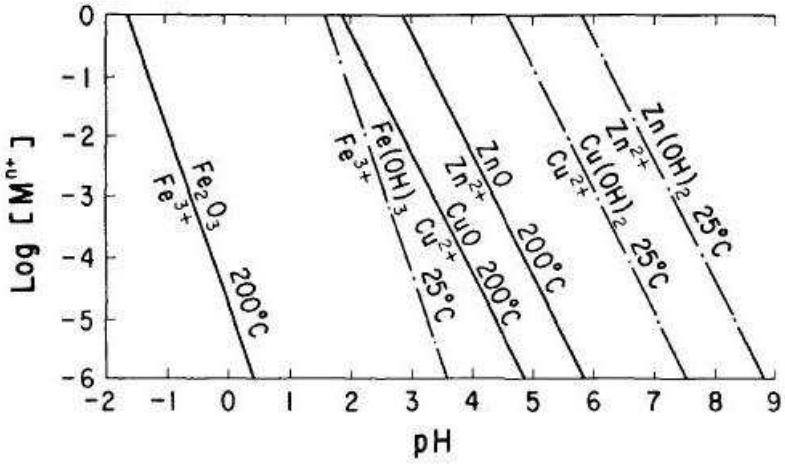

Figure 3.8: Relation between concentration of metal ion and pH at 25˚C and 200˚C [21]

The previous figure shows that the hydrolysis of ferric iron is favored at high temperature and low pH (Figure 3.8) [21]. It can also be seen that for given conditions, only iron precipitates and the other ions stay in solution. Hydrolysis is thus a very efficient way to selectively remove iron from solution.

3.4.2 Effect of zinc sulfate

Because of the importance of the Hematite Process in the zinc industry, most studies related to hematite precipitation thermodynamics have been performed in acidic ferric sulfate solutions, with addition of zinc. The addition of zinc sulfate to the Fe-O-S system promotes the formation of hematite over a wider range of temperature and free acidity [2], [21]. Sulfur content in the precipitate decreases when zinc sulfate is present. Adding zinc sulfate to the leach solution also shifts upward the critical concentration of sulfuric acid allowing hematite precipitation (Figure 3.9) [39].

Table 3.5: Free acidity upper limit for hematite precipitation in absence and presence of zinc at 200˚C [39]

Zinc Concentration	0 g/L Zn	69-74 g/L Zn	99-103 g/L Zn
Free Acidity Limit	64 g/L	103 g/L	111 g/L

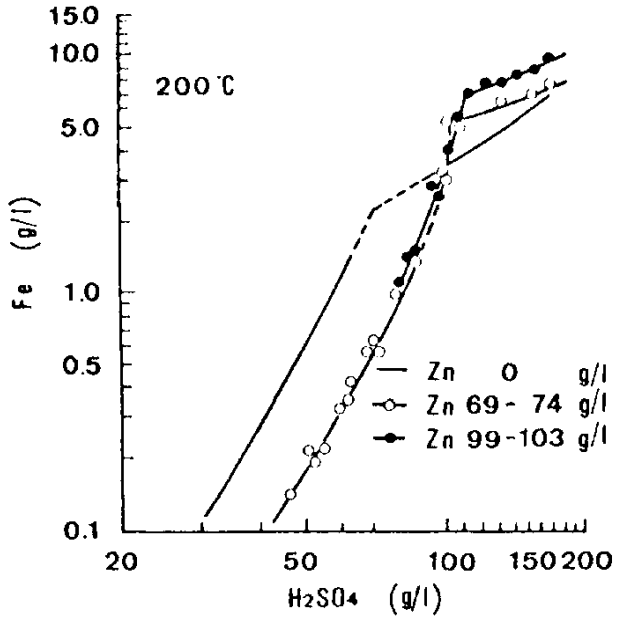

Figure 3.9: Relationship between concentration of ferric ion and free sulfuric acid in the presence of zinc sulfate at 200˚C [39]

3.4.3 Effect of copper sulfate

Tozawa and al. also investigated the influence of copper sulfate on the Fe-O-S system (Figure 3.10). The observations are similar than when adding zinc sulfate. The following table provides an estimation of the effect of copper sulfate on the upper free acid limit for hematite precipitation. Not all authors agree on the limit, and the value varies with for each specific system.

Table 3.6: Free acidity upper limit for hematite precipitation in absence and presence of copper at 200˚C [39]

Cu Concentration	0 g/L Cu	50 g/L Cu	70 g/L Cu
Free Acidiy Limit	64 g/L	76 g/L	80 g/L

Experiments have also been conducted with addition of sodium or magnesium sulfate. Adding sodium sulfate resulted in the formation of sodium jarosite. Magnesium sulfate had a similar effect on the system than zinc and copper.

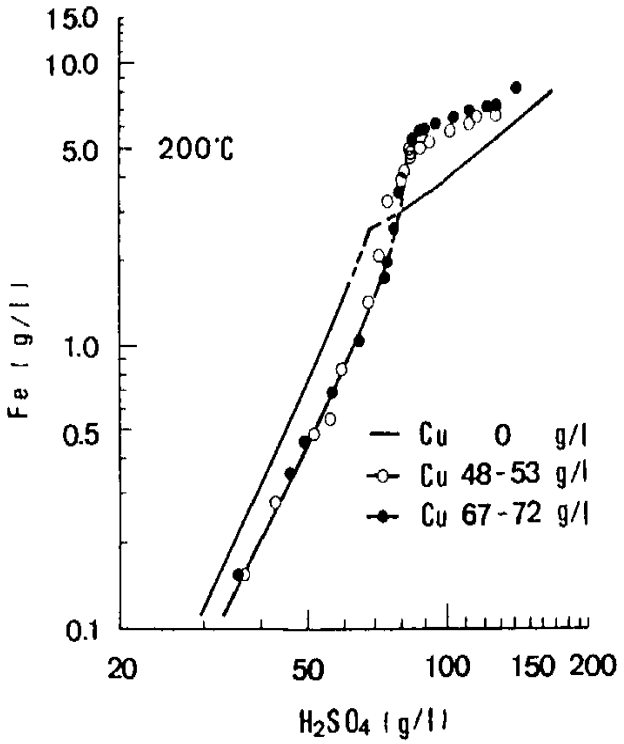

Figure 3.10: Relationship between concentration of ferric ion and free sulfuric acid in the presence of copper sulfate at 200˚C [39]

3.4.4 Buffering effect of metals sulfates

The hematite precipitation equilibrium can be rewritten as:

$$Fe^{3+} + 1.5\ H_2O = 0.5Fe_2O_3 + 3H^+ \quad \text{(Equation 3.12)}$$

The reaction constant is $K = \frac{a_{H+}^3}{a_{Fe^{3+}}}$ and at first sight is independent of coexisting sulfates. Yet, the upper acidity limit of hematite precipitation is shifted at higher level when other sulfate species are added to the system. The stabilizing effect of sulfates is due to the SO_4/HSO_4^- equilibrium (Equation 3.13), also referred as the "buffering action of the second dissociation of sulfuric acid" [39]. When adding sulfate, the free H^+ form bisulfate ions HSO_4^- , decreasing the overall free acidity and thus allowing for wider hematite stability conditions (Equation 3.12).

This theory is backed up by that bisulfate and undissociated sulfates are more stable at high temperatures.

$$H^+ + SO_4^{2-} = HSO^{4-} \qquad \text{(Equation 3.13)}$$

3.5 Leaching of artificial solutions

This section details the preparation of the experimental phase. Using the previously detailed observations, experimental work was subdivided in several steps. First, the conditions at which BIS is precipitating from a simple Fe-O-S system were investigated, in the specific setup allowed by Colorado School of Mines equipment. Several matrices which composition was based on previous studies were tested. The operating parameters which could be modified were composition (i.e. iron and acid concentration), temperature and oxygen overpressure. To be considered suitable, the matrix needed to produce significant amount of BIS, and enough residue to be tested by XRD and Leco.

Once BIS were effectively recovered in the residue, the acid concentration in the vessel was slowly decreased to find the limit conditions yielding BIS over hematite. At this point, it was paramount to keep initial ferrous sulfate concentration constant (22.3 g/L Fe). The range of acidity tested was 5-98.6 g/L, and allowed to produce 9 samples which yielded from 100% to 2% hematite, the rest of the samples being iron hydroxysulfates.

Keeping the same initial iron concentration and the autoclave's operating parameters constant, three different matrices were then chosen:

- a low acid matrix yielding pure hematite ($[H_2SO_4]_{initial}$ = 20g/L)
- an intermediate acid matrix yielding a mixture of BIS and hematite ($[H_2SO_4]_{init}$ = 40g/L)
- a high acid matrix yielding mostly BIS ($[H_2SO_4]_{initial}$ = 60g/L)

The second experimental phase consisted in assessing the hindering effect of copper sulfate on BIS precipitation. To do so, various amounts of copper sulfate ($[CuSO_4]_{initial}$ = 12.7-63.5 g/L) were added to the previously defined matrices ($[H_2SO_4]_{initial}$ = 20-60 g/L) and the residues produced were compared.

The third phase aimed at testing the impact of initial iron concentration on residue composition, by using the same sulfuric acid and copper sulfate content in the previously tested matrices, but changing the initial iron sulfate content. 3 batches of three different initial iron compositions were tested:

- Batch A: 83.4g $FeSO_4$ i.e. $[Fe(II)]_{initial}$ = 16.7g/L
- Batch B: 111.2g $FeSO_4$ i.e. $[Fe(II)]_{initial}$ = 22.3g/L
- Batch C: 152.9g $FeSO_4$ i.e. $[Fe(II)]_{initial}$ = 30.7g/L

Finally, the influence of iron's initial oxidation state on the system was also investigated. Within sulfides, the oxidation state of iron can be II or III and thus form ferrous or ferric sulfate when leached in sulfuric acid. During the first phases of testing, the oxidation of ferrous ions to ferric was believed to be complete because of favorable thermodynamics. However, most studies conducted prior this thesis were based on the use of ferric sulfate for leach solution preparation and it appeared necessary to verify the extent of iron oxidation in solution. As a result, two batches of identical iron concentration (22.3g/L) were compared: one batch was prepared with ferrous sulfate and the other with ferric sulfate.

CHAPTER 4 EXPERIMENTAL AND ANALYTICAL PROCEDURES

In this chapter, the equipment and operating parameters are presented. The analytical procedures used to characterize the solid and liquid products are described in details.

4.1 Description of the autoclave

Experiments were performed in a 2L autoclave made of titanium. The autoclave sealing is achieved by a spring holding the vessel and the shaft together. A magnetic drive on the impeller driving shaft provided agitation at 500rpm. The autoclave is equipped with two cooling coils, to rapidly cool the vessel and the impeller if needed. Four valve-controlled openings correspond to a sampling tube, oxygen inlet, gas outlet and pressure transducer. Pressure, temperature and rotation speed were set and changed through a controlling unit next to the autoclave. Titanium baffle bars were placed inside the vessel. Figure 4.1 shows the equipment used and figure 4.2 represents a schematic diagram of the vessel and the impeller.

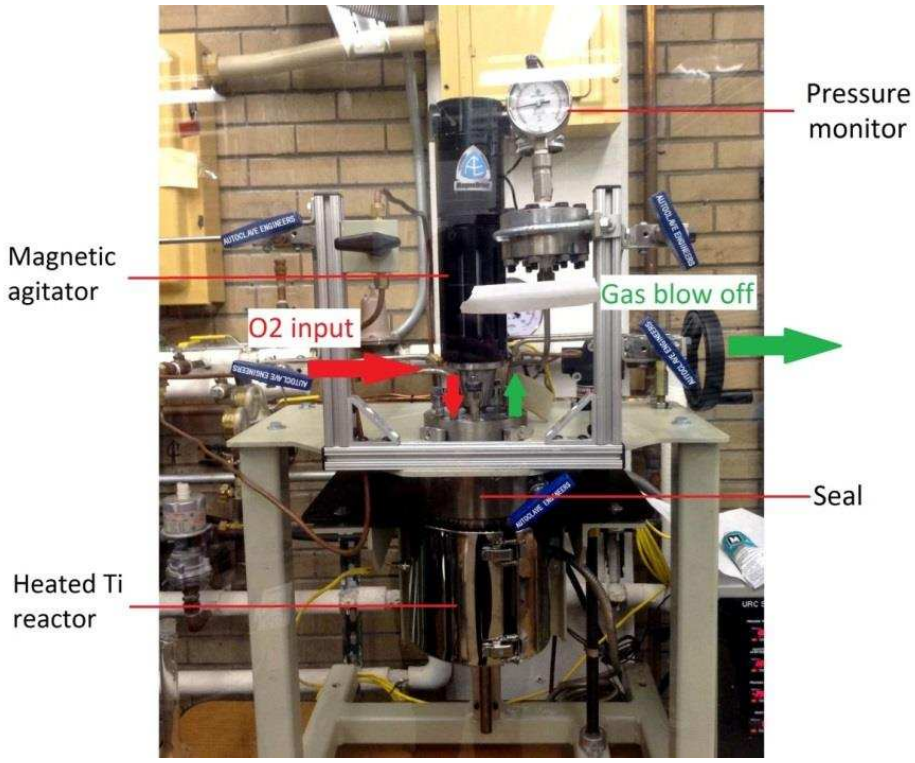

Figure 4.1: Photograph of Colorado School of Mines autoclave

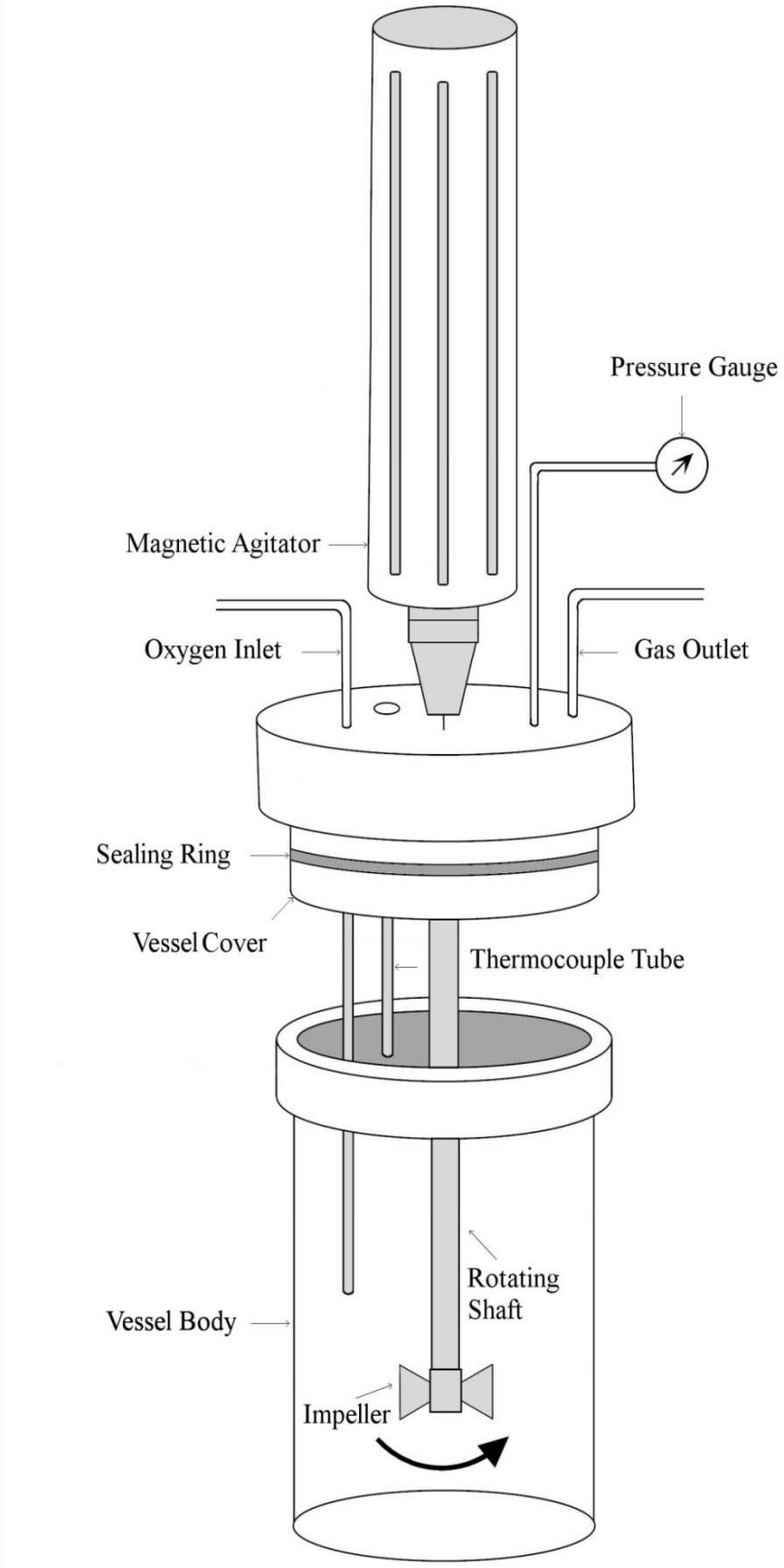

Figure 4.2: Detailed diagram of the autoclave

4.2 Experimental procedure

This section details the chemicals used, as well as the experimental procedure followed for all tests.

4.2.1 Chemicals used for matrix preparation

Reagent grade chemicals and deionized water were used for all the experiments. Each experiment was carried out using 1 liter of solution in the 2 liter vessel. The solutions were prepared using:

- Ferrous sulfate heptahydrate $FeSO_4.7H_2O$
- Ferric sulfate hydrate $Fe_2(SO_4)_3.xH_2O$
- Cupric sulfate pentahydrate $CuSO_4.5H_2O$
- Sulfuric acid H_2SO_4

Accounting for chemicals purity, initial iron concentration ranged from 16.7 to 30.7 g/L, initial copper concentration varied between 0 and 63.6 g/L and sulfuric acid concentration varied between 5 and 98.6 g/L. The sulfate salts were completely dissolved in 1 liter of deionized water in a volumetric flask before being transferred into the vessel.

4.2.2 Preheating and retention phase

In order to reach the required temperature and pressure for hematite precipitation, the vessel was preheated during ~60 min. During this time, neither oxygen nor agitation was applied. After 60 min, the temperature in the vessel reached about 185˚C, which is the minimum required temperature for the hematite process. The rotating drive was then started (500 rpm) and 40 psi oxygen overpressure was added. Within 5 minutes, the temperature and pressure in the vessel stabilized to the following conditions: 195ºC and 225 psi. The control range for the temperature was ±2ºC. Retention time was 3 hours. Figure 4.3 presents the typical evolution of pressure and temperature during a test.

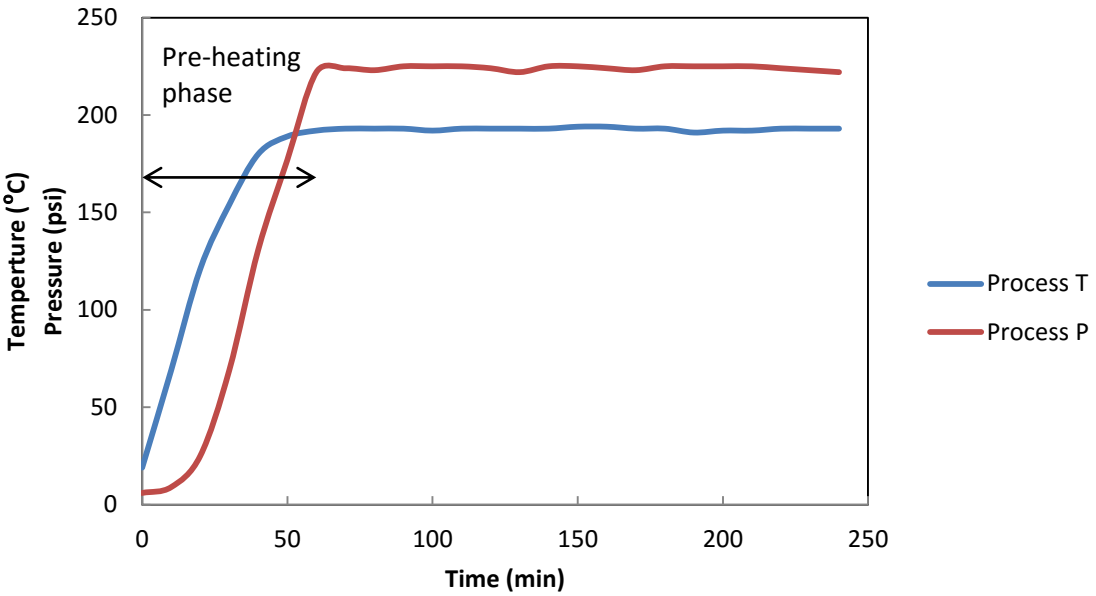

Figure 4.3: Temperature and pressure evolution during autoclave run

Table 4.1: Steam pressure values at 160, 185 and 195ºC

Temperature (ºC)	160	185	195
Steam Pressure (psi)	75.0	148.2	188.1

4.2.3 Cooling and samples handling

After 3 hours residence time, agitation and heater were stopped. Cooling took about 1h30 min to reach a temperature less than 100˚C in the reactor. The vessel was depressurized and safely opened. Another 30 minutes of cooling were necessary for the vessel and the solution to be safely handled. The solution was filtered on a Buchner vacuum filter using Whatman 50 filter papers and washed with 1 to 2 liters of deionized water. The solutions were bottled for analysis and the residues were dried at least 24 hours at 75˚C. Once bagged, residue samples were sent to Newmont Metallurgical Services in Greenwood Village, CO for analysis.

4.3 Free Acidity measurement

Free acidity was measured using an auto titrator (model: DL15 Metler-Toledo) and a Sigma Aldrich 0.5M NaOH titrant solution. The procedure is detailed in appendix A. Because of

the possibility of hydrolysis for metallic ions in solution, potassium oxalate was added before the titration as complexing agent (Equations 4.1 and 4.2) (Figure 4.4). Any hydroxide consumption due to the presence of cupric and ferric ions was thus prevented.

$$Fe^{3+} + 3C_2O_4^{2-} = Fe(C_2O_4)_3^{3-} \qquad \text{(Equation 4.1)}$$

$$Cu^{2+} + 2C_2O_4^{2-} = Cu(C_2O_4)_2^{2-} \qquad \text{(Equation 4.2)}$$

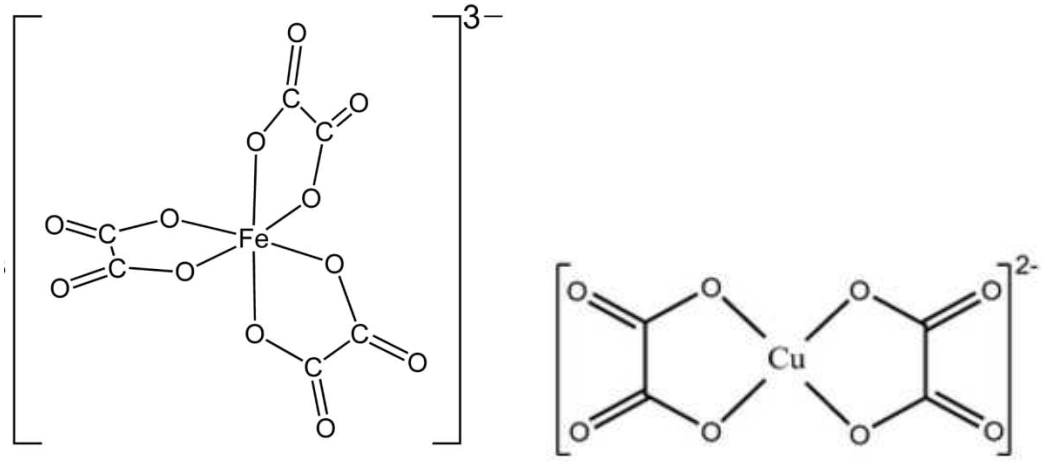

Figure 4.4: Complexation of Fe(III) and Cu(II) by oxalate

The titration uses the first derivative method: the first derivative of pH with respect to titrant volume (dpH/dV) is calculated and plotted. The highest peak on the plot corresponds to the volume of titrant (Appendix A). Using equation 4.3, free acidity could be calculated.

$$\text{Free acidity (g/L)} = \frac{49 * \text{mL titrant} * \text{mol titrant}}{\text{mL sample}} \qquad \text{(Equation 4.3)}$$

Free acidity refers to the "free" amount of sulfuric acid or in other word the total amount of sulfate ions that are not bound to ferric sulfate or copper sulfate (Equation 4.4) [38]:

$$[H_2SO_4] = [SO_4]_{total} - 3/2[Fe(III)]_{total} - [Cu]_{total} \qquad \text{(Equation 4.4)}$$

4.4 Flame Atomic Absorption Spectrometry

FAAS was chosen for analysis of the PLS because of its reliability for copper and iron. All dilutions were made using a 2% nitric solution, in order to match the standard matrix composition. Functional parameters of the machine are presented in table 4.2.

Table 4.2: Functional parameters used for atomic absorption analyses

Element	Wavelength	Lamp current	Characteristic Concentration	Linear Range	Slit
Fe	302.1 nm	30 A	0.4 mg/L	10 mg/L	0.2 nm
Cu	216.5 nm	15 A	0.117 mg/L	20 mg/L	0.2 nm

4.5 X-Ray Diffraction

X-Ray Diffraction (XRD) analyses were performed at Newmont Metallurgical Services. The XRD patterns helped identifying and quantify the phases in the residue.

Javed and al. used XRD patterns to make observations on the crystallinity of their hematite residue [40]. Indeed, the intensity peaks shape provides information on the crystals. Sharp, well delimited peaks are characteristic of well crystallized species. Poor crystallinity means wider peaks. When possible, the XRD patterns produced in this project were compared. In mixtures, peaks intensity and shape are related to phase abundance. As a result, only pure hematite samples were used for pattern comparison (no pure iron hydroxysulfate residues were produced).

4.6 Sulfur content

Sulfur content measurements were performed at Newmont Metallurgical Services using a Leco analyzer. This technology consists in heating less than 0.1g of sample at 1350˚C in an induction furnace. During heating, oxygen is flowed through the machine, releasing sulfur dioxide which is measured by an infra-red detection system [41].

Samples were analyzed for total sulfur content. They were compared to sulfur content in the most common species encountered in this study (Table 4.3).

Table 4.3: Sulfur content in hematite and iron hydroxysulfates

Hematite	BIS	Fibroferrite	Jarosite
0	18.98%	12.39%	13.34%

4.7 QEMSCAN

A mineral characterization was performed at the Colorado School of Mines QEMSCAN Facility, within the Department of Geology and Geological Engineering. Quantitative Evaluation of Minerals by Scanning Electron Microscopy or QEMSEM is a recent method of analysis designed to provide quantitative analysis of minerals or rocks. It is associating a scanning electron microscope and energy dispersive x-ray spectroscopy detectors to integrated software called QEMSCAN. Surface images of the samples are generated in function of their mineralogy, integrating petrography data to the analysis.

A first recognition step gives an exhaustive list of present minerals. By grouping the minerals into appropriate sections, a primary list is created. It allows narrowing the composition to minerals of interest. Boundary zones between minerals were closely looked at. Mixed x-ray spectra are common during acquisition and can lead to misidentification of the minerals.

Three samples susceptible to be representative of the various types of precipitates were analyzed. The sample preparation procedure followed at Colorado School of Mines is presented in appendix B.

CHAPTER 5 RESULTS

This chapter presents the results obtained from the four experimental phases.

5.1 Leaching of a pure ferrous sulfate solution

This section presents the results obtained from the leaching of a solution of 22.3g/L initial iron concentration (111.24g/L $FeSO_4$) at varying initial free acidity.

5.1.1 Free acidity

Free acid generation/consumption in function of initial free acidity is presented in figure 5.1. At low initial sulfuric acid concentration, free acid is produced in solution. With increasing initial free acid, less acid is released until it reaches equilibrium at $[H_2SO_4]_{initial}$ = 40g/L = $[H_2SO_4]_{final}$. Above this point, acid is consumed during the leaching process.

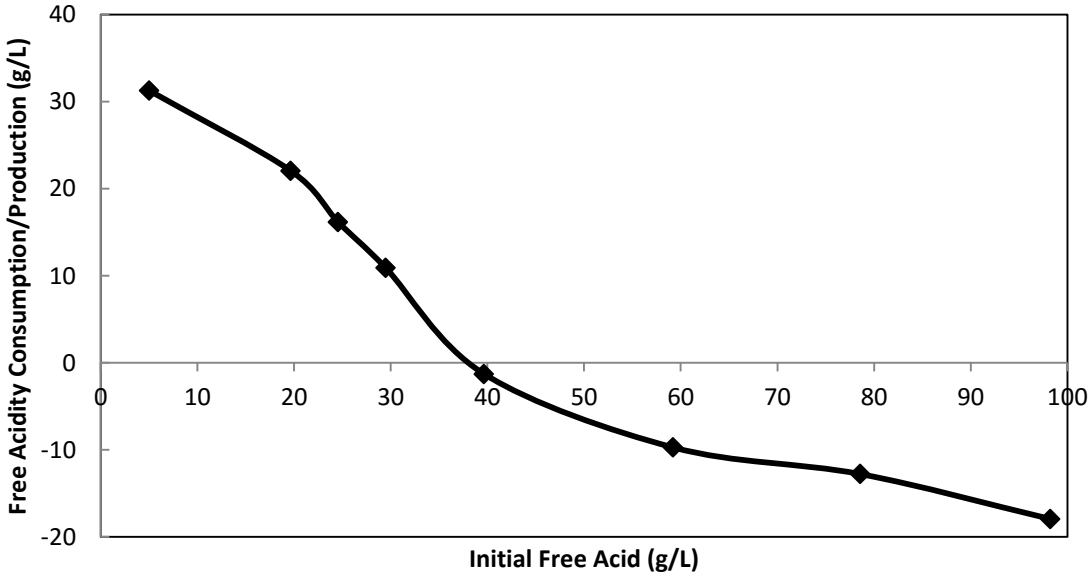

Figure 5.1: Free acid Consumed/Produced in function of initial free acid content

This pattern can be explained by the residue composition. At “low” initial free acidity, hematite is preferentially formed. For each mole of hematite precipitated, two moles of sulfuric acid are formed. At intermediate initial sulfuric content, the residue is composed of hematite, BIS and to a lesser extent jarosite. As mentioned in paragraph 3.1, jarosite precipitation produces

less acid than hematite, and BIS precipitation does not release any. Because the proportion of hematite produced decreases, final acidity in the system drops as well. At high initial free acidity, when BIS are predominant in the system, free acid is consumed for the oxidation of ferrous sulfate. If the hydrolysis of ferrous sulfate to hematite is not complete, there is no acid production to balance the initial consumption.

5.1.2 Final iron in solution

The following graph shows the relationship between final ferric concentration in solution and final free acidity (Figure 5.2). At high free acid concentration, more iron remains in solution. High sulfuric acid levels are promoting precipitation of BIS and jarosites, two species which have lower iron content than hematite. Consequently, more ferric is remaining in solution at high acidity.

At the point of initial sulfuric concentration of 40g/L, a breaking point in the curve is seen. Above this point, BIS is the main phase (see Figure 5.3). Below this point, BIS content in the precipitate gradually increase from 0 to 90%. The other stable phase is hematite. These observations correlate previous publications [21], [39].

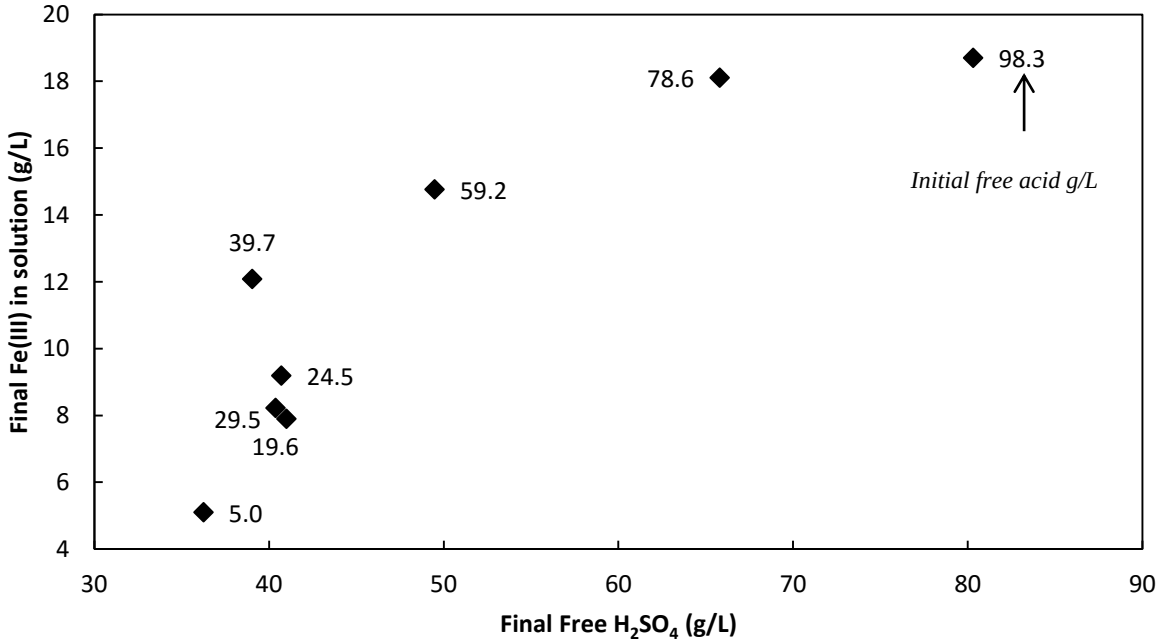

Figure 5.2: Relationship between final ferric and free sulfuric acid concentrations
The numbers by the data points are the initial free acid concentration in g/L.

5.1.3 Residue characterization

The residue characterization by XRD and Leco is presented in this paragraph. The percentage of hematite in the residue gradually decreases with increasing initial free acid concentration. In parallel, the BIS content increases. Some hydronium jarosite has been detected in one of the samples.

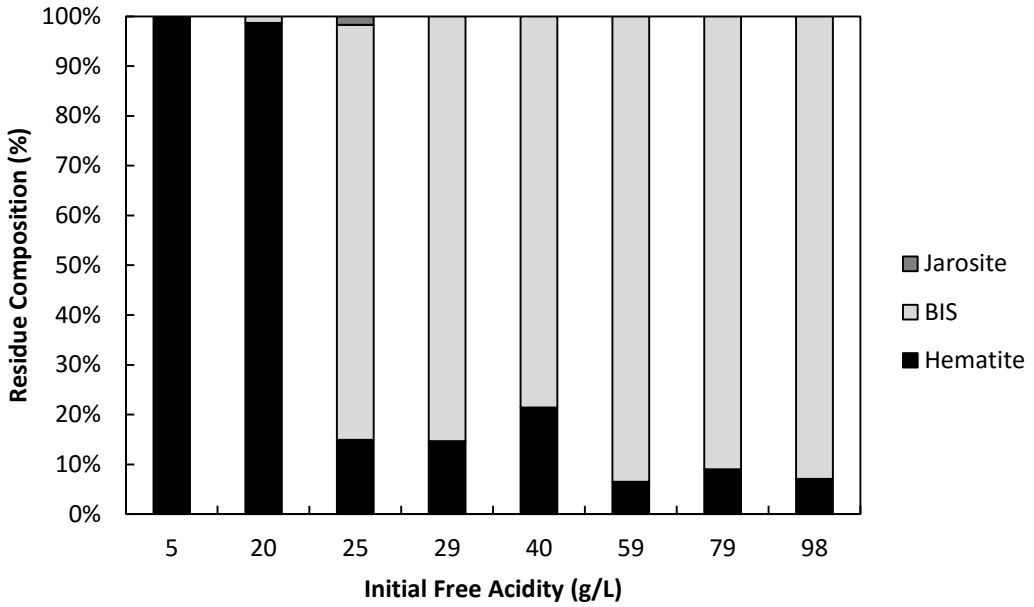

Figure 5.3: Effect of free acidity on residue composition

Figure 5.4 shows the relationship between the sulfur content in the residue and final sulfuric acid concentration. It is correlated to the composition of the residue: a net increase above 41g/L initial free acidity marks the limit for BIS precipitation.

By comparing XRD patterns, Javed et al. observed that increasing sulfuric acid concentration is negatively influencing hematite crystallinity [40]. For this project, at constant copper and iron concentration, increasing free acidity readily forms BIS or jarosite in the residue. Only one sample yielded 100% hematite, thus it was not possible to compare a significant number of patterns.

XRD patterns for hematite, BIS and a mixture of jarosite-hematite are presented in figures 5.5 and 5.6.

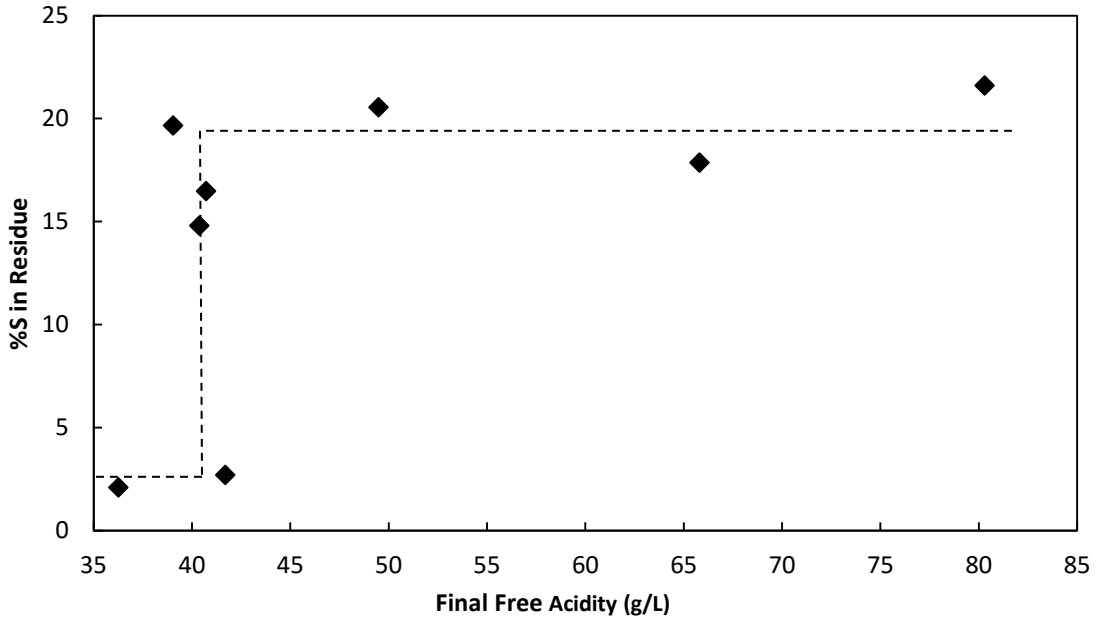

Figure 5.4: Relation between sulfur content in residues and free sulfuric acid concentration

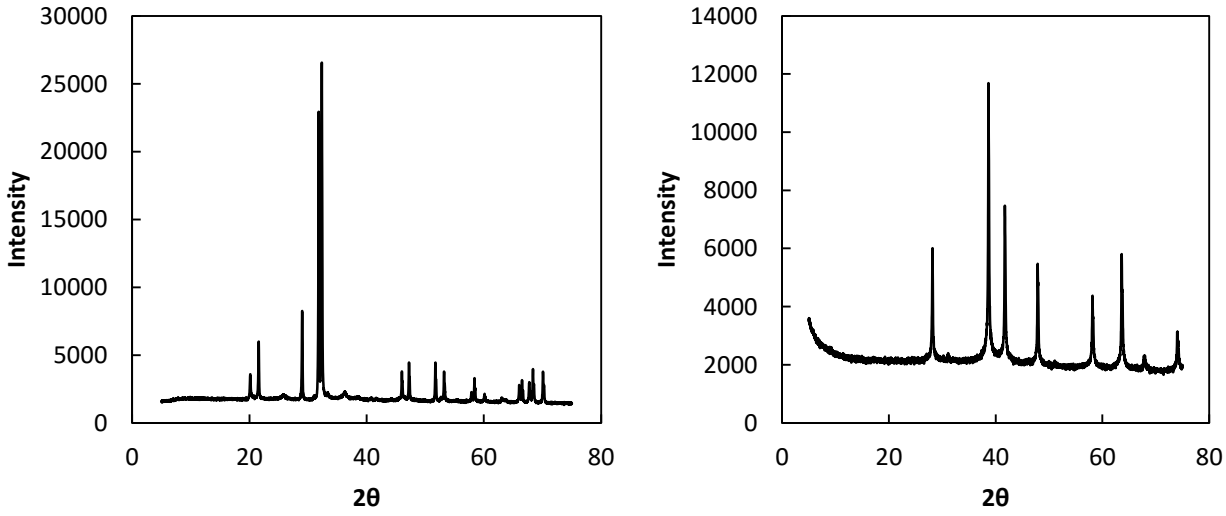

Figure 5.5: Typical XRD patterns for hematite (left) and BIS (right)

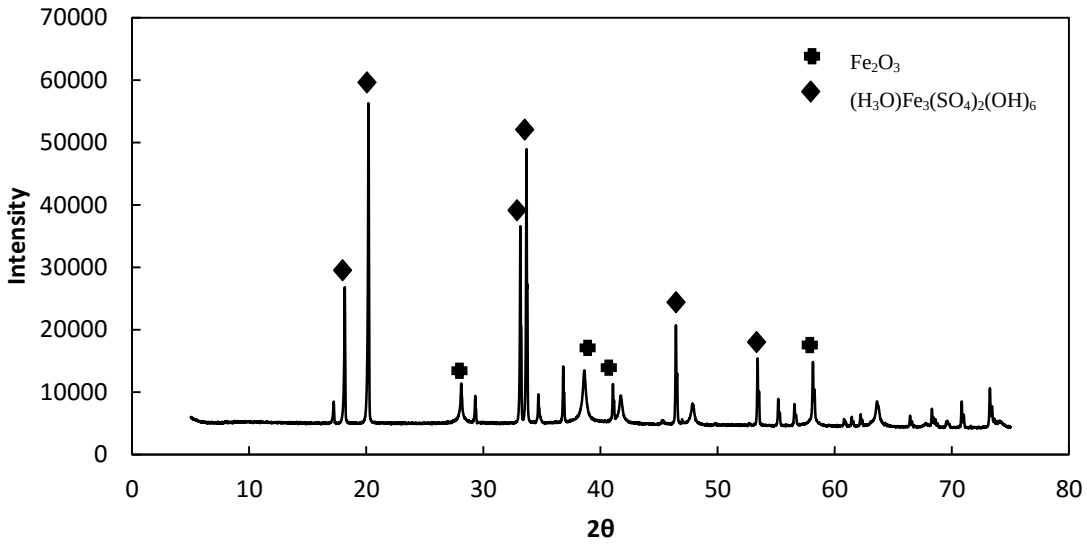

Figure 5.6: XRD pattern for a mixture of hydronium jarosite – hematite

5.2 Effect of copper sulfate

Using the same initial matrices composition (in terms of Fe(II) and H_2SO_4 concentrations), copper sulfate was increasingly added in the system.

5.2.1 Free Acidity

Figure 5.7 shows the influence of copper sulfate on final free acidity. Three initial free acidity compositions were investigated: 20g/L, 40g/L and 60g/L, as they were respectively expected to yield hematite, a mixture, and BIS. In presence of copper sulfate, the amount of acid produced increases. At high copper sulfate concentration (63.5g/L Cu), the limit is shifted up to point where there is no acid consumption at 60g/L initial free acid.

5.2.2 Final iron in solution

The effect of copper sulfate on final iron remaining in solution is presented in figure 5.8. The breaking point in the curve is observed for copper concentrations below 25.4g/L (appearance of BIS in the residue). At 38.1g/L and above, there is no visual shift and final free acidity steadily increases. This correlates well to the residue composition: there is no BIS in the samples prepared from “intermediate” free acidity solutions. From figure 5.8, it can also be seen that copper sulfate helps decreasing the iron left in solution only at low initial sulfuric concentration.

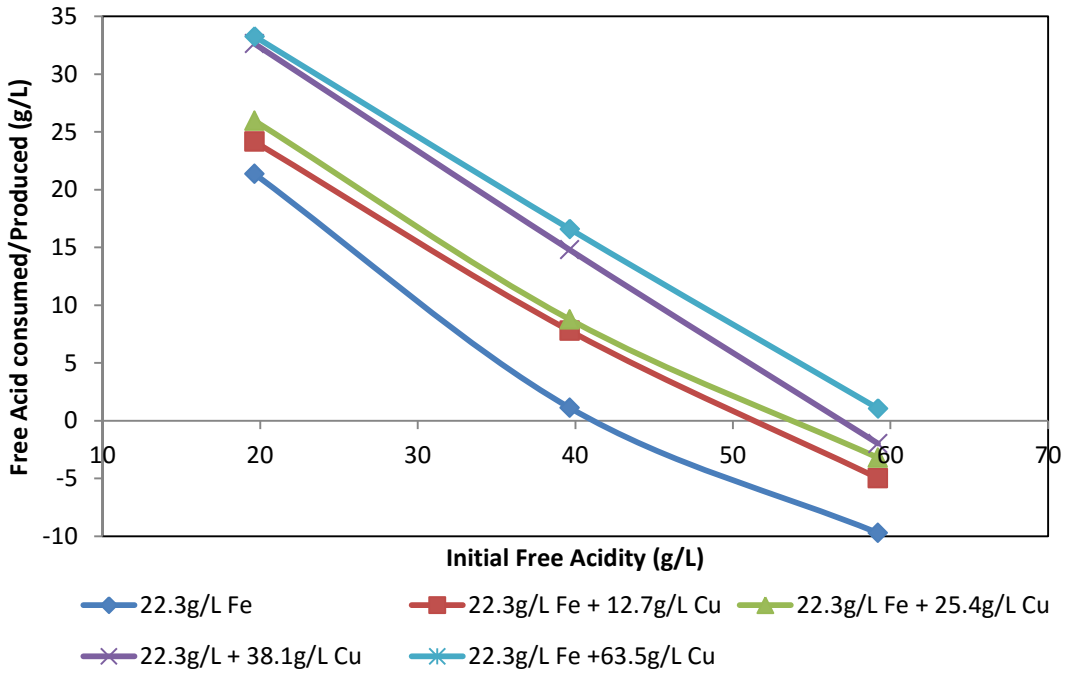

Figure 5.7: Free acid consumed/produced in presence of copper sulfate

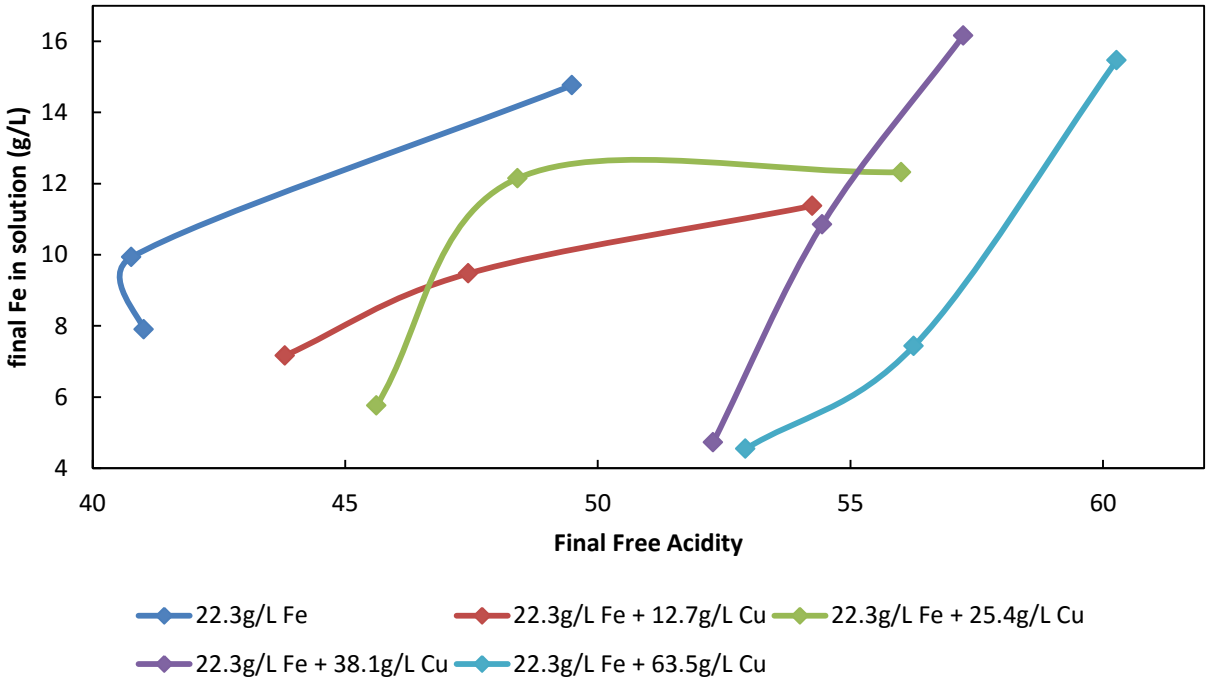

Figure 5.8: Relation between final ferric and free sulfuric acid concentrations in presence of copper sulfate

5.2.3 Final copper in solution

Figure 5.9 presents the concentration of copper in the rinse solution with increasing final free acidity and various initial copper contents. Above a limit of approximately 53g/L H_2SO_4, copper concentration increases in the rinse solution. There obviously is an effect of the initial copper concentration on the copper remaining in the rinse. But free acidity seems to have an influence as well since batches with same initial copper content show different final copper concentrations.

Copper sulfate solubility is influenced by the amount of free sulfate ions in solution (Equation 5.1). Higher sulfuric acid concentration means more sulfate ions are available. The solubility of copper sulfate can be decreased to the point where some copper sulfate precipitates along with hematite/BIS. When the residue is washed with distilled water, copper sulfate dissolves and is transferred to the rinse solution.

$$CuSO_4 = Cu^{2+} + SO_4^{2-} \qquad \text{(Equation 5.1)}$$

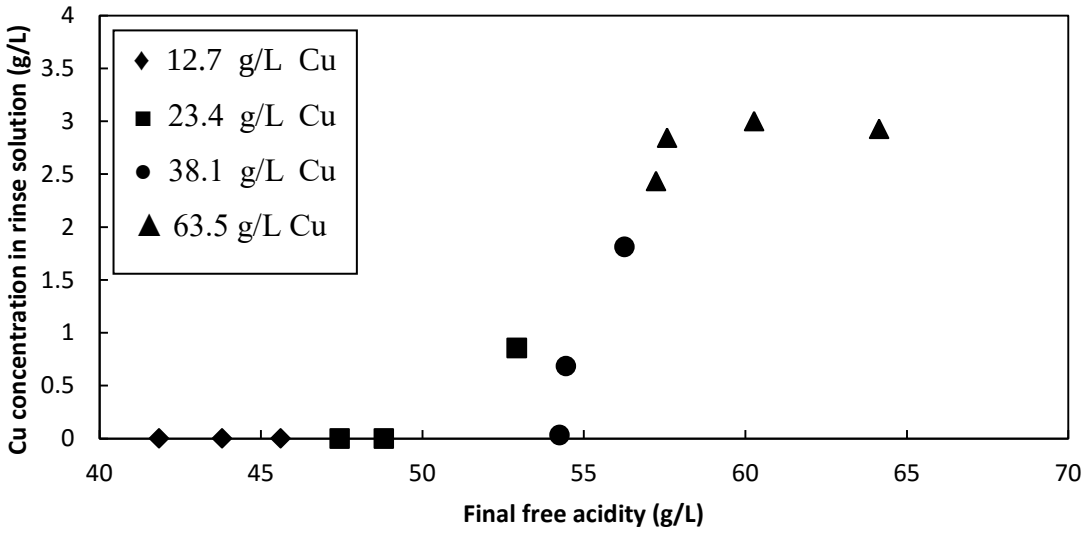

Figure 5.9: Influence of free acidity on copper concentration in the rinse solution

5.2.4 Residue characterization

Copper sulfate influences the residue composition by hindering the formation of BIS, as shown in figure 5.10. Looking at the sulfur content as a function of acidity, it is seen that copper sulfate shift upwards the free acidity limit for hematite vs. BIS precipitation (Figure 5.11 and

table 5.1). This is related to the buffer effect of sulfates in solution, decreasing the acidity, and thus promoting hematite precipitation (paragraph 3.4).

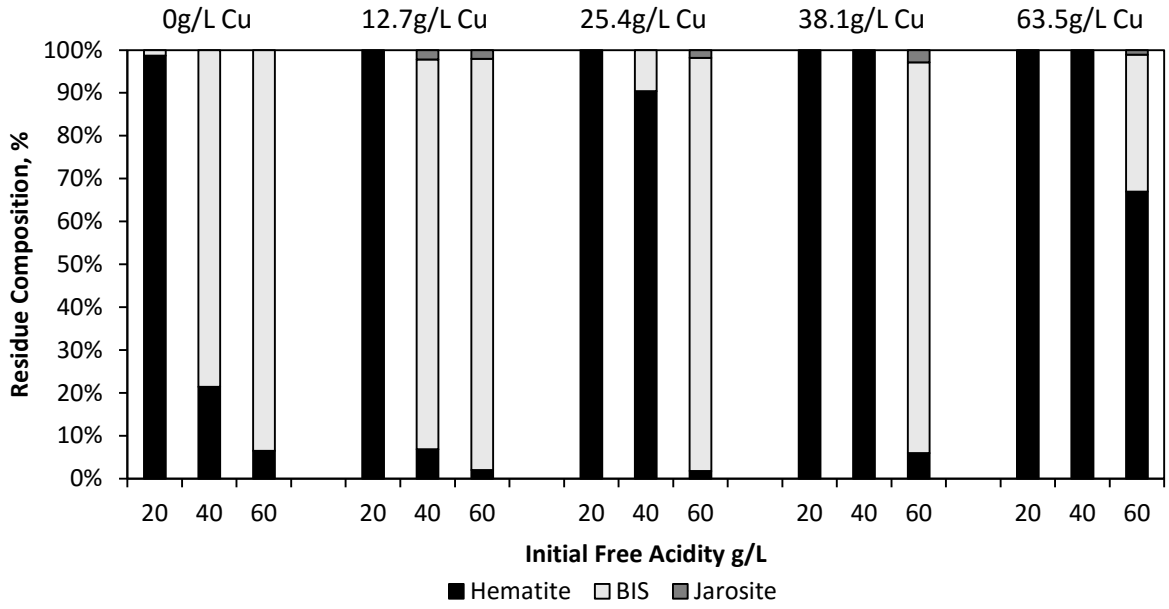

Figure 5.10: Effect of copper sulfate on residue composition

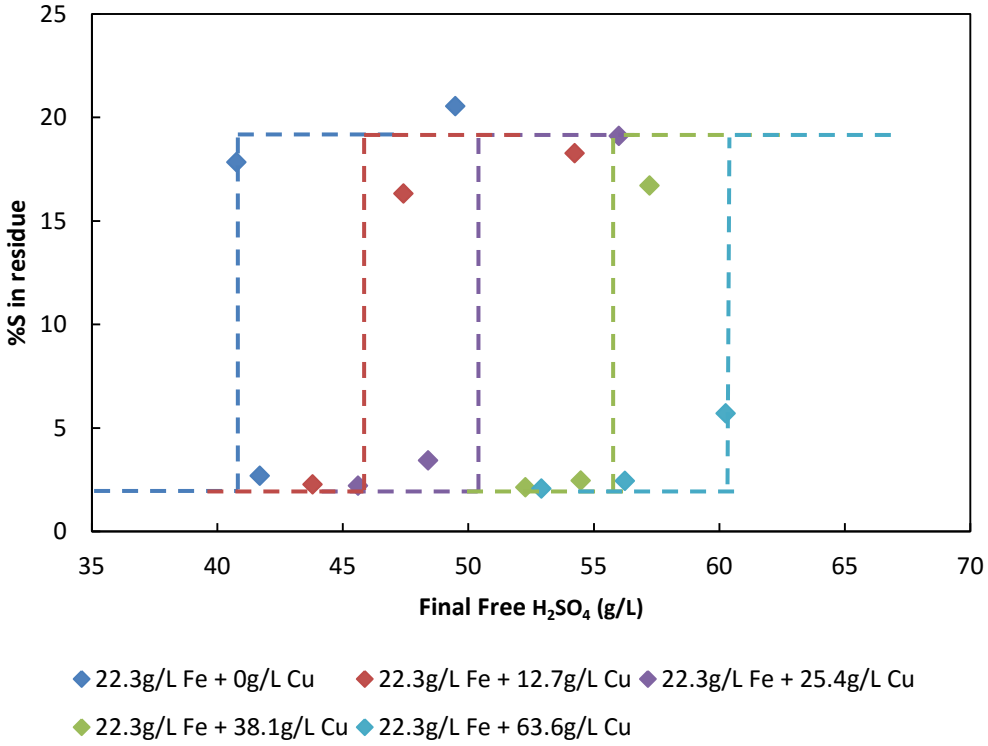

Figure 5.11: Relation between sulfur content in residues and free sulfuric acid concentration

Table 5.1: Influence of copper sulfate on free acidity upper limit for hematite precipitation

Initial [Cu]	0g/L Cu	12.7g/L Cu	25.4g/L Cu	38.1g/L Cu	63.6g/L Cu
Limit [Free Acid]	41 g/L	46 g/L	50.5g/L	56 g/L	>61g/L

As mentioned in paragraph 3.5., three initial free acidity conditions were tested. At 20g/L initial free acid and [Cu]>12.7g/L, the residue produced is 100% hematite. The XRD patterns of these samples were compared in order to assess a potential influence of copper sulfate on hematite crystallinity (see appendix C). Residues precipitated from high copper sulfate solutions seem to be better crystallized (sharper peaks). This observation needs to be taken with caution and would need to be confirmed with additional testing.

5.3 Effect of increasing iron concentration

In this third phase, 3 batches of three different initial iron compositions were tested:

- Batch A: 83.4g $FeSO_4$ i.e. $[Fe(II)]_{initial}$ = 16.7g/L
- Batch B: 111.2g $FeSO_4$ i.e. $[Fe(II)]_{initial}$ = 22.3g/L
- Batch C: 152.9g $FeSO_4$ i.e. $[Fe(II)]_{initial}$ = 30.7g/L

For each batch, three different copper concentrations (0, 12.7 and 38.1 g/L) and three different sulfuric acid concentrations were tested (20, 40 and 60g/L).

5.3.1 Free Acidity

Free acid generation/consumption in function of initial free acidity is presented in figure 5.12. The same previously reported trend is observed for batch A, B and C:

- low initial free acidity is correlated to the highest acid production (>15g/L)
- high initial free acidity is correlated to acid consumption
- intermediary initial free acidity leads to acid production or consumption depending on the copper sulfate concentration in the system

Increasing the initial iron concentration in solution yielded unclear results. One could expect an increase in acid production because more iron is available for hydrolysis. It cannot be confirmed here since batch B sulfuric acid concentrations are higher than batch C.

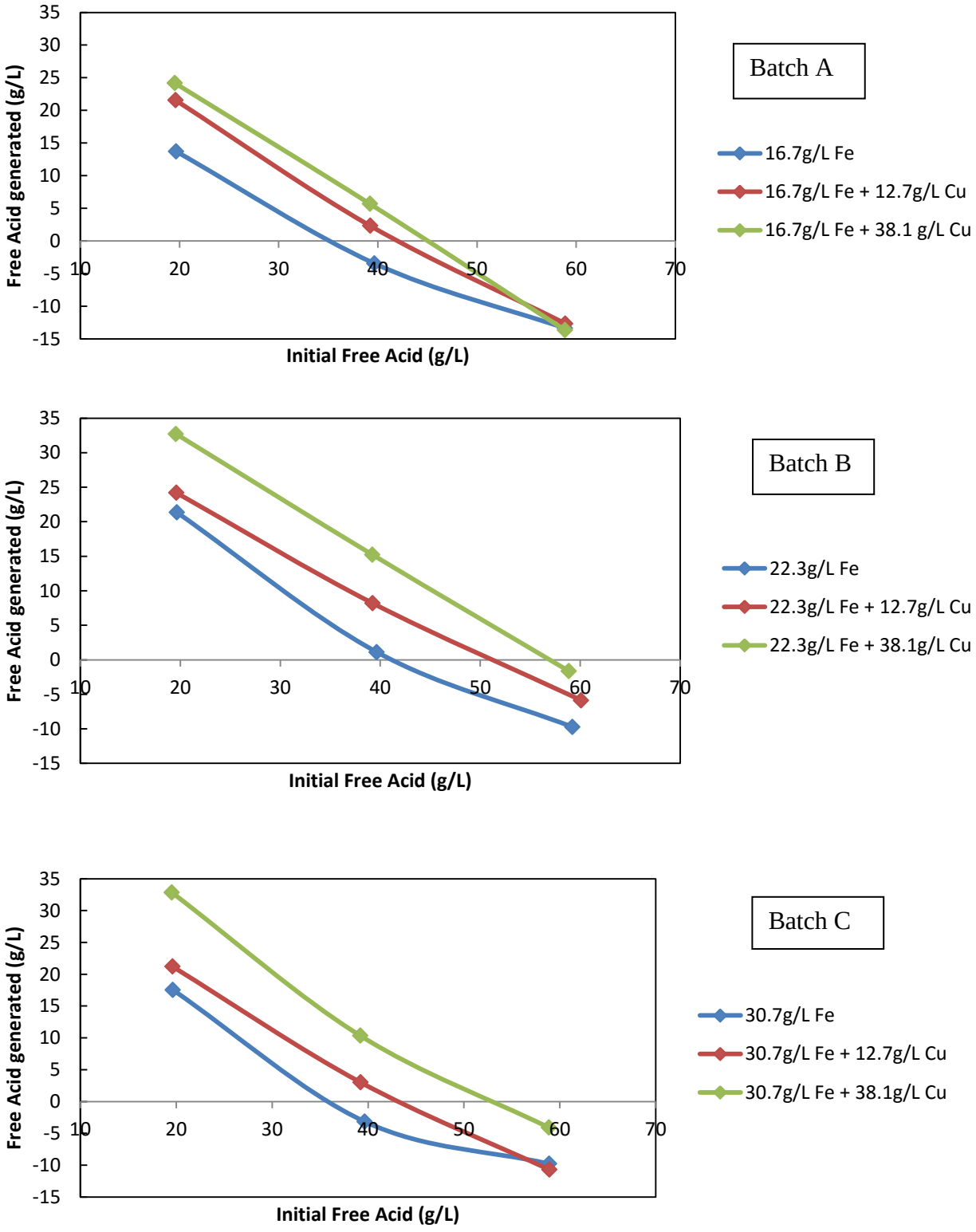

Figure 5.12: Influence of varying initial Fe concentration on free acid consumed/produced

5.3.2 Final iron in solution

The three graphs in figure 5.13 illustrate the final amount of iron left in solution over free acidity. It shows that:

- An increasing copper sulfate concentration is associated with a decrease in the final free acid content. As a result, more iron precipitates out of solution when copper is present.
- It is unclear how initial iron concentration is influencing the conversion % to hematite.

For batch A and B, there is no (or very little) shift in the curve at high copper sulfate concentrations. This is related to hematite being the main component in the residue under these conditions.

For Batch C, it is unclear why the concentration of iron remaining in solution is higher at intermediate initial free acidity. The corresponding residues do not show high amounts of BIS which could have explained such pattern.

5.3.3 Final copper in solution

Figure 5.14 compares the concentration of copper in the rinse solution for batch A, B and C. Again, because of sulfate concentration, higher free acidity is related to greater amount of copper in the rinse solution.

Less data was available to analyze batch A and C. As a result, the observations made for these two batches must be analyzed with caution. One could expect that increasing iron concentration would lower the solubility of copper sulfate and thus increase the amount of copper in the rinse solution for batch C. It is not the case since batch A shows higher levels of residual copper in the rinse solution than B and C. The rinsing step was overall consistent, but some small variations in the volume of DI used to rinse the precipitates might explain these results.

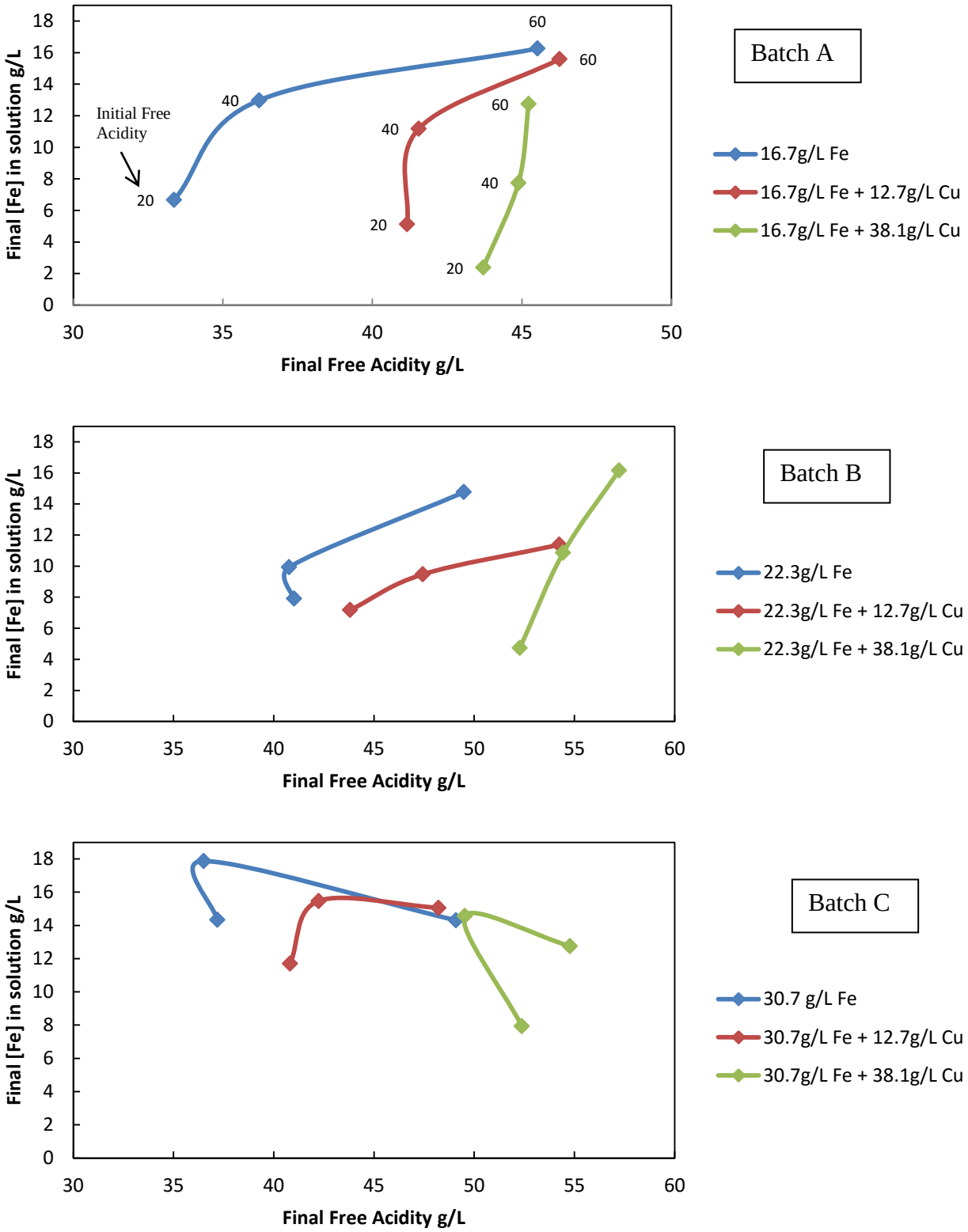

Figure 5.13: Relation between concentration of ferric remaining in solution and final free acidity in presence and absence of copper sulfate

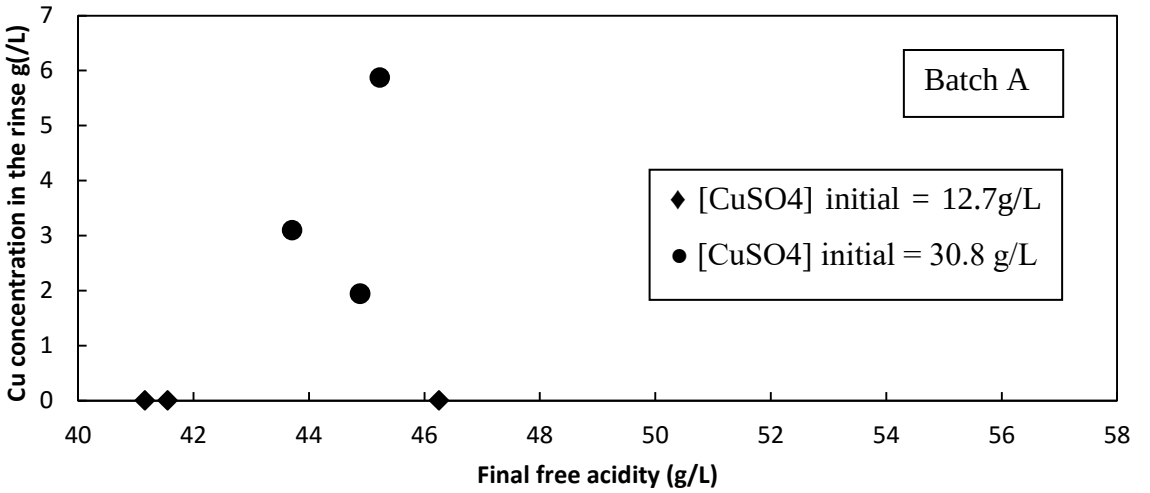

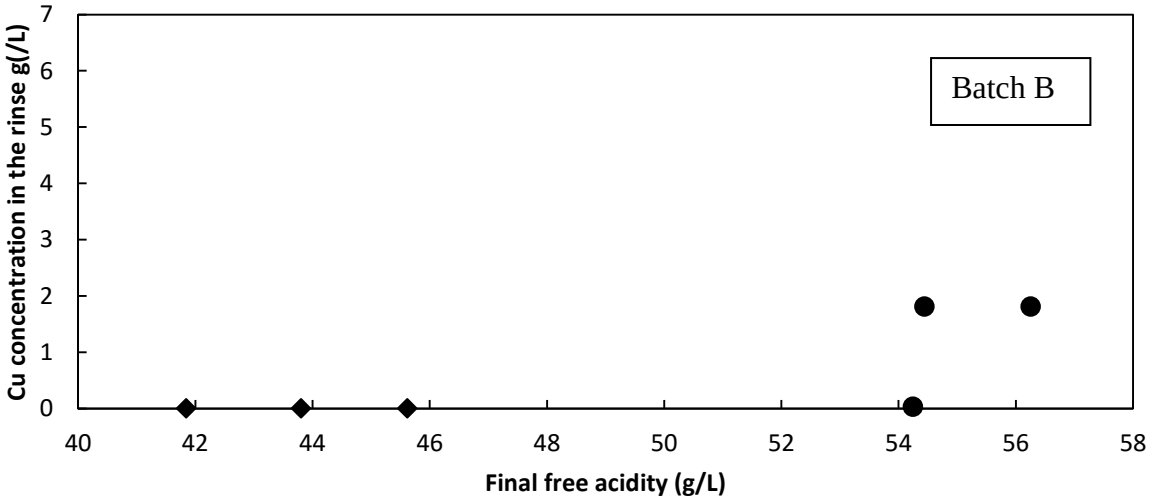

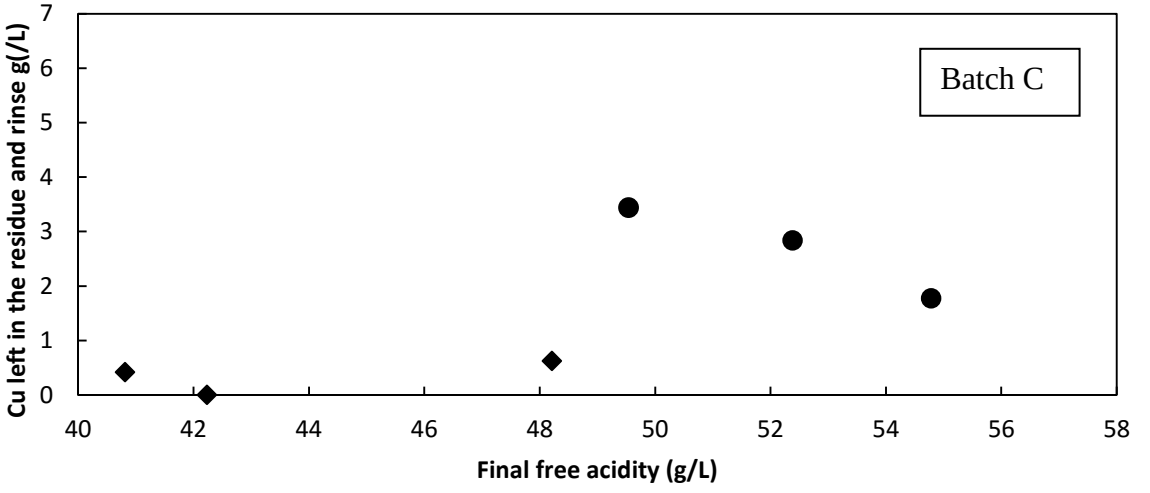

Figure 5.14: Influence of free acidity on copper concentration in the rinse solution

5.3.4 Residue characterization

Figure 5.15 compares the effect of copper sulfate on residue composition for batch A, B and C. As noticed in paragraph 5.2, copper sulfate hinders the formation of BIS and jarosite.

The following observations are made for the influence of iron concentration:

- The proportion of hydronium jarosite in the residue decreases with increasing iron concentration. No jarosite was detected in batch C
- When no copper sulfate is added in the initial solution, the influence of iron sulfate concentration is unclear
- When copper sulfate is present, batch B and C show similar trends. However, batch A has much lower BIS content, indicating that low initial iron concentration hinders BIS formation

Plotting the sulfur content in the residue against final free acidity shows the limit for BIS formation (Figure 5.16). Table 5.2 summarizes the influence of initial iron concentration on this limit.

Table 5.2: Upper free acidity limit for the precipitation of hematite

Initial Fe	0g/L Cu	12.7g/L Cu	38.1g/L Cu
Batch A - 16.7 g/L	35 g/L	38 g/L	> 45 g/L
Batch B - 22.3 g/L	41 g/L	46g/L	56 g/L
Batch C - 30.7 g/L	37 g/L	42 g/L	54 g/L

Each limit was defined with only three points, which led to a probable error of ±2g/L. When the residue formed at high free acidity did not yield BIS, the limit was considered to be above the highest point measured. As seen earlier, copper sulfate shifts upward the limit free acid concentration for the precipitation of BIS.

When increasing the iron content in the leach solution from 16.7 to 22.3g/L, the free acid limit is moved forward. At 30.7g/L, it moves back to a slightly lower value. Thus batch B shows an optimum iron concentration to shift up the free acidity limit. There is no clear correlation between figures 5.14 et 5.15 to make a definitive conclusion on the effect of iron concentration.

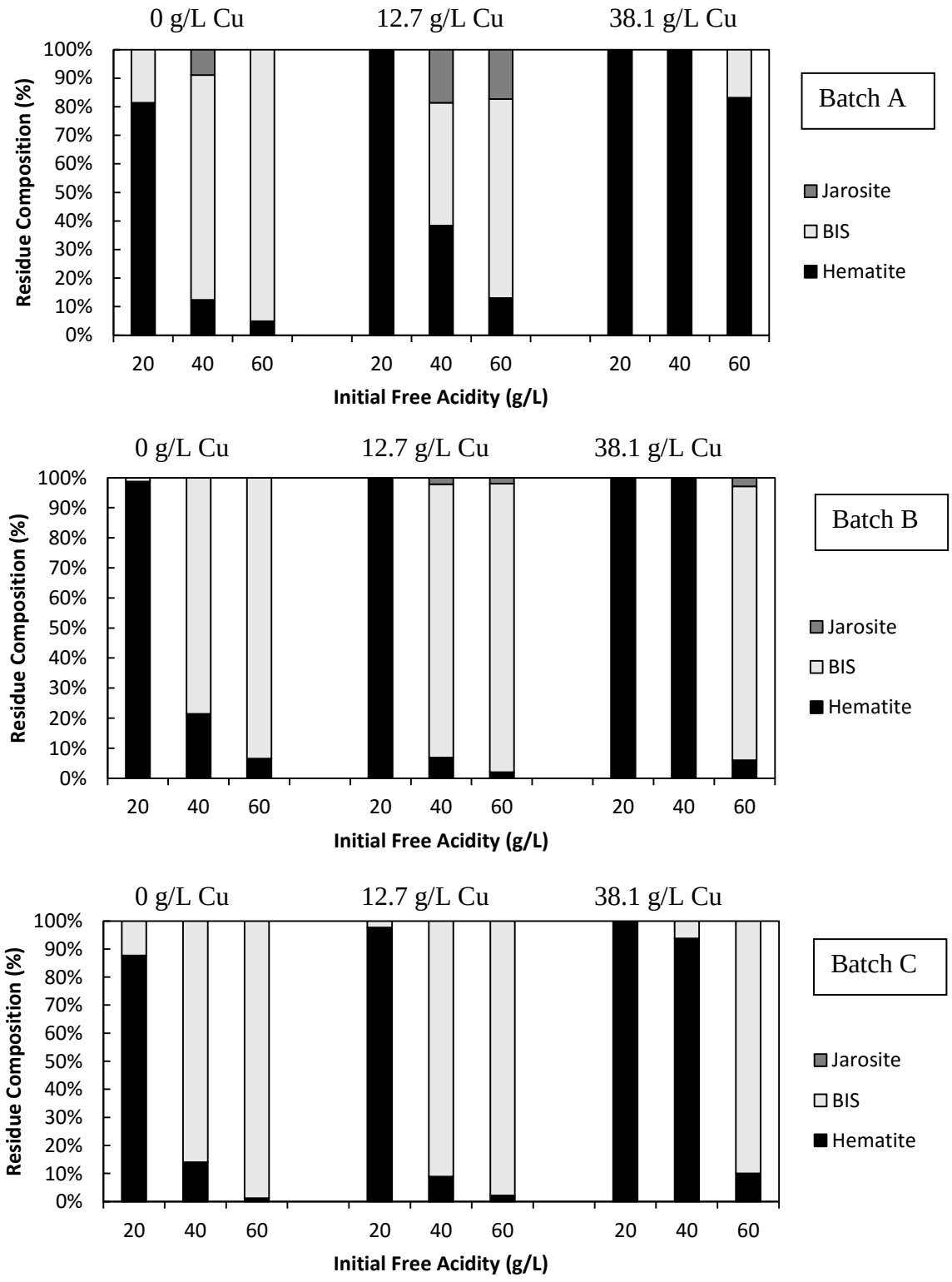

Figure 5.15: Influence of initial iron concentration on residue composition

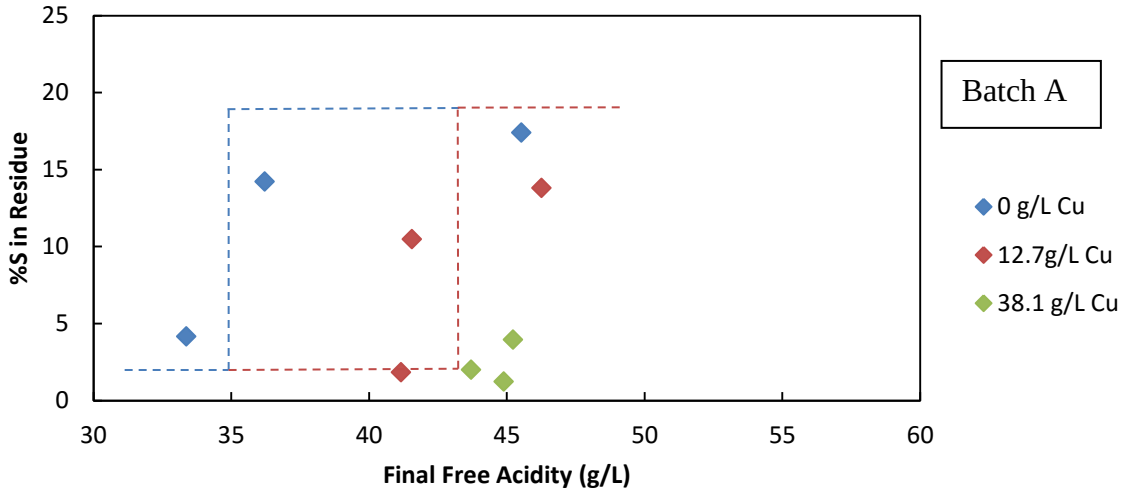

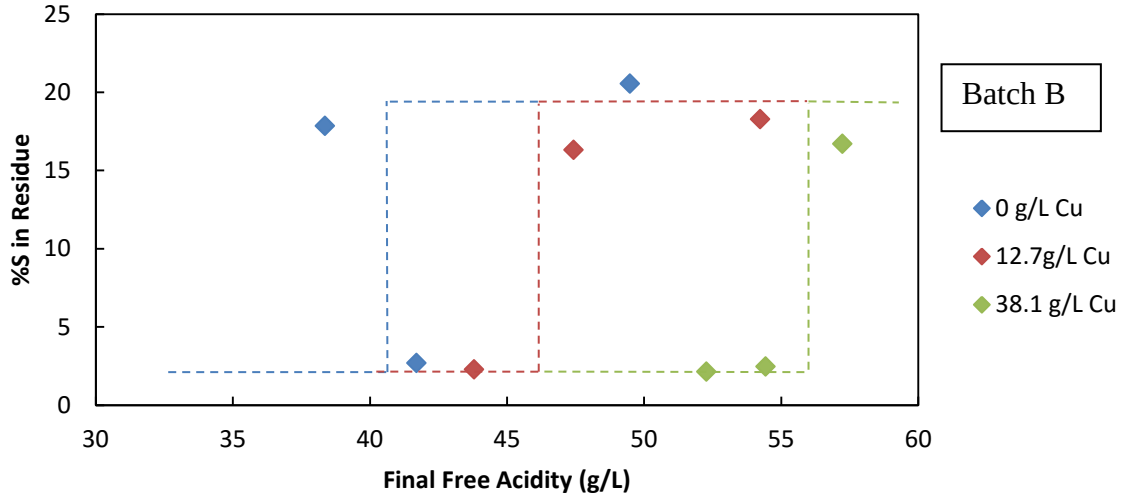

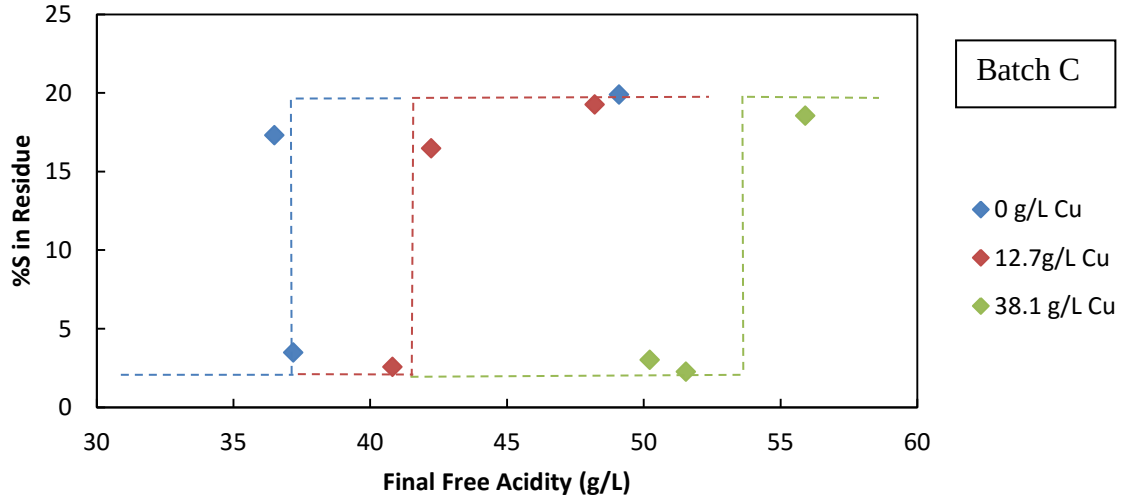

Figure 5.16: Relation between sulfur content in residues and free sulfuric acid concentration

XRD patterns of 100% hematite samples were also compared. No clear trend could be identified for the effect of initial iron concentration on the residue crystallinity.

5.4 Effect of initial iron oxidation state

In this section, the effect of initial oxidation state of iron on the system is investigated.

5.4.1 Ferrous ion titration

Following the process presented in appendix D, the remaining ferrous iron was titrated in the cooled solutions right after leaching (Table 5.4). All the solutions were initially composed of 22.3g/L iron and 25.4g/L copper.

Table 5.3 Ferrous iron titration data

	Initial H_2SO_4 (g/L)	Fe(II) titrated in final solution (g/L)	Fe(III) in final solution (g/L)	%Fe(II) not oxidized from initial
Initial	20	0.25	7.5	1.12
Iron:	40	0.25	11.2	1.12
Fe(II)	60	0.2	13.5	0.9
Initial	20	0.05	15.3	-
Iron:	40	0.025	17.1	-
Fe(III)	60	0.05	21.3	-

When titrating the solution prepared from ferric sulfate, a color change happened after two or three drops added. Because leaching takes place in an oxidative environment, the possibility for ferrous ions to be in solution is null. Thus the residual potassium dichromate added before saturation of the solution (<0.05g/L) was not accounted for. Instead, a ±0.05g/L error on ferrous titration was considered.

Titration of the solutions prepared with ferrous iron revealed that a very little portion of the total iron was not oxidized (1% or less). As a result, it was considered that all the iron originally dissolved in solution was available for hematite or BIS precipitation.

5.4.2 Free Acidity

At low and intermediate initial free acidity, liquors prepared from ferric sulfate produced less free acid than liquors prepared from ferrous sulfate (Figure 5.16). When using ferric sulfate, the first oxidation reaction does not take place (Equation 3.3). Yet, this reaction consumes most free acid in solution. The resulting large excess of free acid in solution hinders hematite precipitation and as a result sulfuric acid production. At 60g/L initial free acidity, when BIS are stable, there is no acid consumption. Because of high sulfuric concentration in solution, acid consumption has stabilized.

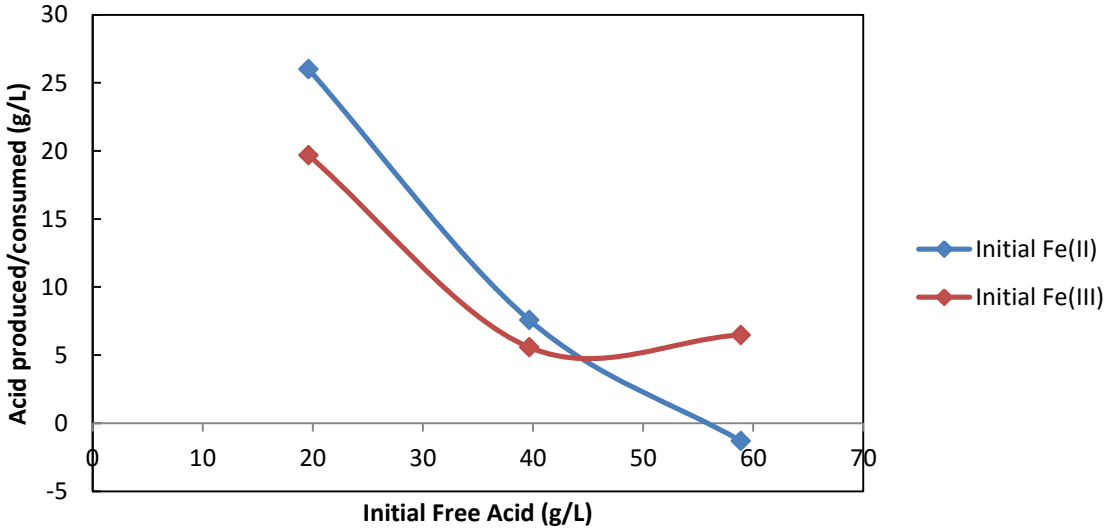

Figure 5.17: Comparison of free acid consumed/produced after leaching of ferric and ferrous sulfate solutions

5.4.3 Final iron in solution

Comparison between solutions prepared with ferric or ferrous iron in terms of final iron concentration is shown in figure 5.18. Ferric iron yielded much less residue than ferrous iron. Additionally, the characteristic curve shift related to BIS formation is not seen when using ferric iron.

This increase in ferric iron remaining in solution can be explained by the excess of free acid. Hydrolysis reactions for BIS and hematite precipitation produce sulfuric acid. Thus, at higher concentrations, the hydrolysis reactions are shifted backwards.

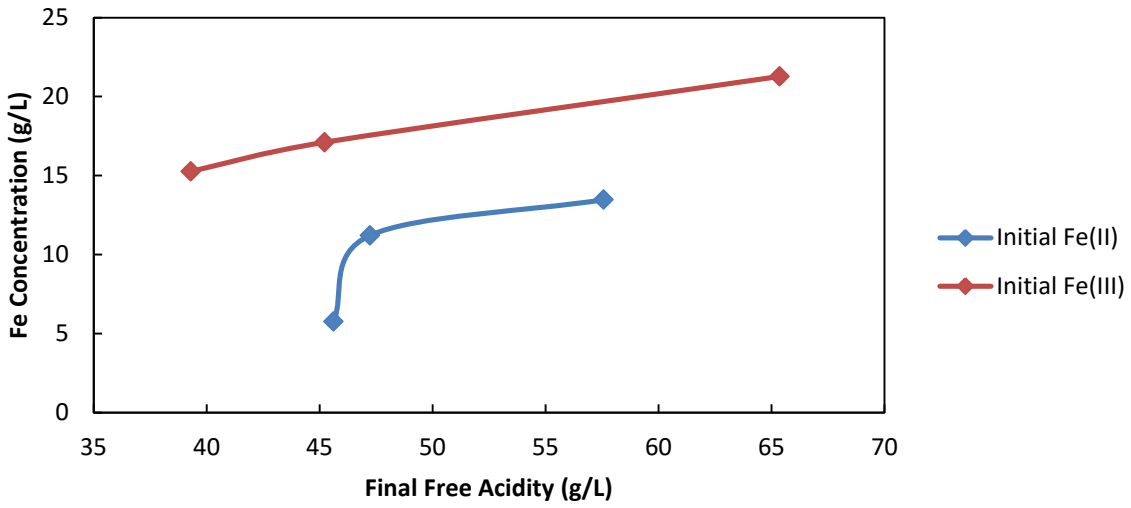

Figure 5.18: Comparison of final iron concentration in solution after leaching of ferric and ferrous sulfate solutions

5.4.4 Final copper in solution

Figure 5.19 compares the amount of copper in the rinse solution when using ferric or ferrous iron sulfate. No specific trend can be inferred from the few graph points. However, the solutions leached at intermediary initial free acidity show an unexpectedly high copper concentration in the rinse solution.

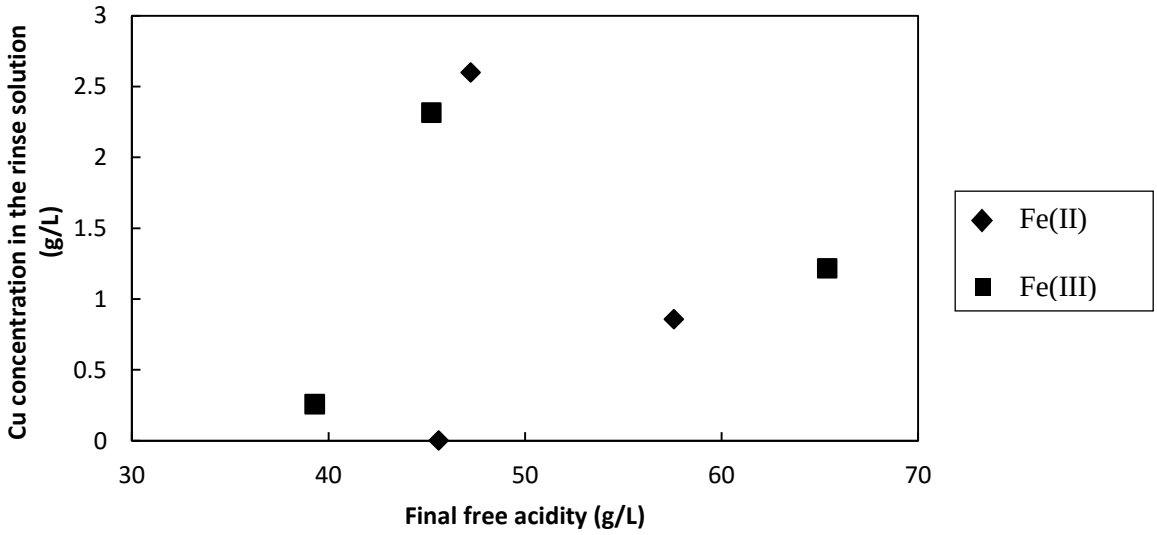

Figure 5.19: Influence of free acidity on copper concentration in the rinse solution

5.4.5 Residue characterization

Figure 5.20 compares the residue composition of solutions prepared with ferrous or ferric sulfate. The following observations can be made:

- For solution prepared from ferrous sulfate, increasing the initial free acid concentration promotes the formation of BIS
- Residues from solutions prepared from ferric sulfate do not seem to be influenced by the initial free acid concentration
- No specific trend explains the episodic formation of jarosite in the residue

The results for the batch prepared from ferric sulfate suggest that the free acidity limit for precipitation of BIS is already reached at 20g/L.

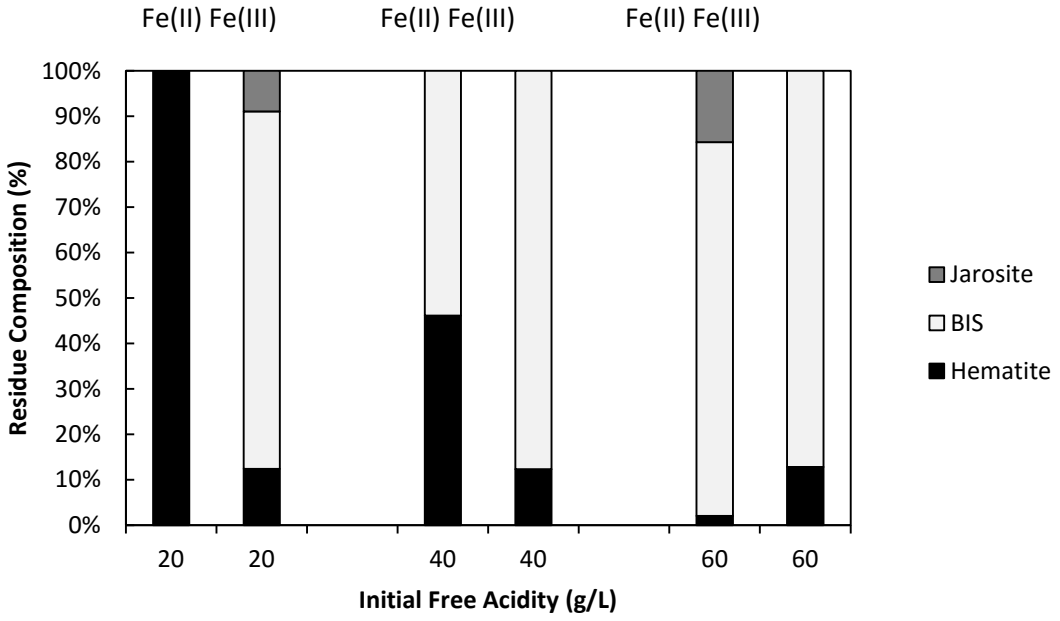

Figure 5.20: Effect of iron oxidation state on residue composition

When looking at the sulfur content in the residues (Figure 5.21), the limit free acidity is logically higher in the ferrous sulfate case where the system is not saturated by sulfate ions. The lower limit is unclear for the Fe(III) solutions since none of the residues majority yielded BIS. It was set at 41 g/L or lower (Table 5.4).

Table 5.4: Free acidity limit for the precipitation of BIS

Initial Fe	Fe(II)	Fe(III)
Free Acid Limit	50.5 g/L	<41 g/L

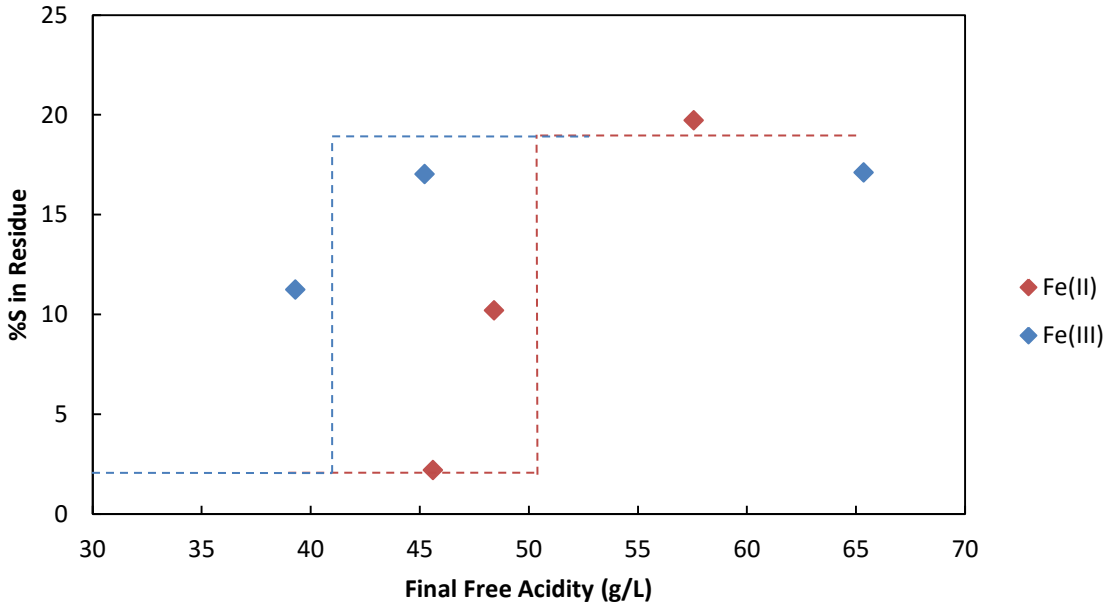

Figure 5.21: Relation between sulfur content in residues and free sulfuric acid concentration

5.4.6 Discussion

The previous results were presented in terms of free acidity. This choice was made since the literature review and the results obtained in paragraph 5.1 indicated that free acidity is the main factor influencing the precipitation. In this specific case, at equal initial iron concentrations, the ratio Fe:S is quite different when preparing a solution from ferric sulfate or ferrous sulfate. It becomes more difficult to compare tests which molar ratios are very unalike. As a result, the effect of iron oxidation state on the residue chemistry must be confirmed by leaching solutions with similar molar ratios before making a definitive conclusion.

5.5 Stat-Ease model

Design-Expert® by Stat-Ease® is a software providing statistical modelling on design of experiment (DOE) for process development optimization. In this project, it was used to generate a prediction of the system's behavior. Two different analyses were performed.

A first approach consisted in using a regular two-level factorial design. Two-Level factorial design is useful for estimating main effects and interactions. The second approach consisted in using a general factorial design, which allowed analyzing three factors, with three levels for each of them. The factors analyzed where [$FeSO_4$], [$CuSO_4$] and [H_2SO_4]. The response factor analyzed was %BIS (=%$FeOHSO_4$ + %$(H_3O)Fe_3(SO_4)_2(OH)_6$) in the residue. A model separating BIS and jarosite as response factors was produced, but was not conclusive.

More details about Stat-Ease® plots interpretations can be found in appendix F.

5.5.1 First approach

Table 5.5 presents the factors and levels used. The model is performed based on the extreme values for each factor. A two-level design using three factors gave 8 runs.

Table 5.5: Factorial DOE – first approach

	Factor 1	Factor 2	Factor 3	Response 1
Run	A:[FeSO4] g/l	B:[CuSO4] g/l	C:[H2SO4] g/l	%BIS
1	83.40	0.00	20.00	18.6
2	152.93	0.00	20.00	12.3
3	83.40	150.08	60.00	16.8
4	152.93	150.08	20.00	0
5	152.93	150.08	60.00	90
6	152.93	0.00	60.00	98.8
7	83.40	0.00	60.00	95.1
8	83.40	150.08	20.00	0

According to the Box-Cox Plot recommendations, a square root transform was used. The Half-Normal Plot (Figure 5.22) and Pareto Chat (Figure 5.23) determined that [$CuSO_4$] and [H_2SO_4] had the most effect on the %BIS.

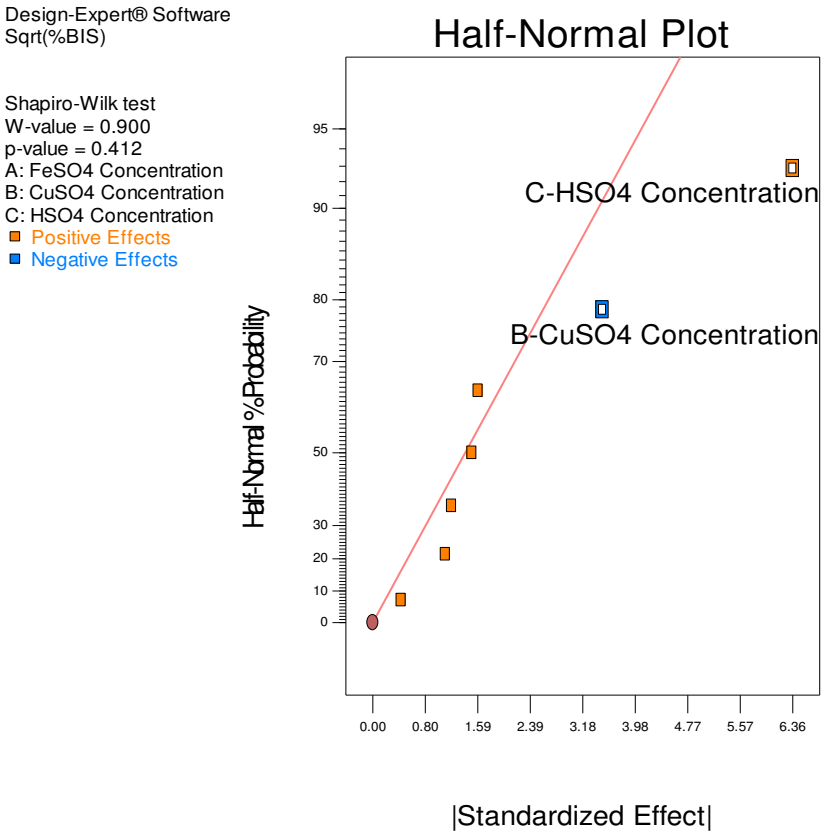

Figure 5.22: Half-Normal Plot – First approach

Following on, the ANOVA analysis (analysis of the variance) validated the model and calculated a final equation in terms of actual factors (Equation 5.2). This equation can be used to make predictions about the response for given levels of each factor.

Table 5.6: ANOVA for selected factorial model – First approach

Source	Sum of Squares	df	Mean Square	F Value	p-value Prob > F	
Model	105.25	2	52.63	17.28	0.0057	significant
B-CuSO4 Concentration	*24.24*	*1*	*24.24*	*7.96*	*0.0370*	
C-HSO4 Concentration	*81.01*	*1*	*81.01*	*26.60*	*0.0036*	
Residual	15.22	5	3.04			
Cor Total	120.48	7				

$$\text{Sqrt(\%BIS)} = 0.51355 - 0.023197*[CuSO_4] + 0.15911*[H_2SO_4] \qquad \text{(Equation 5.2)}$$

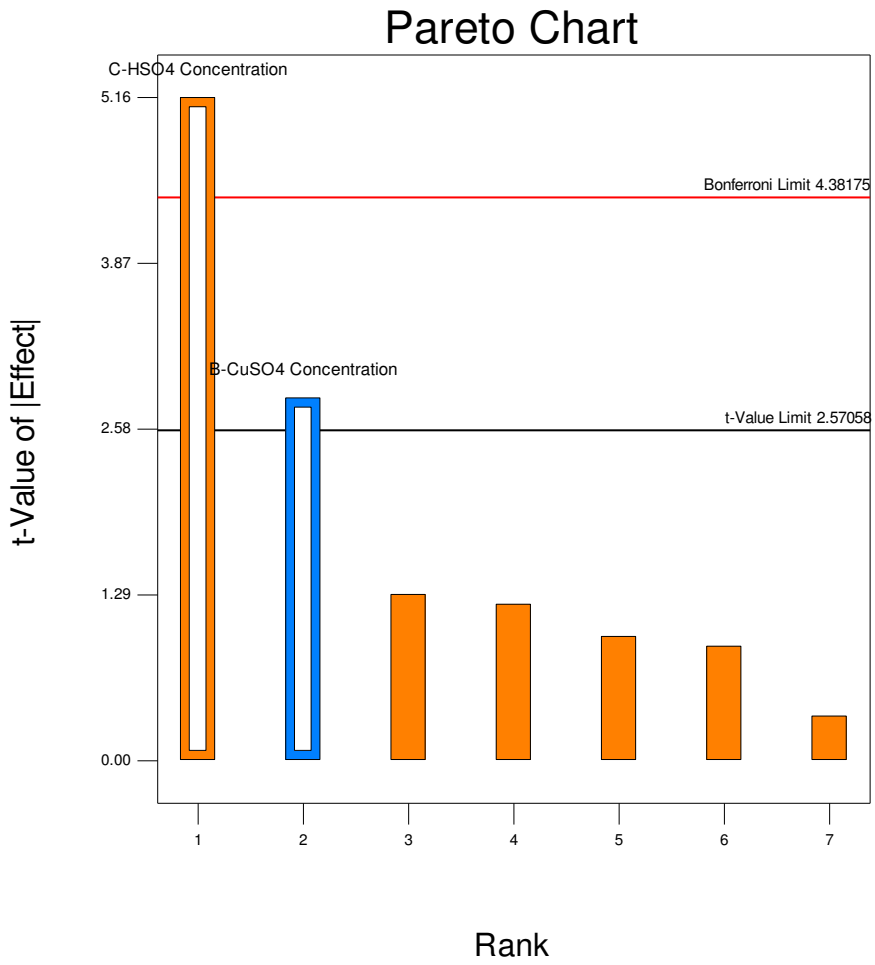

Figure 5.23: Pareto Chart – First approach

As recommended by the software, diagnostic plots where used to assess the viability of the model. Even though not enough points were available to extremely accurately predict the response, the major trends shown by the 3D surface plot (Figure 5.24) explain the response factor behavior. Varying [$FeSO_4$] does not change the appearance of the surface, correlating the observation made that initial ferric concentration has little impact on the residue composition.

Sulfuric acid has the most positive impact on %BIS, while copper sulfate negatively influences its value. The combination of the two factors did not improve the model.

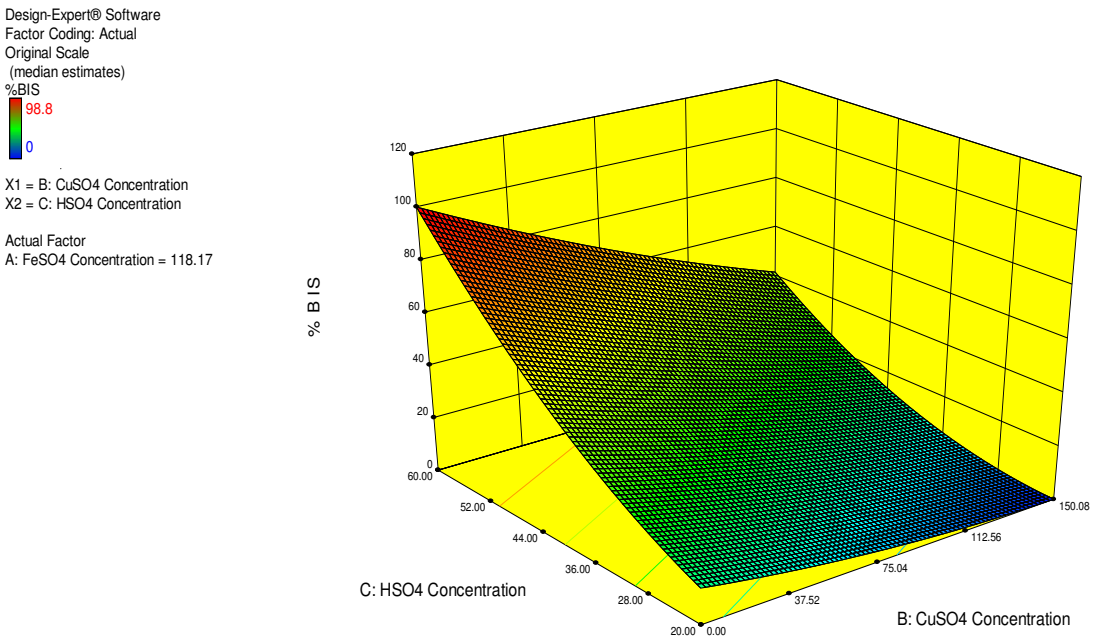

Figure 5.24: 3D surface model – First approach

5.5.2 Second approach

Because of the evident lack of intermediate values in the previous model, a better estimation was attempted with 26 data points (Table 5.7). According to the Box-Cox Plot recommendations, a square root transform was used. The Half-Normal Plot (Figure 5.25) showed that [$CuSO_4$], [H_2SO_4], and the combination [$CuSO_4$]/[H_2SO_4] had the most effect on the %BIS.

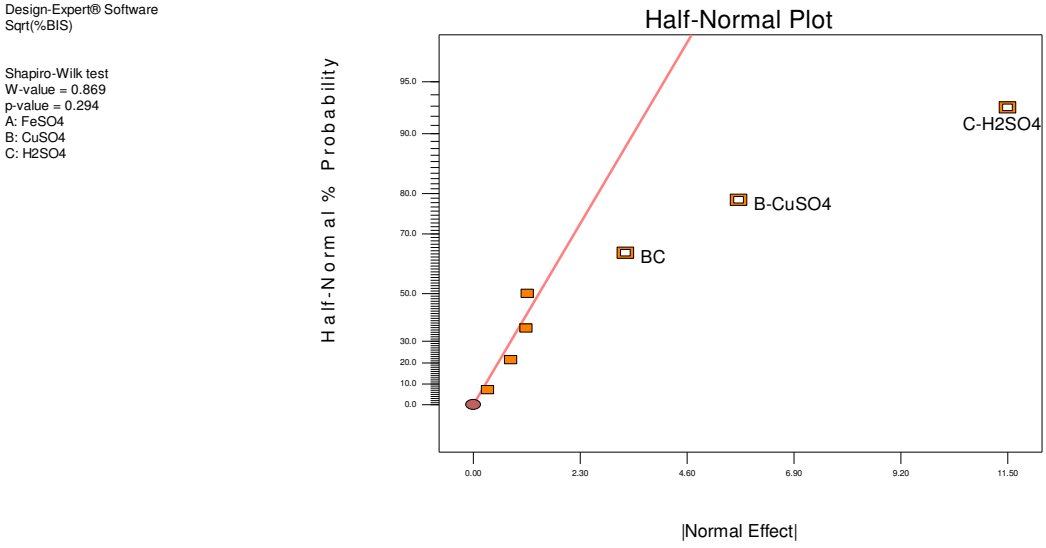

Figure 5.25: Half-Normal Plot – Second approach

Table 5.7: Factorial DOE – first approach

Run	Factor 1 A:FeSO4	Factor 2 B:CuSO4	Factor 3 C:H2SO4	Response 1 %BIS
	g/L	g/L	g/L	%
1	111.24	0	60	93.5
2	152.93	150.083	60	90
3	152.93	50.03	40	91.1
4	83.405	50.03	20	0
5	111.24	50.03	60	97.9
6	83.405	150.083	20	0
7	111.24	0	20	1.3
8	83.405	150.083	60	16.8
9	111.24	150.083	60	93
10	152.93	150.083	20	0
11	111.24	150.083	20	0
12	111.24	50.03	40	93.1
13	83.405	0	20	18.6
14	83.405	0	60	95.1
15	83.405	50.03	40	61.6
16	83.405	0	40	87.6
17	152.93	0	60	98.8
18	83.405	50.03	60	77
19	111.24	150.083	40	0
20	152.93	0	20	12.3
21	83.405	150.083	40	16.8
22	111.24	0	40	78.6
23	152.93	150.083	40	6.2
24	152.93	50.03	60	97.8
25	111.24	50.03	20	0
26	152.93	50.03	20	2.4
27	152.93	0	40	86

ANOVA analysis was conducted again (Table 5.8). If F and p-value are indicating that the model is significant, no simple equation to predict the factor's response could be obtained.

Table 5.8: ANOVA for selected factorial model – Second approach

Source	Sum of Squares	df	Mean Square	F Value	p-value Prob > F	
Model	412.34	8	51.54	24.06	< 0.0001	significant
B-CuSO4	*78.46*	*2*	*39.23*	*18.31*	*< 0.0001*	
C-H2SO4	*294.56*	*2*	*147.28*	*68.76*	*< 0.0001*	
BC	*39.32*	*4*	*9.83*	*4.59*	*0.0099*	
Residual	38.55	18	2.14			
Cor Total	450.90	26				

Because of the complexity of the response to [$CuSO_4$] and [H_2SO_4], the 3D surface model is symbolized by columns. The model errors seem to be related to the intermediate values which were not accounted for in the first approach. The fact that the intermediate values used are not actually equidistant from the extreme values likely is a partial reason for the differences between the prediction and the actual values. As for approach 1, changing [$FeSO_4$] had a very few influence on the 3D model (Figure 5.26).

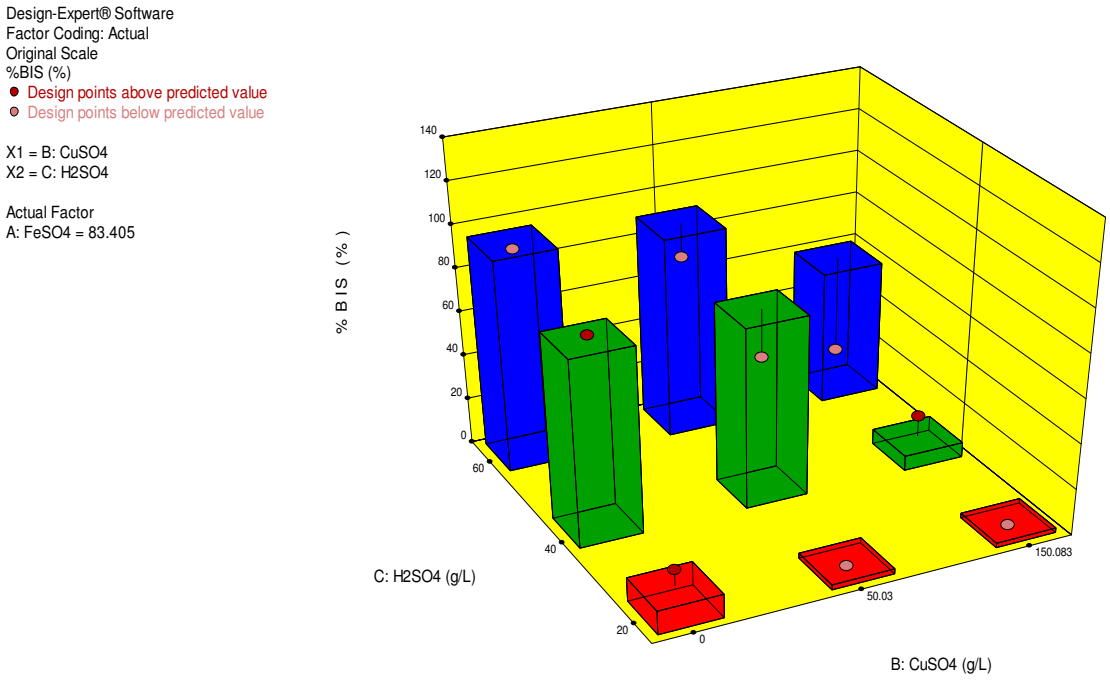

Figure 5.26: 3D surface model for the second approach

5.6 Ternary diagrams

In order to visualize the influence of PLS composition on the Fe-Cu-S system, experimental data was plotted in ternary graphs, using the software OriginLab®. The purpose is to obtain a continuous approach of the results, and complete to the discrete data described in the experimental paragraph.

5.6.1 Residue composition

First, the XRD data was plotted within the Fe-Cu-S ternary diagram to observe the species distribution. One example (Batch B) is shown figure 5.27, where the stability area of BIS and hematite have been extended for better reading. The original plots for batches A, B and C are shown in appendix F. The switch between BIS and hematite seems to occur in limited conditions, with a very small area in the diagram where the two species are coexisting. The limit is not as clear for batches A and C, but this is most likely related to the fact that less data points were available to draw the diagram.

For batches A, B and C, this small “coexisting domain” was represented as a line, and the result is compiled in figure 5.28. It appears that an increasing initial iron concentration shifts this limit to the lower part of the graph.

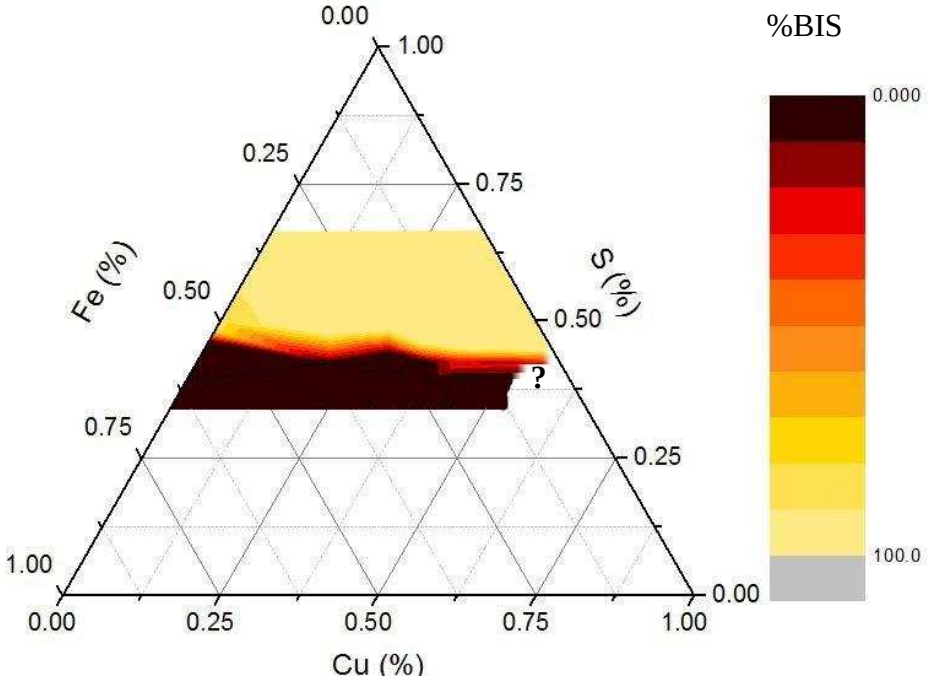

Figure 5.27: Ternary plot showing hematite vs. BIS stability in the Fe-Cu-S system

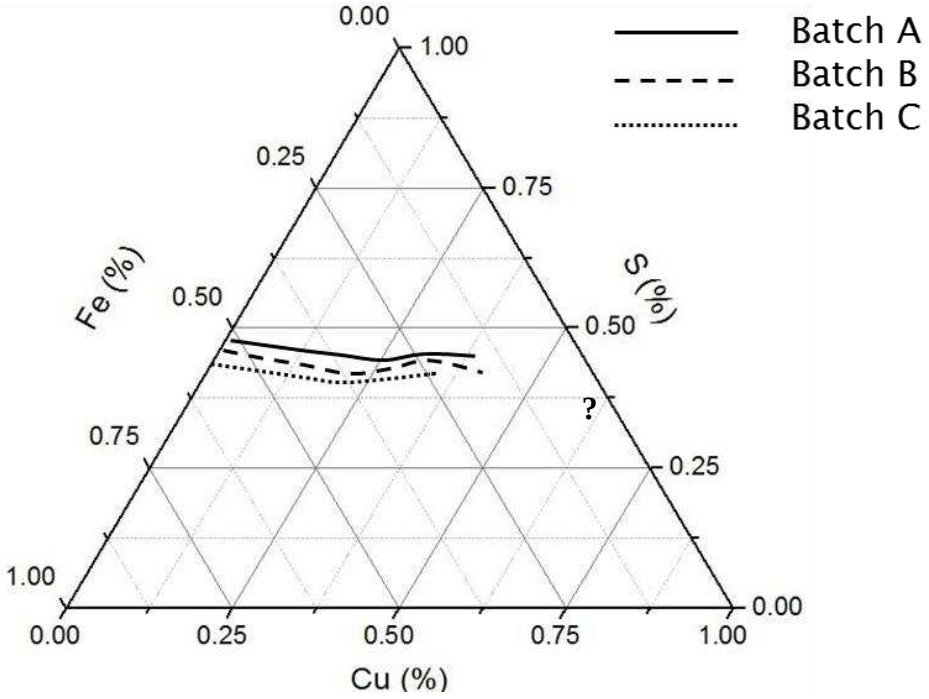

Figure 5.28: Ternary plot showing the influence of initial iron concentration on the limit of BIS stability

Figure 5.27 could be used to predict the residue composition obtained after the leaching of a concentrate. Knowing the percentages of copper, iron and sulfur in the concentrate, they can be reported to the ternary diagram (assuming the total iron concentration is also known) and the corresponding point will provide information on the amount of BIS expected in the residue.

5.6.2 Percentage iron recovered in the residue

Identically, %Fe recovered in the residue was plotted (Figure 5.29). Plots for batches A and C are visible in Appendix E. Accordingly to iron content difference in hematite and BIS, less iron remains in PLS when iron oxide precipitates.

If these graphs show well the correlation between residue chemistry and efficiency of the precipitation process, they should be used with caution. They were plotted with a limited amount of points and should be completed for better accuracy.

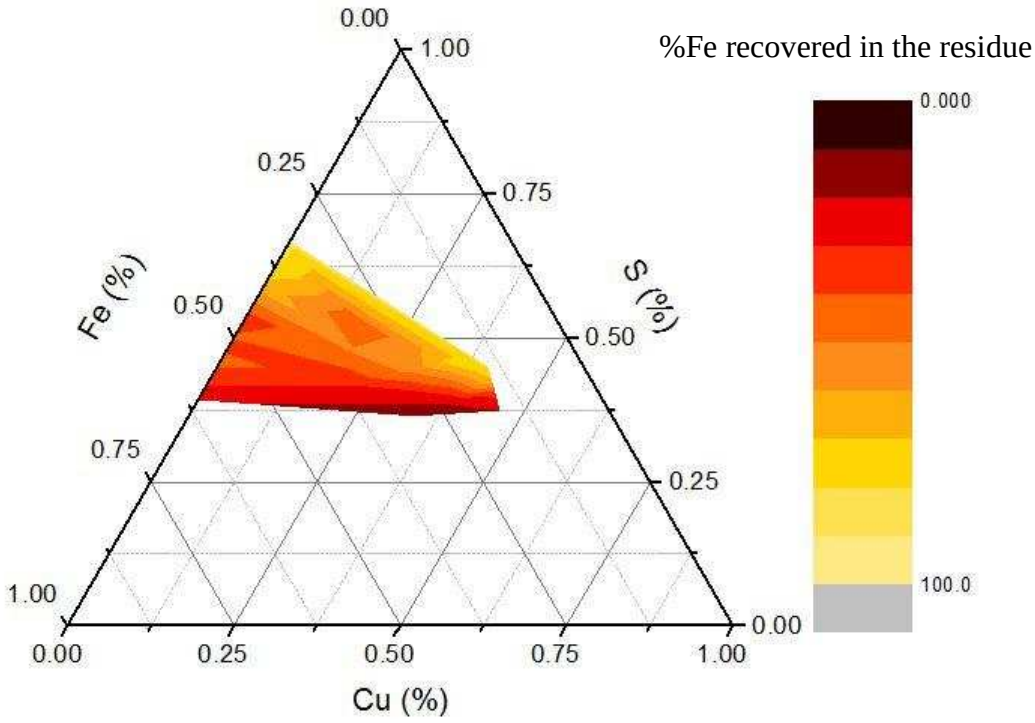

Figure 5.29: Ternary Diagram showing %Fe recovered in the residue for batch B

Again, if a concentrate's composition is known, this ternary diagram could be used to predict how much of the total iron should be recovered in the residue after leaching.

5.7 QEMSCAN analysis

This section presents the results obtained by QEMSCAN data analysis.

5.7.1 Mineralogy of the samples

The analysis was made in order to collect more information on mineralogy of the residue, especially particle size distribution (PSD), shape and mineral association. Three samples were analyzed; their initial solution composition is detailed in table 5.9.

Table 5.9: Initial solution composition of the samples analyzed by QEMSCAN

Sample #	42	43	44
$[Fe]_{initial}$ in g/L	22.3	22.3	22.3
$[Cu]_{initial}$ in g/L	25.4	25.4	25.4
$[H_2SO_4]$ in g/L	19.6	39.2	58.9

After processing the data, seven mineral categories were brought out:

- Hematite, and more generally all the pixels detected as iron oxides species
- BIS, including the synthetic product $FeOHSO_4$ and one of its hydrated species fibroferrite ($FeOHSO_4.5H_2O$)
- BIS-Hematite interphase, which describes all the areas where the beam shot was directed at a boundary between the two phases without being able to detect which one was dominant
- Jarosite, as hydronium jarosite
- Elemental sulfur, i.e. the pixels characterized by an unusually high sulfur content when compared to the other elements
- Ferric Sulfate
- Other minerals i.e. quartz, which has been found contaminating a couple samples.

Tests 42 and 43 are mainly composed of hematite, with BIS and jarosite in traces. Test 44 mostly shows BIS with less than 5% of hematite and jarosite. The images as well as composition of each samples is presented in appendix G.

QEMSCAN percentages are matching the XRD data up to a ±5% difference. The reason for this difference relies in the detection limit of QEMSCAN (5µm). When analyzing a pixel, an average measurement from the whole pixel area is produced, but it does not account for the heterogeneity of the pixel. All intermediary pixels were associated with the closest category matching their global composition, which means that part of each pixel could have actually belong to another category.

5.7.2 Particle Size and shape

PSD of the three samples is presented in Figure 5.30. Test 42 and 43 show similar fine particle sizes (inferior to 150µm) and are quite homogeneous overall. Test 44 shows a much wider distribution ranging from the detection limit 7µm up to over 1mm. The bigger particles do not seem to have agglomerated: they are round and show concentric hematite and jarosite growth rings. The intermediary particles show stretched out, irregular shapes.

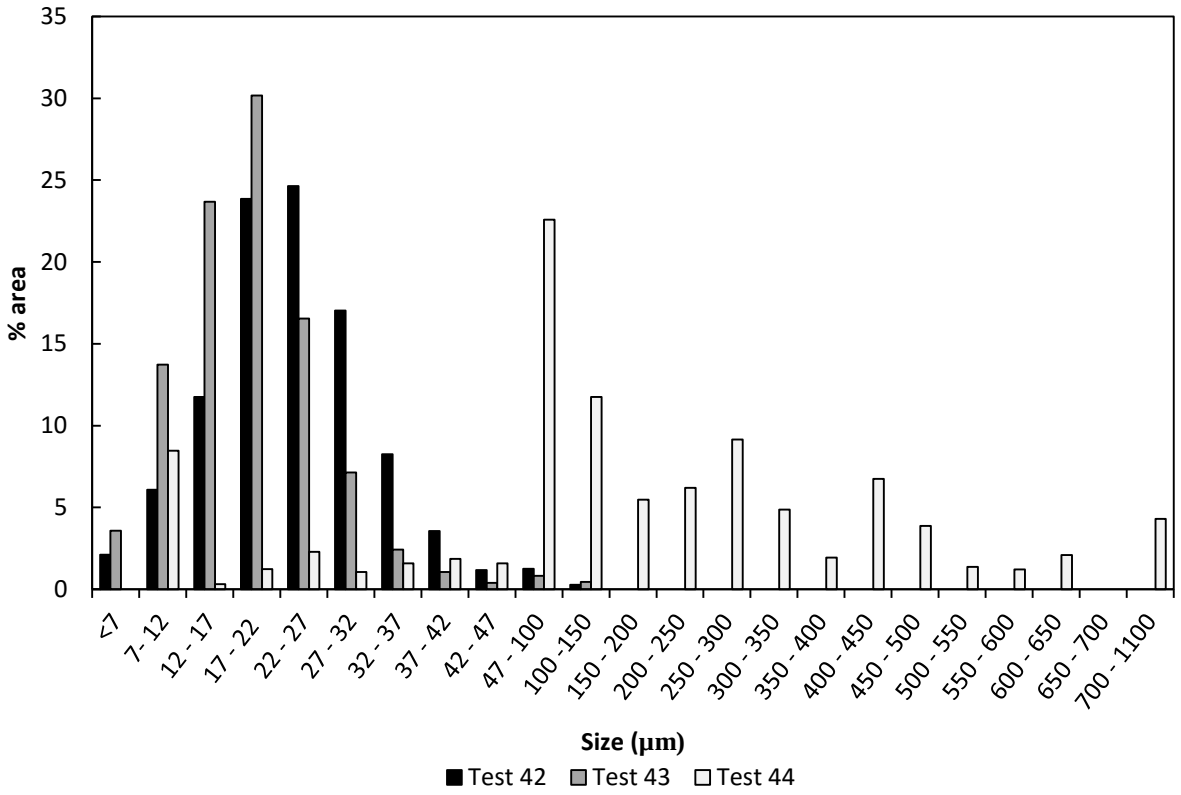

Figure 5.30: Particle size distribution of test 42, 43 and 44

Individually, each mineral PSD was also plotted and the results are presented in appendix G (each mineral was specifically considered as a grain). The observations are:

- Hematite particle size is homogeneous and fine (<150µm), no matter the sample type. Particle size does not seem to be influenced by leaching conditions.
- BIS particle size is fine and homogeneous for tests 42 and 43. At higher free acidity, the particle size distribution is much wider and is mainly larger than 100µm.
- The very fine BIS-hematite grain particle size confirms that those pixels were identified at boundaries between the two species.
- Jarosite is overall very finely grained (<50µm), but tends to be slightly coarser at higher acidity, as does BIS.
- Elemental sulfur is finely disseminated in all three samples (<30µm), slightly coarser for test 44.

A lot of coarse hematite grains show a “doughnut” shape. No literature was found on the topic to explain this unusual result. Two hypotheses can be made:

- Hematite crystallized around a species which progressively became unstable at high temperature and pressure, and dissolved (this supposes high porosity within hematite).
- The inner part of the particles was separated during sample preparation.

5.8 Moisture content

Table 5.10 shows that moisture content is more than doubled when the residue composition exceeds 90% BIS. The numbers shown are an average of all samples showing BIS content either inferior to 10% or superior to 90%. The data showed a greater dispersion in between these percentages.

Table 5.10: Average moisture content depending on %BIS

%BIS in residue	<10% BIS	>90% BIS
Average moisture content	18.8 %	45.1 %

CHAPTER 6 PROPOSED ECONOMIC ANALYSIS

A general analysis was performed in order to assess which economic indicator would be the most impacted by a decrease of the BIS content in the autoclave discharge.

6.1 Assumptions

The following economic evaluation will be based on a simplified flowsheet where pressure oxidation is used Leach/Solvent Extraction/Electrowinning circuit for copper and cyanidation for gold. The following assumptions were made:

- Feed head grade is presented in table 6.1
- Overall recovery is presented in table 6.3 and based on the assumptions concerning the residue presented in table 6.2
- Capital and operating costs are calculated for the circuit presented in Figure 6.1
- 560,660 tonnes of concentrate feed per annum and 800,940 tonnes of feed per annum
- Grinding circuit functioning at full capacity
- The concentrate mineral composition is 60% chalcopyrite, 35% pyrite, 5% gangue
- At this stage, the income related to gold production will not be included in the analysis
- Conditions of leaching: 220˚C, 40 psi oxygen overpressure
- Operating costs do not include neutralization of the leach solution. Sulfuric acid is considered to be reused for heap leaching
- Capital costs include the expenditures related to building a new mill, they do not include refining costs for Cu cathode if needed
- The mill is operating 325 days/year to account for maintenance shutdowns
- Pressure leaching and solvent extraction – electrowinning circuits are located on the same site; therefore, no transportation costs were included
- By-products are not marketable
- 10 year cash flow

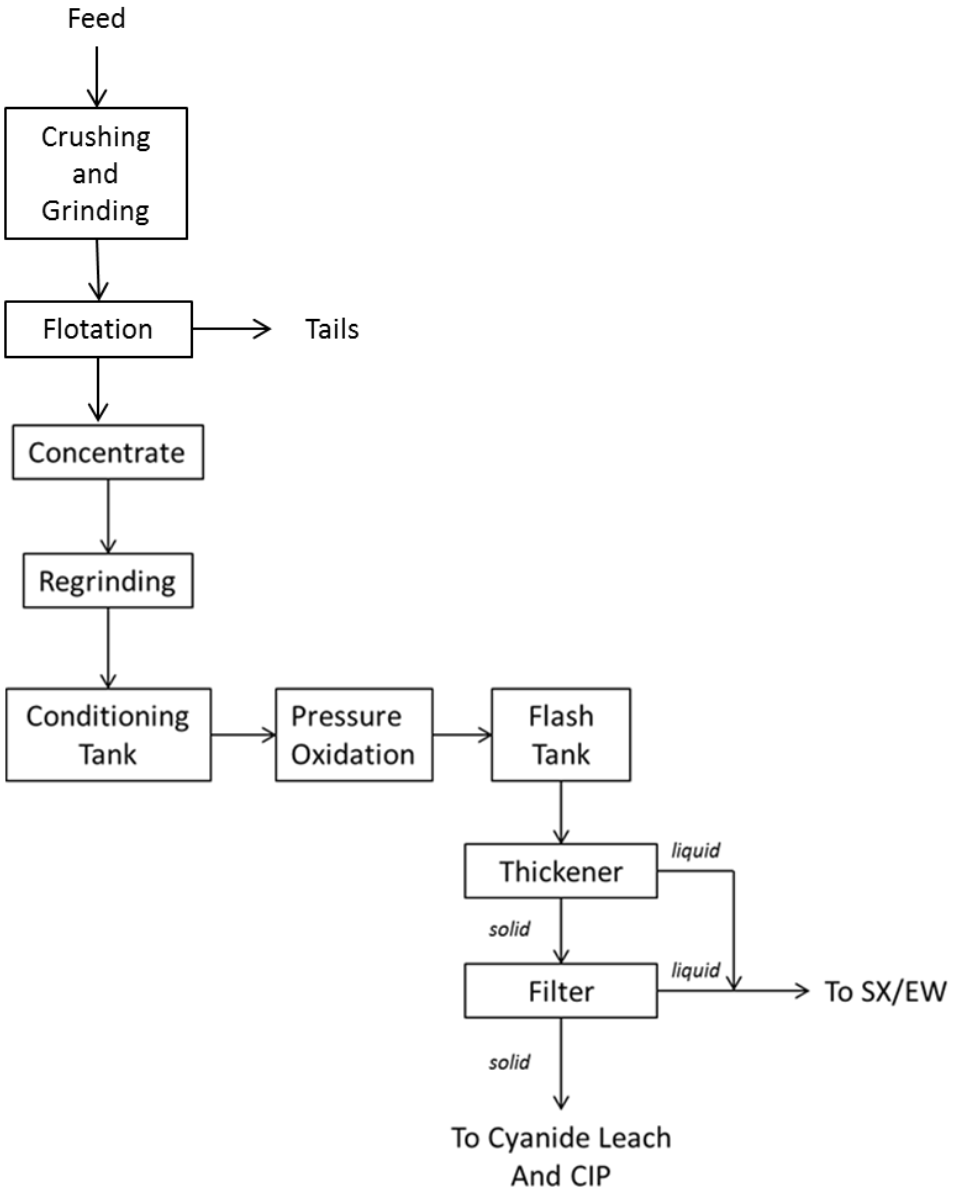

Figure 6.1: Proposed flowsheet for economic analysis
Note: SX=Solvent Extraction – EW=Electrowinning

The model aims at trying to predict the feasibility of treating a concentrate with the following composition:

Table 6.1: Assay data for Concentrate X

Cu (%)	Fe (%)	S (%)	Au (g/t)
18.2	31.1	35.0	30.5

Recalculating the percentages within Fe-Cu-S system, the compositions of the concentrates in the ternary diagram are the following: 21.6% Cu, 41.5% S, 36.9% Fe. Implementing the feed composition in the ternary plots (paragraph 5.6), we can predict the percentage of BIS in the residue as well as the percent of iron recovered in the residue (Table 6.2).

Table 6.2: Composition of the residue and %Fe recovered

%BIS in residue	%Fe recovered in residue
10	90

Table 6.3: Overall %Recovery assumptions based on residue composition

Au	Cu
90%	98%

Accounting for table 6.2, we will also assume that:

- %Fe recovered in residue has an influence on the overall copper recovery during the solvent extraction and electrowinning stages
- We will neglect the impact of other contaminating ions in solution such as Zn, Pb or alkali metals

Costs estimates for actualization of the costs were used following equation 6.1 and table 6.4:

$$2014\ \text{Cost} = [\text{Year}]\ \text{Cost} * \frac{2014\ \text{cost index}}{[\text{Year}]\ \text{cost index}} \qquad \text{Equation 6.1}$$

Table 6.4: Cost indexes for CAPEX and OPEX estimation [44]

Year	CAPEX	OPEX
1995	80.1	83.0
2014	101.5	98.5

6.2 Copper pressure leaching circuit

The estimation of operating and capital costs for the copper recovery circuit was made using the Proceedings of COPPER 95-COBRE 95 International Conference [44]. The detailed tables are presented in appendix H.

Table 6.5: Total Operating Costs for production and marketing of cathode copper per annum in M$

Parameter	1995 Cost	2014 Cost
Autoclaving concentrates	30.75	
SX/EW	30.86	
Copper losses, tailing disposal, freight, marketing, etc	21.61	
Total operating costs	83.22	98.76

Table 6.6: Total Capital costs for hydrometallurgical treatment of copper concentrate per annum in M$

Parameter	1995 Cost	2014 Cost
Direct capital costs	170.14	
Indirect capital costs	65.00	
Total capital costs	235.14	297.78

6.3 Grinding and flotation mill

The estimation of operating and capital costs for the primary grinding and flotation circuit was based on the Flotation Mill Model of CostMine 2014 [42]. The values for a 2,500 tpd feed throughput were extrapolated from values for 1,000 and 2,000 tpd feed throughput. The detailed calculation can be found in appendix H.

Table 6.7: Total Capital and Operating Costs for grinding and flotation Mill

Parameter	2014 Cost
Capital Costs in M$	37.60
Operating Costs in $ per tonne of feed	13.81
Operating Costs in M$ per annum	11.06

6.4 NPV Analysis

Copper price used at the time of this analysis is $2.1 /lb Cu. An additional 14% annual capital write-off was added, based on 100,000 tonnes of Cu produced annually.

Table 6.10 presented the cash flow diagram based on overall operating and capital costs for mine life duration of 10 years. Annual Cu cathode production is 100,000 tonnes, i.e. 220.462 Mlb Cu.

Table 6.8: NPV analysis for the 10 years cashflow

Discount Rate	NPV
0%	2,725,288,000
8%	1,591,067,724
10%	1,404,789,083
20%	$789,830,429.43

Table 6.9: Economic indicators for the 10 years cash flow

Plant life	10 years
IRR	91%
Payback Period	1.1 years

The project seems extremely viable in terms of economic factors. This can be explained by the simplified flowsheet considered: some intermediary equipment might not have been accounted for. Additionally, the calculations made using [44] are most likely to be underestimated. Pressure leaching circuits are difficult to control and prone to higher maintenance costs than expected.

Table 6.10: 10 year Cashflow

Year	0	1	2	3	4	5	6	7	8	9	10
Gross Revenue		462,840,000	462,840,000	462,840,000	462,840,000	462,840,000	462,840,000	462,840,000	462,840,000	462,840,000	462,840,000
Operating Costs											
Leaching/SX/EW		(98,760,000)	(98,760,000)	(98,760,000)	(98,760,000)	(98,760,000)	(98,760,000)	(98,760,000)	(98,760,000)	(98,760,000)	(98,760,000)
Grinding/Flotation		(11,060,000)	(11,060,000)	(11,060,000)	(11,060,000)	(11,060,000)	(11,060,000)	(11,060,000)	(11,060,000)	(11,060,000)	(11,060,000)
Total OPEX		(109,820,000)	(109,820,000)	(109,820,000)	(109,820,000)	(109,820,000)	(109,820,000)	(109,820,000)	(109,820,000)	(109,820,000)	(109,820,000)
Capital Costs											
Leaching/SX/EW	($297,780,000.00)										
Grinding/ Flotation	($37,600,000.00)										
Total CAPEX	($335,380,000.00)										
Capital Write-Off		($46,953,200.00)	($46,953,200.00)	($46,953,200.00)	($46,953,200.00)	($46,953,200.00)	($46,953,200.00)	($46,953,200.00)	($46,953,200.00)	($46,953,200.00)	($46,953,200.00)
Net Cashflow	($335,380,000.00)	$306,066,800.00	$306,066,800.00	$306,066,800.00	$306,066,800.00	$306,066,800.00	$306,066,800.00	$306,066,800.00	$306,066,800.00	$306,066,800.00	$306,066,800.00
Cumulative Cashflow	($335,380,000.00)	($29,313,200.00)	$276,753,600.00	$582,820,400.00	$888,887,200.00	$1,194,954,000.00	$1,501,020,800.00	$1,807,087,600.00	$2,113,154,400.00	$2,419,221,200.00	$2,725,288,000.00

6.5 Sensitivity Analysis

Figure 6.2 shows NPV sensitivity for CAPEX, OPEX and gross revenue. The later has the most influence on NPV, since fluctuating copper price have a considerable impact on the revenue made from a 100,000 tonnes annual production. Operating costs have more influence on NPV than capital costs, which could be explained by the operating challenges associated with Pressure Leach/SX/EW circuits.

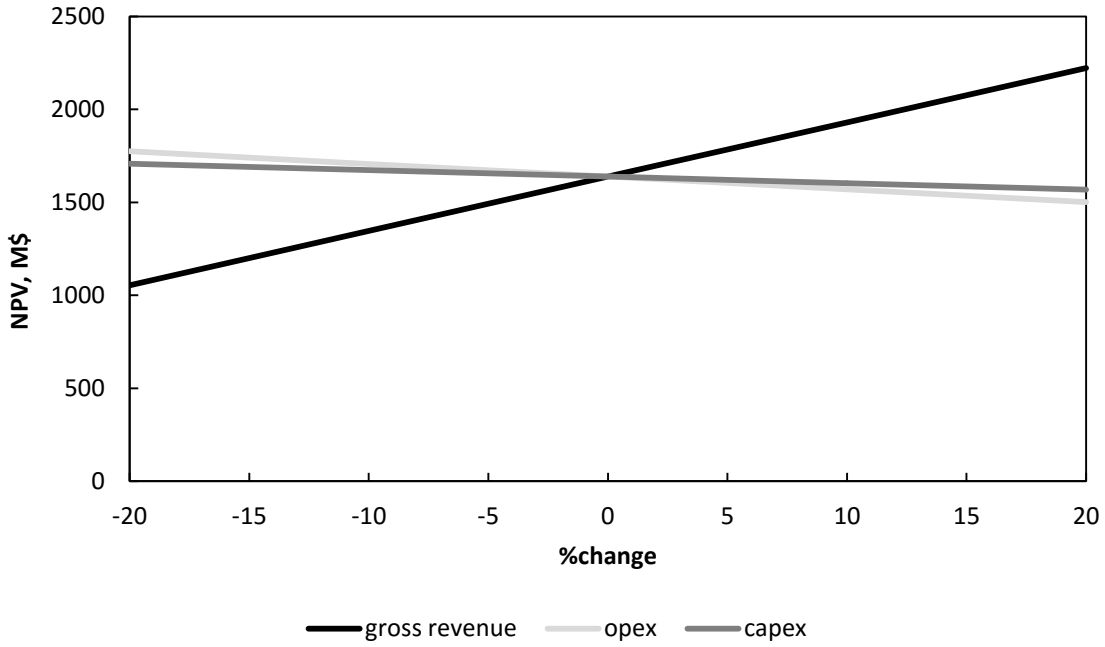

Figure 6.2: Sensitivity analysis

Within a copper leach operation where iron contamination is a major issue, diminishing the amount of BIS in the residue would have two main financial consequences:

- Slightly decrease operating and capital costs (because of tailing disposal and filtering savings)
- Highly increase the gross revenue by improving copper recovery

For this estimation, a copper recovery increase of 1% would represent a NPV increase of $30M. Again, it is likely that some costs have been underestimated in this analysis. But the previous remark shows that effectively hindering BIS allows a significant increase of NPV.

CHAPTER 7 CONCLUSIONS AND RECOMMENDATIONS

This project aimed at better understanding the influence of leaching solution composition on the precipitate chemistry during high pressure oxidative leaching. It was achieved by leaching artificial solutions of varying compositions at temperature and pressure usually implemented in copper sulfide POX circuits. The main application to the observations made in this thesis would be to predict the response of any copper-iron sulfide concentrate and change the solution chemistry to hinder the formation of BIS. This is, of course, a theoretical approach since synthetic solutions prepared from sulfates were used to recreate a certain concentrate composition. Contaminants and conditions of leaching would deeply complicate the system's response. However, the statistical model and ternary plots can be used to predict some general trends which can be expected during leaching of copper sulfides.

7.1 Summary

The literature review highlighted the importance of sulfuric acid concentration in the PLS on residue composition. In the conditions of this study, in a simple Fe-O-S system at 22.3g/L Fe, the upper limit for hematite precipitation over BIS is 41g/L. Hematite precipitation is associated with great production of sulfuric acid, whereas BIS formation is consuming it. This explains why high acidity promotes the formation of BIS. Applied to the industry, this suggests that a possible solution to an excessive BIS content in the autoclave discharge would be to decrease the overall sulfuric acid concentration. Of course, this has to be done with caution to avoid diminishing overall recovery.

When progressively adding copper sulfate to the system, the precipitation limit for hematite is shifted upward. At 63.5 g/L Cu, hematite is stable up to 61g/L sulfuric acid. Copper sulfate is thus actively hindering BIS formation. The specific effect of copper on the limit is depending on the matrix composition (i.e. iron concentration and initial acid concentration) and the operating conditions of leaching as well. The results presented here sometimes show great difference with what has been reported in the literature. Overall, this thesis' results mean that adding copper sulfate to an existing circuit could help improving the residue's chemistry.

According to several authors, the stabilizing effect of copper sulfate is a due to the buffering action of the ion sulfate. The type of metal in solution is certainly influencing the process as well since different metal sulfate in comparable concentration yield slightly different results.

The effect of initial iron concentration in solution was investigated over the range 16.7-30.7 g/L. Discrete experimental results did not allow to draw definite conclusions regarding its influence on BIS content in the residue or %Fe left in solution. However, two trends can be highlighted:

- BIS seems to be hindered by low initial iron concentrations.
- Increasing copper sulfate concentrations help reducing the iron left in solution after leaching.

The influence of initial oxidation state of iron was tested by leaching identical solutions prepared from ferric or ferrous sulfate. Ferric sulfate seems to promote BIS formation and increase the amount of iron left in the PLS, no matter the initial free acidity concentration. This can be explained by the consumption of acid for ferrous oxidation to ferrous, which does not happen when using ferric sulfate as reagent. In practice, this would mean that the acid leach concentration can be optimized to fit the type of minerals in the ore, and the oxidation state of iron in these minerals.

Hydronium jarosite was shown to be precipitating along with hematite and BIS. There is no specific trend which could help explaining its stability, besides the fact that it disappears at low initial iron concentration.

Statistical modelling by Stat-Ease® and extrapolation using OriginLab® confirmed that sulfuric acid was the main parameter controlling hematite precipitation, along with copper sulfate to a lesser extent. An equation to predict the model's response was produced, but needs to be used with extreme caution when operating at intermediate free acidity levels. The system does not seem to fit as well when BIS and hematite are coexisting.

Plotting the data into ternary diagram (Fe-Cu-S system) has shown the following points:

- Increasing iron concentrations diminishes the stability area of hematite
- The coexistence area for hematite and BIS is very limited
- %Fe effectively extracted from solution by precipitation correlates well to final residue chemistry. This is logical regarding to higher %Fe in hematite than BIS.

Finally, QEMSCAN analysis is correlating XRD data, and is showing that BIS particles are much coarser and more irregular than hematite.

7.2 Recommendations for future work

- Develop an experimental procedure to thermodynamically characterize BIS and model the data. Missing this information prevented any preliminary analysis and led to estimations based on experimental models only.
- Investigate the reproducibility of the results. A few tests were performed twice and yielded residues showing some composition difference.
- Broadening the range of initial iron concentration tested. Leaching of the three batches highlighted a trend for hematite to become less stable at higher $[Fe]_{initial}$. This would need to be confirmed to see the evolution of the stability limit delineated in the ternary plot.
- Conduct additional "intermediary" acidity leaching tests to better understand the reasons for low iron recovery when BIS and hematite are coexisting.
- Working at larger scale. Many areas of the ternary diagrams could not be investigated because of insufficient amounts of residues formed. They were not suitable for XRD analysis.
- Investigate the influence of other metal sulfates on the system. Especially, $ZnSO_4$, $MgSO_4$, $Na2SO_4$, K_2SO_4. Priority should be given to the most common metal contaminants, as well as alkalis, which readily form jarosites.
- Conduct and analyze tests with actual concentrates, which compositions are similar to those tested in this project. The comparison would provide precious information on the prediction reliability.

REFERENCES

[1] Habashi, F. (2014). Pressure Hydrometallurgy. *Métallurgie Extractive Québec.*

[2] Cheng, T. C., & Demopoulos, G. P. (2004). Hydrolysis of ferric sulfate in the presence of zinc sulfate at 200 C: precipitation kinetics and product characterization. *Industrial & engineering chemistry research*, *43*(20), 6299-6308.

[3] Robert Weir, D. (1984). "Some recent developments in hydrometallurgy." *Canadian Metallurgical Quarterly 23(4)*, 353-363.

[4] Fleming, C. A. (1992). Hydrometallurgy of precious metals recovery. *Hydrometallurgy*, *30*(1), 127-162.

[5] Fleming, C. A. (2010). Basic iron sulfate–a potential killer in the processing of refractory gold concentrates by pressure oxidation. *Minerals & Metallurgical Processing Journal*, *27*(2), 81-88.

[6] 911 Metallurgist. (2015). *Refractory Gold Processes*. Retrieved from http://www.911metallurgist.com/blog/refractory-gold-processes

[7] Habashi, F. (1999). Textbook of Hydrometallurgy. *Métallurgie Extractive Québec.*

[8] Wang, S. (2005). Copper leaching from chalcopyrite concentrates. *JOM*, *57*(7), 48-51.

[9] Marsden, J. O., Brewer, R. E., & Hazen, N. (2003). Copper concentrate leaching developments by Phelps Dodge Corporation. Electrometallurgy and Environmental Hydrometallurgy, Volume 2, 1429-1446.

[10] Free, M. (2013). *Hydrometallurgy: Fundamentals and Applications*. John Wiley & Sons.

[11] Outotec. (2013). *Outotec® Gold Processing Solutions* [PDF file]. Available from www.outotec.com/

[12] Cheng, T. C., Demopoulos, G. P., Shibachi, Y., & Masuda, H. (2003). The precipitation chemistry and performance of the Akita hematite process—an integrated laboratory and industrial scale study. *Electrometallurgy and Environmental Hydrometallurgy, Volume 2*, 1657-1674.

[13] Marchbank, A. R., Thomas, K. G., Dreisinger, D., & Fleming, C. (1996). *U.S. Patent No. 5,536,297*. Washington, DC: U.S. Patent and Trademark Office.

[14] Gupta, C. K., and Mukherjee, T. K. (1990). *Hydrometallurgy in extraction processes*. Vol. 2. CRC Press, 196-200.

[15] La Brooy, S. R., Linge, H. G., & Walker, G. S. (1994). Review of gold extraction from ores. *Minerals Engineering*, *7*(10), 1213-1241.

[16] Conway, M. H., & Gale, D. C. (1990). Sulfur's impact on the size of pressure oxidation autoclaves. *JOM*, *42*(9), 19-22.

[17] Tourre, J-M. (1984). A study of the conditions of formation of silver-containing jarosites in the acid pressure leaching of pyritic ores. PhD Diss. Colorado School of Mines.

[18] Ismael, M. R. C., & Carvalho, J. M. R. (2003). Iron recovery from sulphate leach liquors in zinc hydrometallurgy. *Minerals Engineering*, *16*(1), 31-39.

[19] R. Marsalek. (2011). The Reduction of Zinc using Goethite Process and Adsorption of Pb+II, Cu+II and Cr+III on Selected Precipitate. *International Journal of Environmental Science and Development, 2.4,* 253-258.

[20] Onozaki, A., Sato, K., and Kuramochi, S.. (1986). Effect of some impurities on iron precipitation at the Iijima Zinc Refinery. *Iron Control in Hydrometallurgy*, 742-752.

[21] Umetsu, V., Tozawa, K., & Sasaki, K. I. (1977). The hydrolysis of ferric sulphate solutions at elevated temperatures. *Canadian Metallurgical Quarterly*,*16*(1), 111-117.

[22] Gathje, J.C. (2006). Iron reduction in copper leach liquors using controlled precipitation of sulfate species during high temperature pressure oxidation of base metal ores. *Iron Control Technologies*, 231-246.

[23] Posnjak, E., & Merwin, H. E. (1922). THE SYSTEM, Fe2O3—SO3—H2O. *Journal of the American Chemical Society*, *44*(9), 1965-1994.

[24] Rossman, G. R. (1976). Spectroscopic and magnetic studies of ferric iron hydroxy sulfates: the series Fe (OH) SO4· nH2O and the jarosites. *American Mineralogist*, 61(5-6), 398-404.

[25] Scordari, F. (1981). Fibroferrite: A mineral with a {Fe (OH)(H2O) 2SO4} spiral chain and its relationship to Fe (OH) SO4, butlerite and parabutlerite.*Tschermaks mineralogische und petrographische Mitteilungen*, *28*(1), 17-29.

[26] Lazaroff, N., Sigal, W., & Wasserman, A. (1982). Iron oxidation and precipitation of ferric hydroxysulfates by resting Thiobacillus ferrooxidans cells. *Applied and Environmental Microbiology*, *43*(4), 924-938.

[27] Bigham, J. M., & Nordstrom, D. K. (2000). Iron and aluminum hydroxysulfates from acid sulfate waters. *Reviews in mineralogy and geochemistry*, *40*(1), 351-403.

[28] Mindat. (2015). *Jarosite*. Retrieved from http://www.mindat.org/min-2078.html.

[29] Dutrizac, J. E., & Jambor, J. L. (2000). Jarosites and their application in hydrometallurgy. *Reviews in Mineralogy and Geochemistry*, *40*(1), 405-452.

[30] Burgina, E. B., Kustova, G. N., Nikitenko, S. G., Kochubei, D. I., & Elizarova, G. L. (1996). Comparative study of the structures of some basic iron (III) sulfates. *Journal of structural chemistry*, *37*(2), 240-246.

[31] Dutrizac, J. E., & Chen, T. T. Behavior of Various Impurities during the Precipitation of Hematite from Ferric Sulphate Solutions at 225° C. In *TT Chen Honorary Symposium on Hydrometallurgy, Electrometallurgy and Materials Characterization* (pp. 489-499). John Wiley & Sons, Inc.

[32] Berezowsky, R. M. G. S., & Weir, D. R. (1989). Refractory gold: the role of pressure oxidation. *Proceedings of World Gold, AIME*, 152-156.

[33] Majzlan, J., Stevens, R., Boerio-Goates, J., Woodfield, B. F., Navrotsky, A., Burns, P. C., ... & Amos, T. G. (2004). Thermodynamic properties, low-temperature heat-capacity anomalies, and single-crystal X-ray refinement of hydronium jarosite,(H3O) Fe3 (SO4) 2 (OH) 6. *Physics and Chemistry of Minerals*, *31*(8), 518-531.

[34] Drouet, C., & Navrotsky, A. (2003). Synthesis, characterization, and thermochemistry of K-Na-H 3 O jarosites. *Geochimica et Cosmochimica Acta*,*67*(11), 2063-2076.

[35] Babcan, J. (1971). Synthesis of jarosite KFe3 (SO4) 2 (OH) 6. *Geol. Zb*, *22*(2), 299-304.

[36] Voigt, B., & Göbler, A. (1986). Formation of pure haematite by hydrolysis of iron (III) salt solutions under hydrothermal conditions. *Crystal Research and Technology*, *21*(9), 1177-1183.

[37] Van Santen, R. A. (1984). The Ostwald step rule. *The Journal of Physical Chemistry*, *88*(24), 5768-5769.

[38] Papangelakis, V. G., Blakey, B. C., & Liao, H. (1994). Hematite solubility in sulphate process solutions. In *Hydrometallurgy'94* (pp. 159-175). Springer Netherlands.

[39] Tozawa, K., & Sasaki, K. (1986). Effect of coexisting sulphates on precipitation of ferric oxide from ferric sulphate solutions at elevated temperatures. *Iron Control in Hydrometallurgy*, 454-476.

[40] Javed, T. & Asselin, E. (2015). Hematite precipitation from sulphate – chloride solutions at 150˚C. Canadian Institute of Mining, Metallurgy and Petroleum. COM 2015.

[41] ALS Minerals. (2009). *Sulfur analysis methods* [PDF file]. Available from http://www.alsglobal.com/

[42] Stebbins, S. A. (2014). Flotation Mill Models. *CostMine2014*.

[43] U.S. Department of Labor, Bureau of Labor Statistics (2014). Mining and Milling Cost Indexes. *CostMine2015*.

[44] King, J. A., Dreisinger, D. B. (1995). Autoclaving of copper concentrates. *Proceedings of COPPER 95-COBRE95 – Electrorefining and Hydrometallurgy of Copper*. The Metallurgical Society of CIM, 511-533.

[45] "Wayne, Shari, Pat and Mark". (2009). Handbook for Experimenters. *Stat-Ease 08.1*.

APPENDIX SECTION

APPENDIX A: FREE ACIDITY TITRATION PROCEDURE (MODIFIED AFTER JOSEPH GROGAN)

Solution Preparation

30wt.% (1.6M) Potassium Oxalate Solution

Weigh out 150g of potassium oxalate and mix with 450mL of solution in a beaker. Heat and stir until dissolved. Allow to cool and make up to 500mL in a volumetric flask.

Analytical Method

Procedure:

1. Pipette 1mL of sample into sample beaker

2. Dilute sample with approximately 50mL distilled water.

3. Add 5mL of the oxalate solution (should contain ≈ 8mmol oxalate).

4. Wait to allow oxalate complexes to form (solution will become turbid).

5. Run Method 668. (Input sample info and print report)

6. Titrate with 05n NaOH (ensure tower is filled with NaOH pellets) to pH endpoints of 3.5 and 8.5.

7. The characteristic ‘S’ curve should be between these two pH values. Use the equivalence point to determine mL titrant used. The equivalent point is where the curve is steepest on the pH vs. vol titrant plot, or the highest value/peak corresponding to the ‘S’ curve for the plot of the first derivative (dpH/dvol. titrant) vs. vol. titrant.

Calculation:

Free H_2SO_4 (g/L) = $\frac{49*\text{N Titrant}*\text{mL Titrant}}{\text{mL Sample}} = \frac{49*0.5*\text{mL Titrant}}{1}$

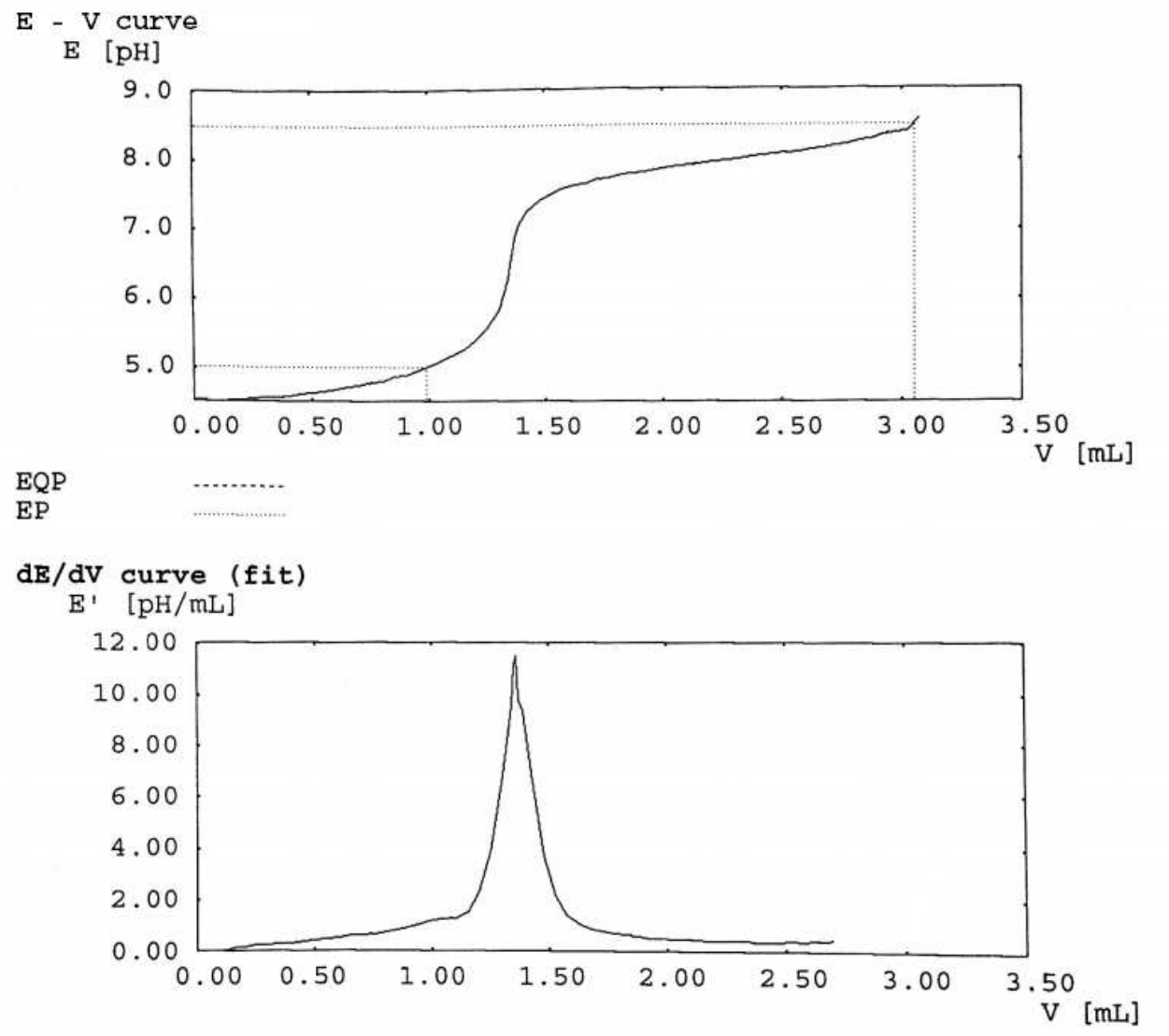

Figure A. 1: Typical titration curve and equivalence point determination

APPENDIX B: QEMSCAN SAMPLE PREPARATION PROCEDURE

Source: Colorado School of Mines QEMSCAN facility (Dr Katharina Pfaff)

To make a grain mount:

1. Measure the total sample weight into a beaker (zero the scale to the beaker's weight). Write the total sample weight in the column.
2. If the sample is too large, cut and quarter it until there is a reasonable amount of material.
3. Riffle the samples until each test tube has one gram of sample material.
4. Choose one test tube of material and measure it into a plastic tube with a label taped around it. Use the test tube opposite the first to create a duplicate sample, again measured and labeled.
5. Add graphite to the sample. Choose graphite size by the closest estimation to the grain size of the sample. If the sample is heterogeneous, choose several graphite sizes. Measure out the graphite in a 3:1 ratio of graphite to sample in the plastic tube by the scale then pour it in with the sample material.
6. Mix up the epoxy in an 8:1 resin to hardener ratio. Mix enough to have ~3-3.5 grams of epoxy per sample, plus some extra just in case.
7. Measure the epoxy into the sample and stir thoroughly with a toothpick.
8. Place the sample into the pressure cooker, close the lid securely, and flip the switch up to create a vacuum. Let the epoxy sit for 12 hours.
9. Remove the samples from the pressure cooker, fix the labels on the top, and backfill the sample with more epoxy, ~1 mm. Place back into the pressure cooker to let sit for another 12 hours.

Polishing:

1. For grain mounts, attach the sample holder to the head of the polisher.
2. Polish the tops of the samples (label side) on the 80 grind with water until flat. Use the level by the QEMSCAN to check the samples before moving on. Once flat, use the 1200 grind on the tops to polish a sheen and make the label readable.

3. Polish the sample side using the sequence 80, 220, 1200, 6 µm, 3 µm, 1 µm. For hard rock samples, use water. For shales or water soluble minerals, use alcohol. After each grind, rinse the samples with water (or methanol for alcohol polished samples) and change the sample holder to make sure there is no granular material remaining during the lower grinds.
4. The 80, 220, and 1200 are grinding pads and the 6, 3, and 1 µm are polishing pads that use a diamond polishing fluid along with water or alcohol lubricant.
5. After the 1 µm, wash the samples in methanol well, dry them with compressed air, and place them in the oven for at least 30 minutes. Use gloves to handle the clean samples from this point on.

Carbon coating:

1. Place the glass ring on the machine, close it, and turn on the vacuum. Wait for the vacuum to reach 10^{-4} (or as close as possible) before turning on the voltage with the Start/Stop button. Crank up the voltage using the knob next to it until the carbon rods begin to spark.
2. Watch the brass piece change color. Stop at red for SEM work, purple/blue for QEMSCAN. Turn down the voltage with the knob before hitting the Start/Stop button again and then turning off the vacuum. Color of the brass piece corresponds to carbon coat thickness (darker=thicker).
3. Carbon coating allows for an electrically conductive surface for the electron beam in the QEMSCAN.

APPENDIX C: XRD PATTERNS

Hematite residues at 12.7, 25.4 and 38.1 g/L CuSO4, 16.7g/L Fe(III), 20g/L H2SO4

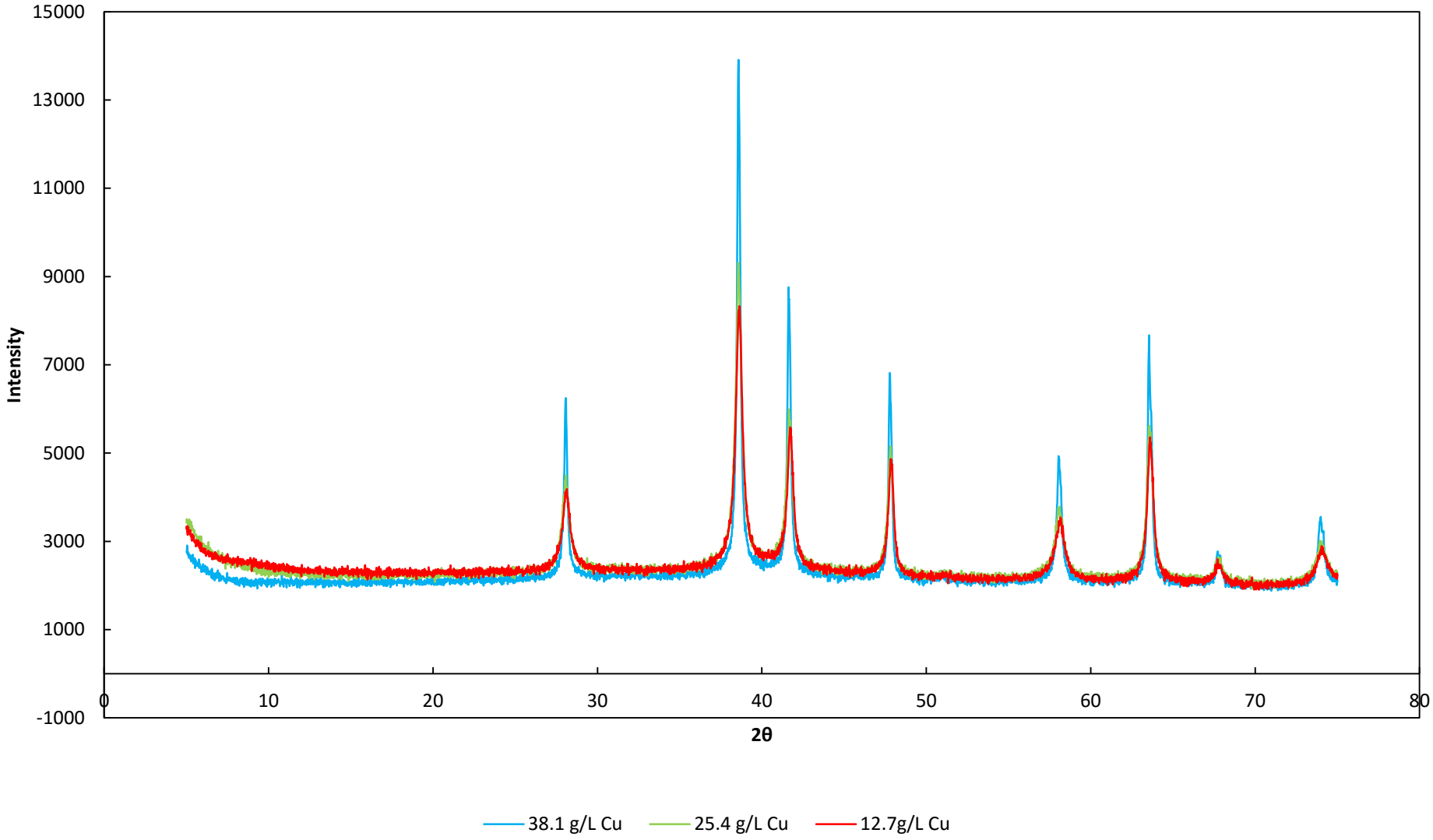

APPENDIX D: FERROUS IRON TITRATION – PASMINCO CLARKSVILLE LABORATORY PROCEDURE

Scope: This procedure is used to determine the amount of ferrous iron in sulfate solutions

Principle: The ferrous salts in cold acid solution are quantitatively oxidized to the ferric oxidation state by potassium dichromate

Reagents: 1. Potassium dichromate solution: 4.4g/L

2. Potassium dichromate solution: 0.44g/L

3. Sodium diphenylaminesulfonate: 10g/L

4. Acid buffer solution: 15% H2SO4, 15% H3PO4 to 1liter with water

Procedure: 1. Pipette 5 or 50mL filtered sample into a 250mL Erlenmeyer flask

2. Add 50mL acid buffer solution and 10 drops diphenylamine sulfonate indicator

3. Titrate with potassium dichromate solution until color changes to purple or violet

Calculation: 5mL sample:

mL 0.44g/L $K_2Cr_2O_7$*0.1 = g/L Fe^{2+}

mL 4.4g/L $K_2Cr_2O_7$*1.0 = g/L Fe^{2+}

50mL sample:

mL 0.44g/L $K_2Cr_2O_7$*0.01 = g/L Fe^{2+}

mL 4.4g/L $K_2Cr_2O_7$*0.1 = g/L Fe^{2+}

Interferences: Cu in quantities > 1mg assists the oxidation of Fe^{2+} by air. As(III) raises results as if oxidized to As(VI) by dichromate.

APPENDIX E: TERNARY PLOTS

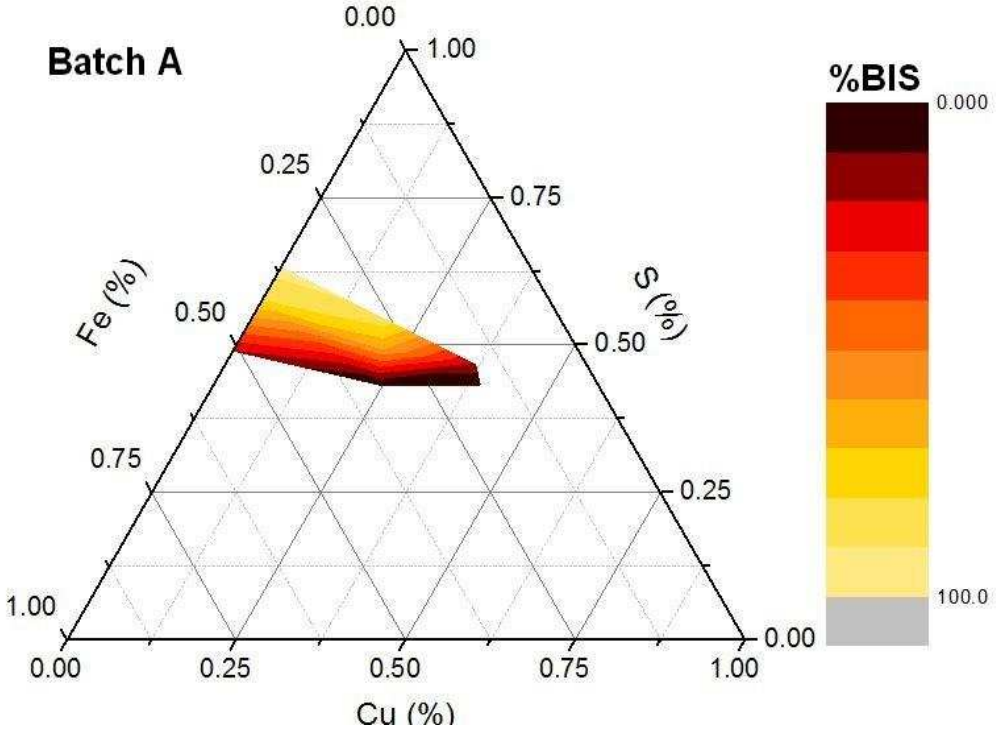

Figure E. 1: Ternary plot showing BIS vs. hematite stability for Batch A

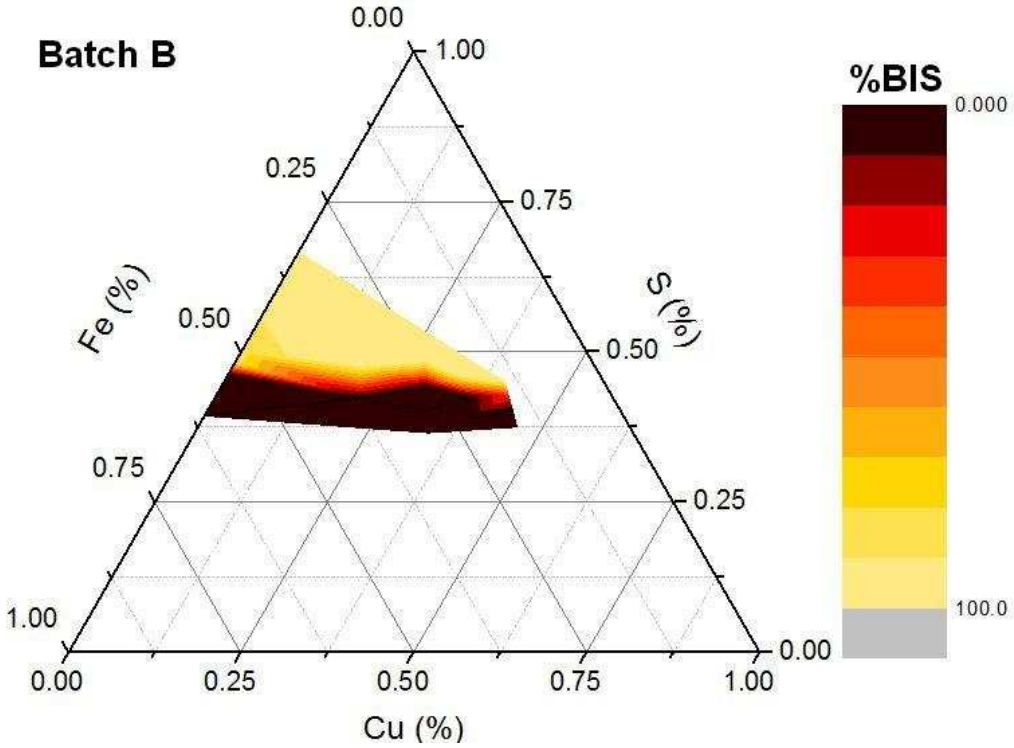

Figure E. 2: Ternary plot showing BIS vs. hematite stability for Batch B

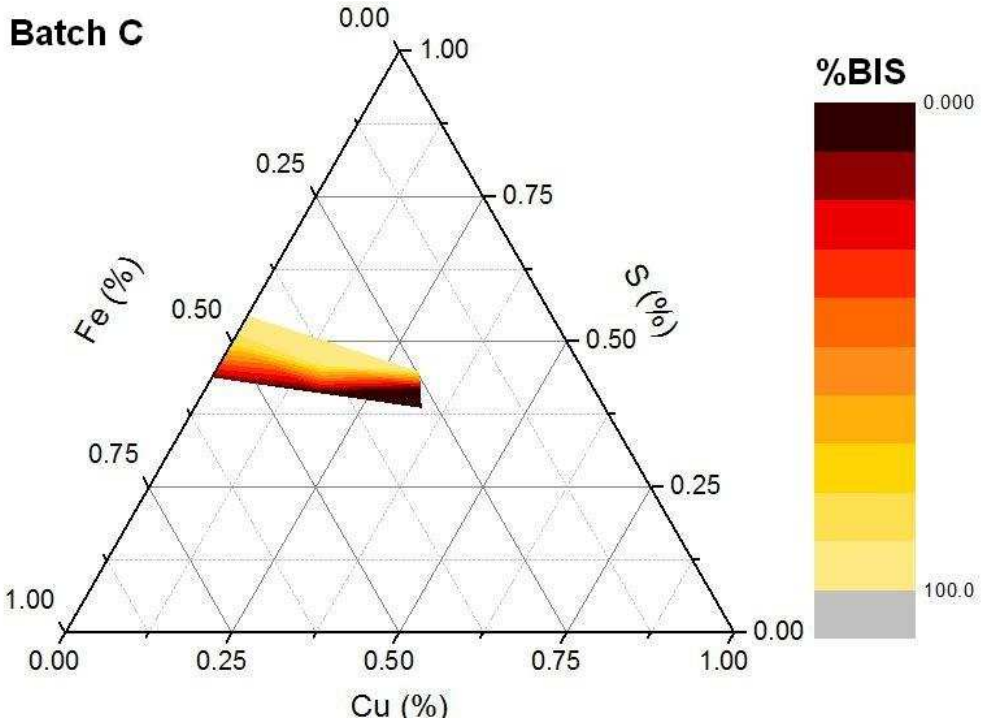

Figure E. 3: Ternary plot showing BIS vs. hematite stability for Batch C

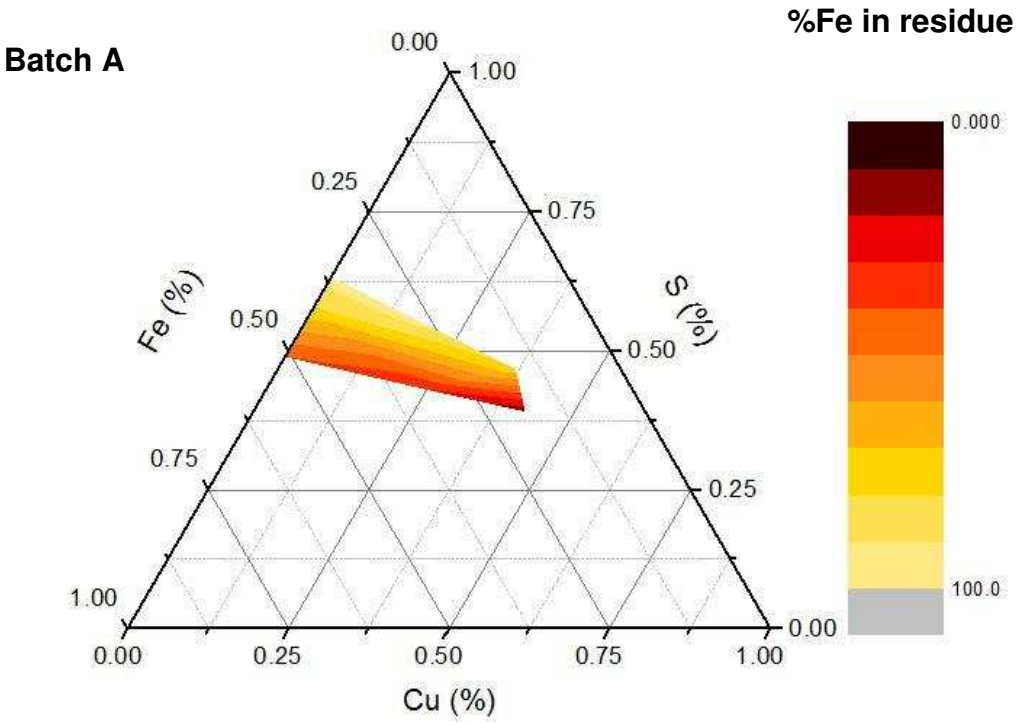

Figure E. 4: Ternary plot showing %Fe precipitated out of solution for Batch A

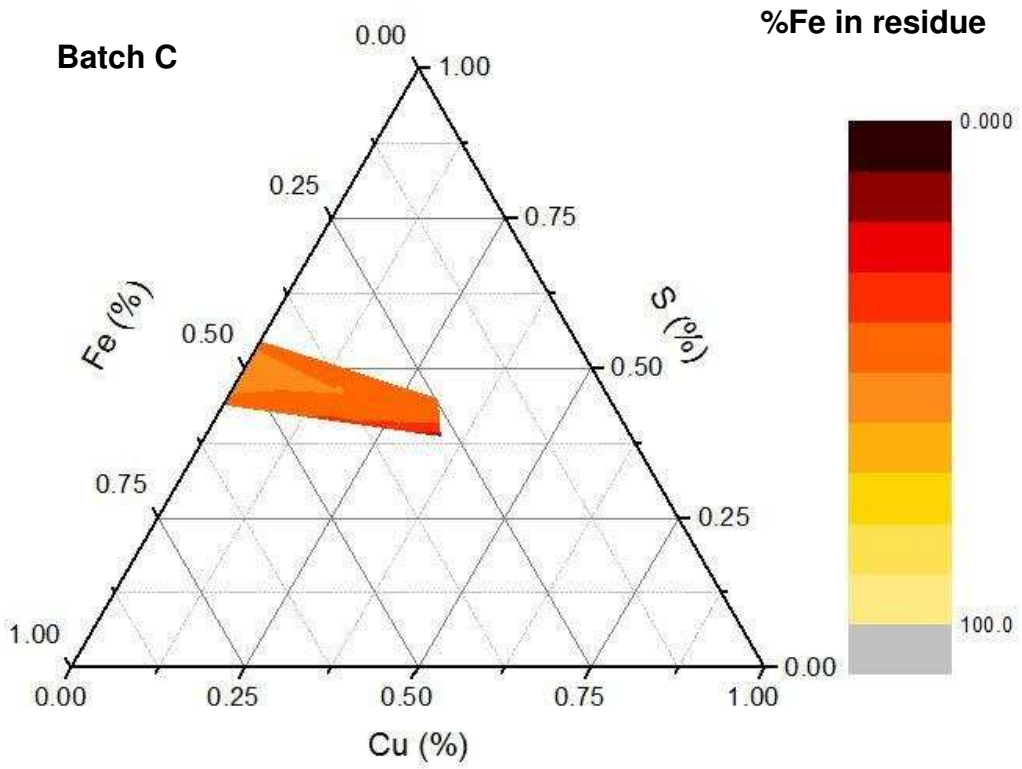

Figure E. 5: Ternary plot showing %Fe precipitated out of solution for Batch A

APPENDIX F: STAT-EASE DATA®

Analysis method provided by Stat-Ease® [45].

1. Compute effects. Use half-normal probability plot to select model. Click the biggest effect (point furthest to the right) and continue right-to-left until the line runs through points nearest zero. Alternatively, on the Pareto Chart pick effects from left to right, largest to smallest, until all other effects fall below the Bonferroni and/or t-value limit.
2. Choose ANOVA and check the selected model:
    a. Review the ANOVA results.
        i. Model should be significant based on F-test:
            1. (Prob > F) is < 0.05 is significant (good).
            2. (Prob > F) is > 0.10 is not significant (bad).
        ii. Curvature and Lack of Fit (if reported) should be insignificant:
            1. (Prob > F) is < 0.05 is significant (bad).
            2. (Prob > F) is > 0.10 is not significant (good).
    b. Examine the F tests on the regression coefficients. Look for terms that can beeliminated, i.e., terms having (Prob > F) > 0.10. Be sure to maintain hierarchy.
    c. c. Check for “Adeq Precision” > 4. This is a signal to noise ratio.
    d. d. Verify the ANOVA assumptions by looking at the residual plots.

Data for the first approach

Normal Plot of Residuals

The normal probability plot indicates whether the residuals follow a normal distribution, in which case the points will follow a straight line. Expect some moderate scatter even with normal data. Look only for definite patterns like an "S-shaped" curve, which indicates that a transformation of the response may provide a better analysis.

The Shapiro-Wilks test for normality is not available on this graph because the test is dependent on the assumption of independence. There is autocorrelation between the residuals, which invalidates the Shapiro-Wilks test. Visual inspection of the graph is sufficient.

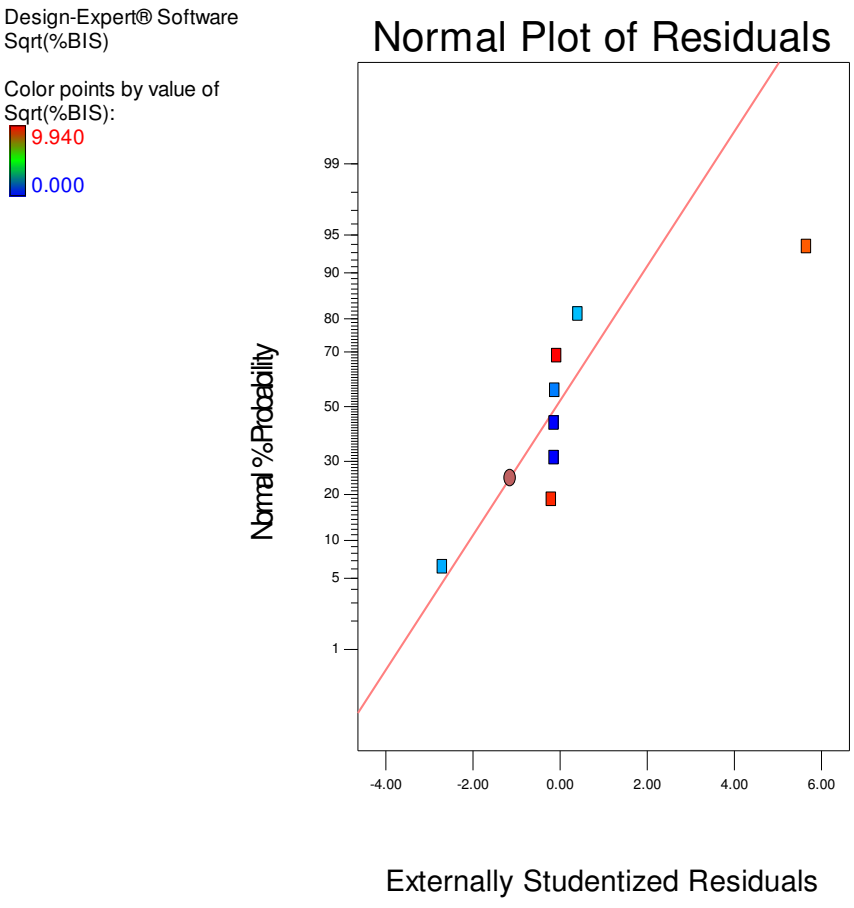

Figure F. 1: Normal Plot of residual – First approach

Residuals vs Predicted Plot

Figure F.2 is a plot of the residuals versus the ascending predicted response values. It tests the assumption of constant variance. The plot should be a random scatter (constant range of residuals across the graph.) Expanding variance ("megaphone pattern <") in this plot indicates the need for a transformation.

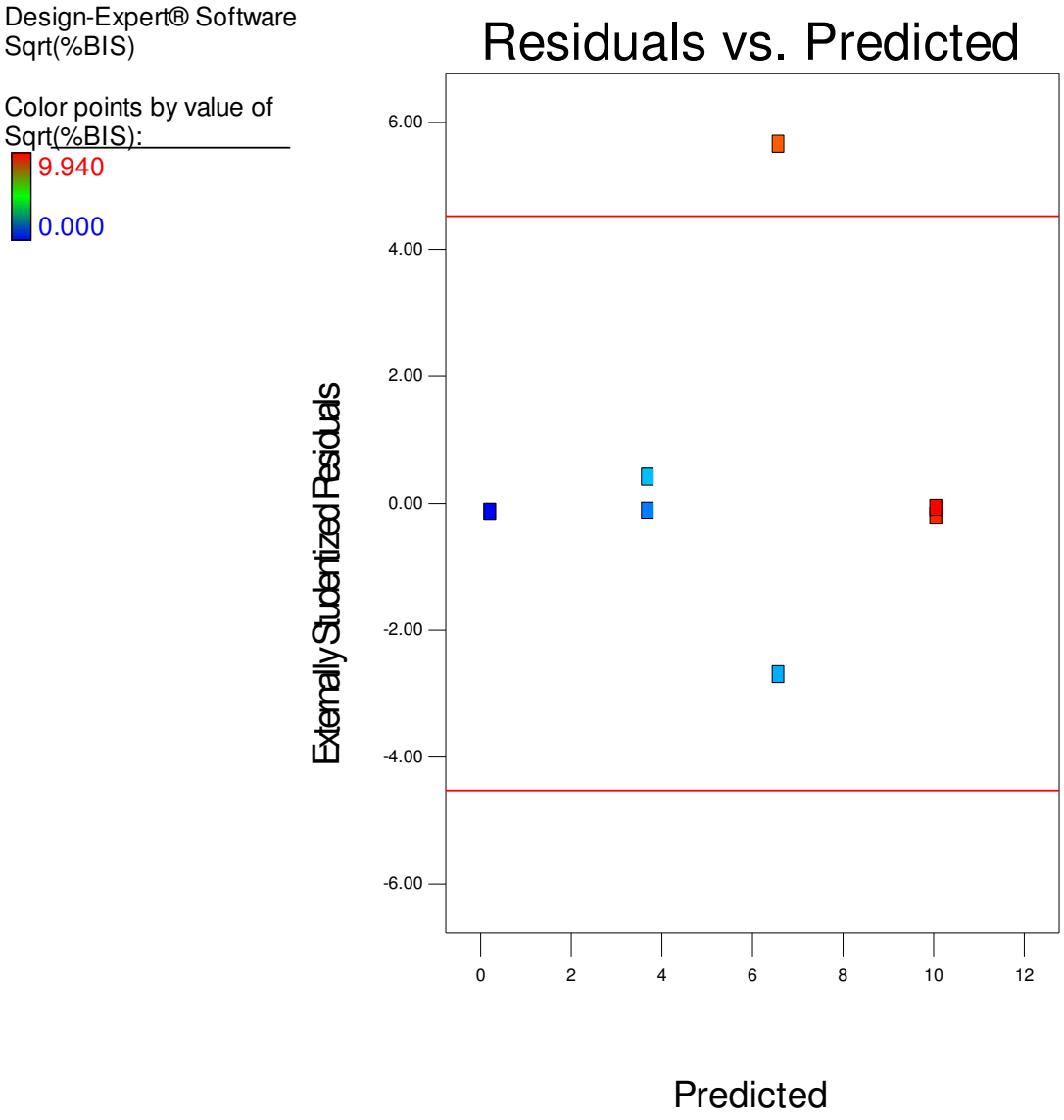

Figure F. 2: Normal Plot of residual – First approach

Residuals vs Run

Figure F.3 is a plot of the residuals versus the experimental run order. It allows to check for lurking variables that may have influenced the response during the experiment. The plot should show a random scatter. Trends indicate a time-related variable lurking in the background. Blocking and randomization provide insurance against trends ruining the analysis.

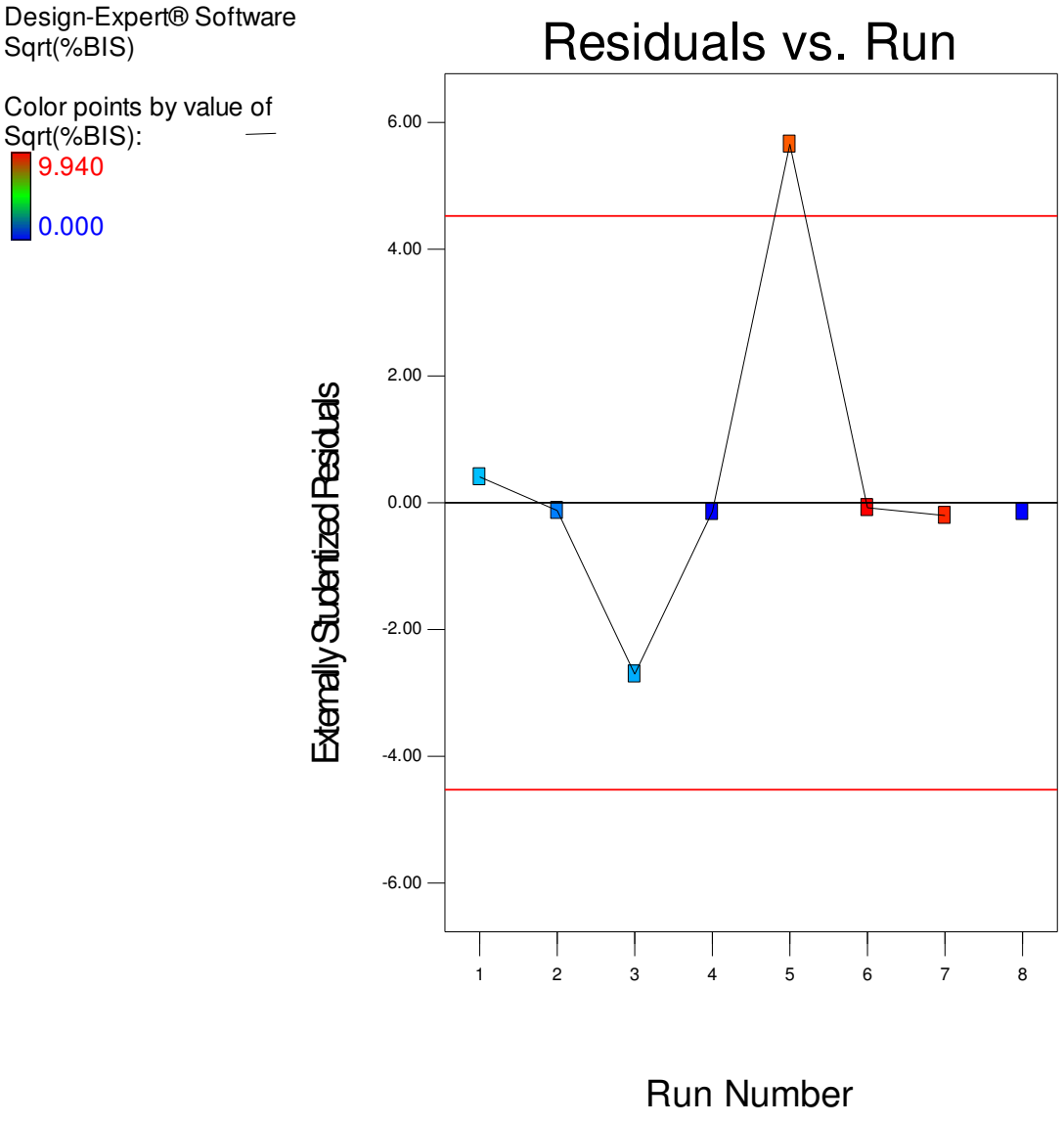

Figure F. 3: Residuals vs. Run – First Approach

Predicted vs Actual

A graph of the observed (actual) response values versus the predicted response values. It helps to detect a value, or group of values, that are not easily predicted by the model. The data points should be split evenly by the 45 degree line. If they are not, try a transformation (check the Box-Cox plot) to improve the fit.

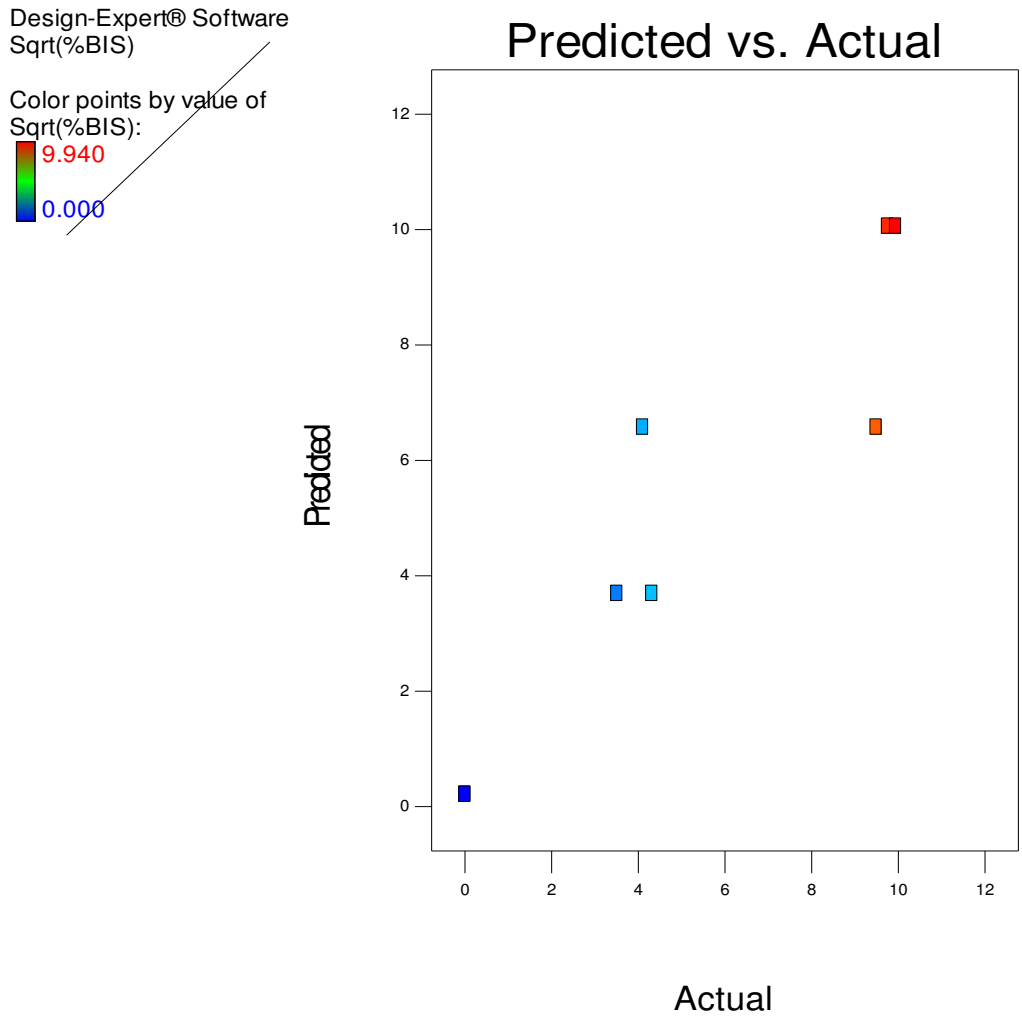

Figure F. 4: Predicted vs. Run – First Approach

Box-Cox Plot

This plot provides a guideline for selecting the correct power law transformation. A recommended transformation is listed, based on the best lambda value, which is found at the

minimum point of the curve generated by the natural log of the sum of squares of the residuals. If the 95% confidence interval around this lambda includes 1 then the software does not recommend a specific transformation. This plot is not displayed when either the logit or the arcsine square root transformation has been applied.

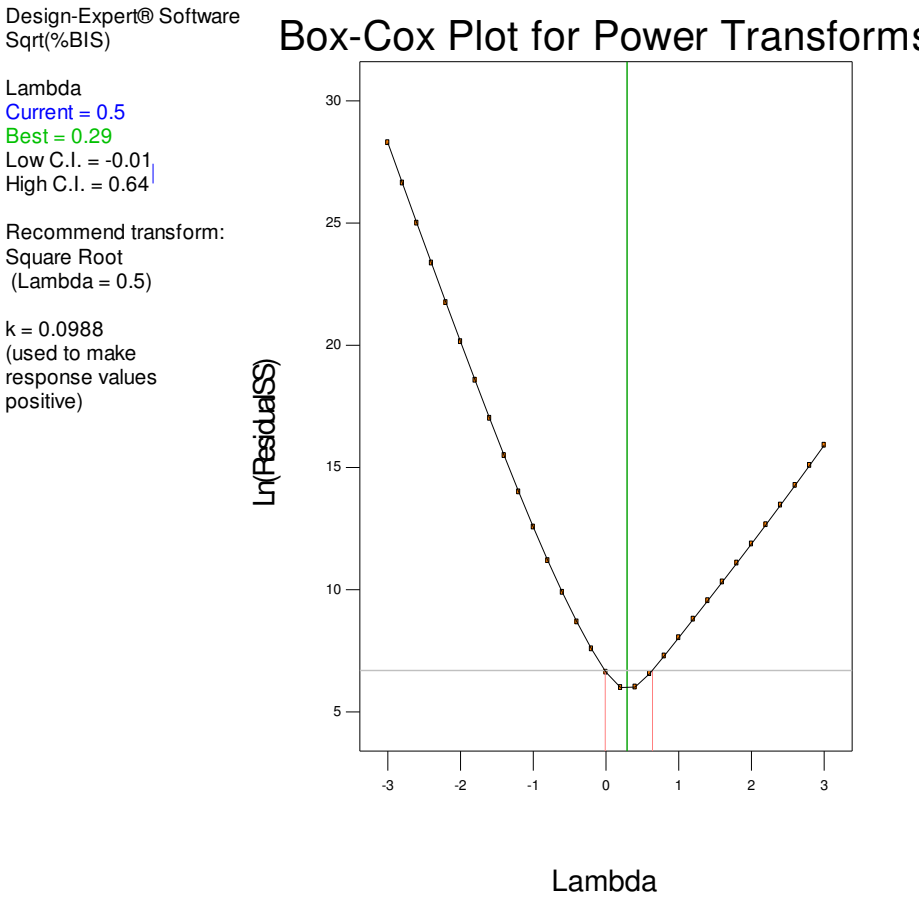

Figure F. 5: Box-Cox Plot – First Approach

Cook's Distance

A measure of how much the regression changes if the case is deleted. Relatively large values are associated with cases with high leverage and large studentized residuals. Large values should be investigated – they could be caused by recording errors, an incorrect model, or a design point far from the remaining cases.

"Large" is the value of the red line which is set as the minimum of 1 or the F critical value at alpha of 0.5 using p and n-p degrees of freedom, where p is the number of terms in the model including the intercept and n is the number of runs. =min(finv(0.5,p,n-p), 1).

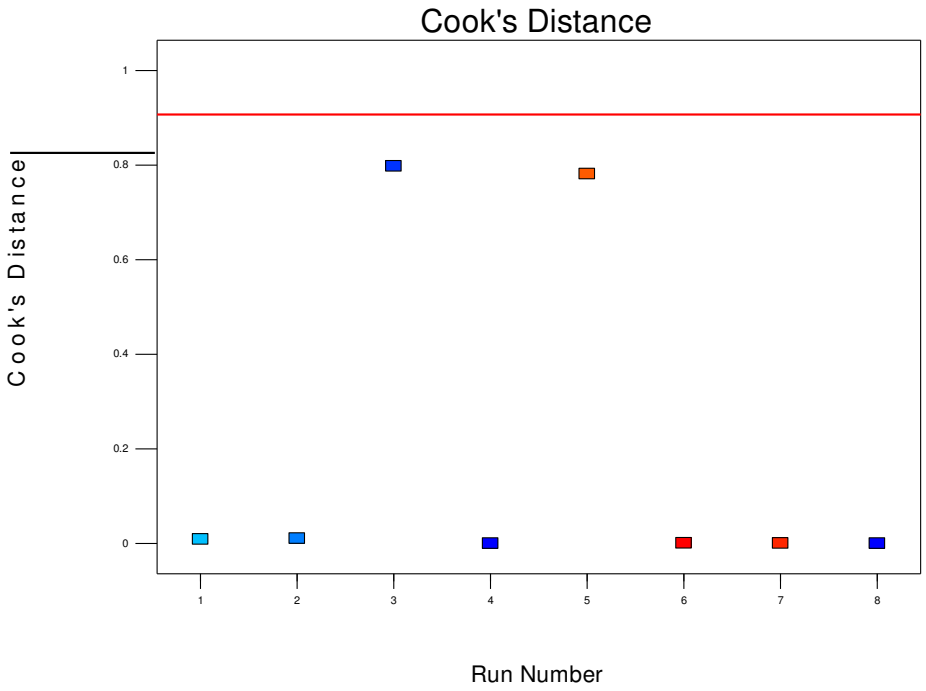

Figure F. 6: Cook's Distance – First Approach

Leverage

Numerical value between zero and one that indicates the potential for a design point to influence the model fit. A value of one means that the predicted value will be forced to be exactly equal to the actual value, with zero residual. The sum of the leverage values across all cases equals the number of parameters fit by the model. The maximum leverage an experiment can have is 1/k, where k is the number of times the experiment is replicated. Values larger than 2 times the average leverage are flagged. A high leverage point is "bad" because if there is a problem with that data point (unexpected error) that error strongly influences the model.

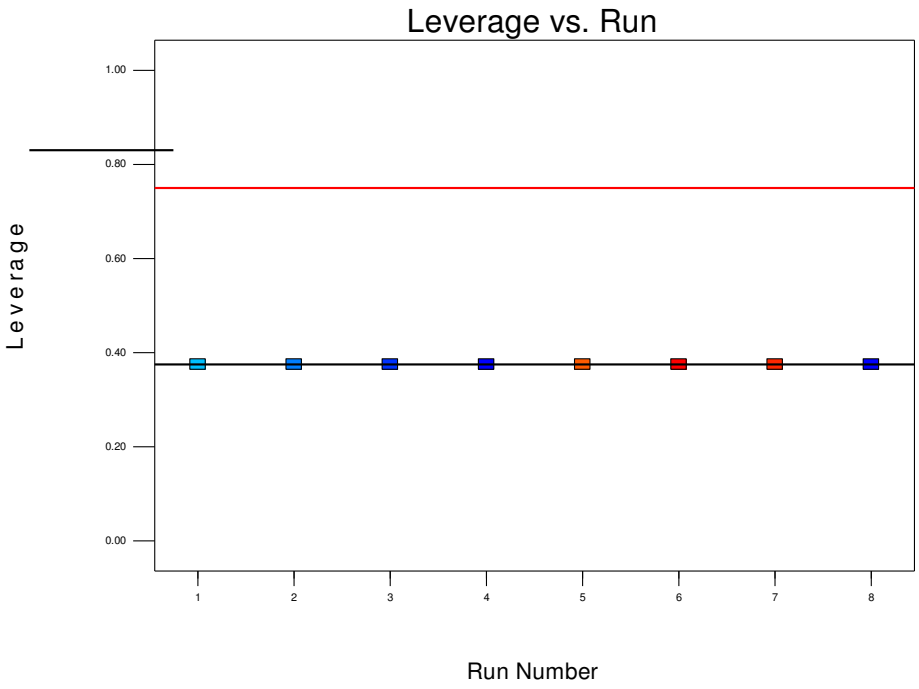

Figure F. 7: Leverage – First Approach

Second Approach

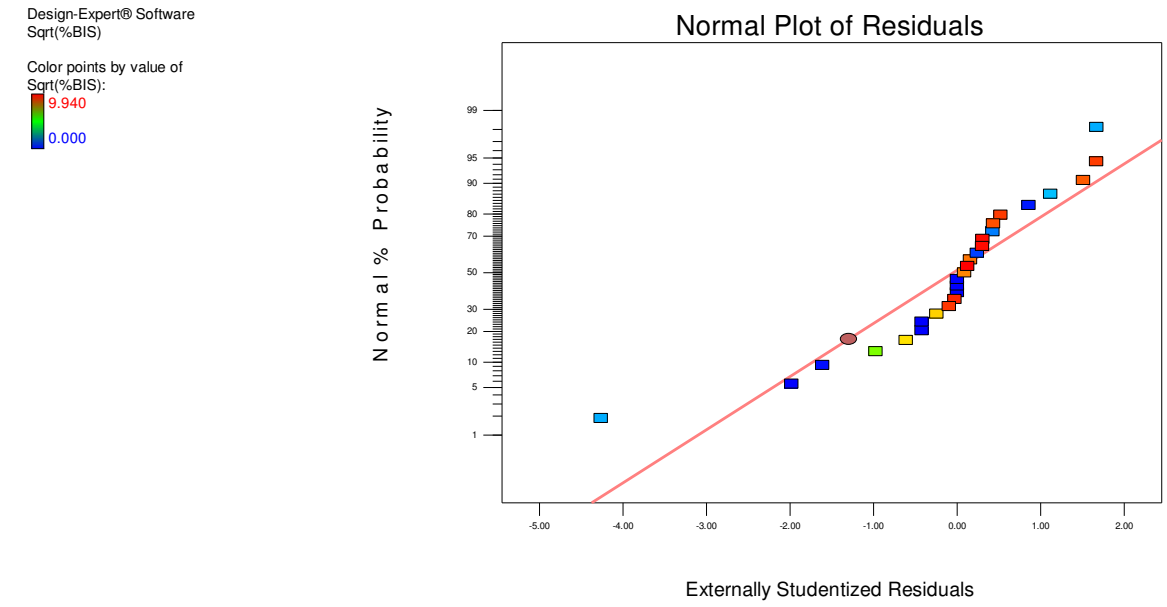

Figure F. 8: Normal Plot – Second Approach

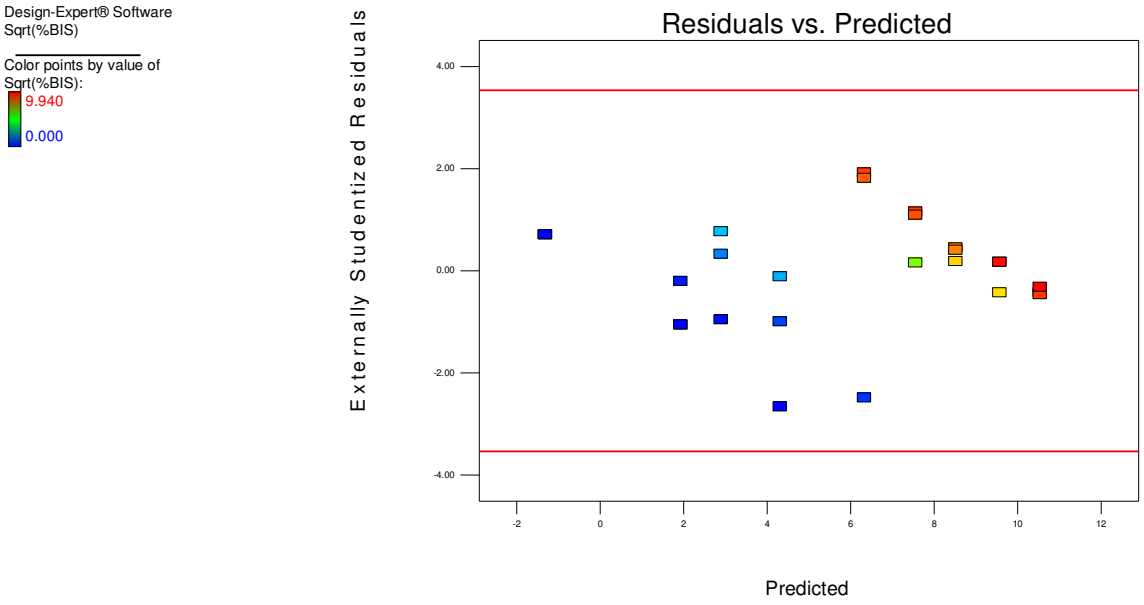

Figure F. 9: Residual vs. Predicted – Second Approach

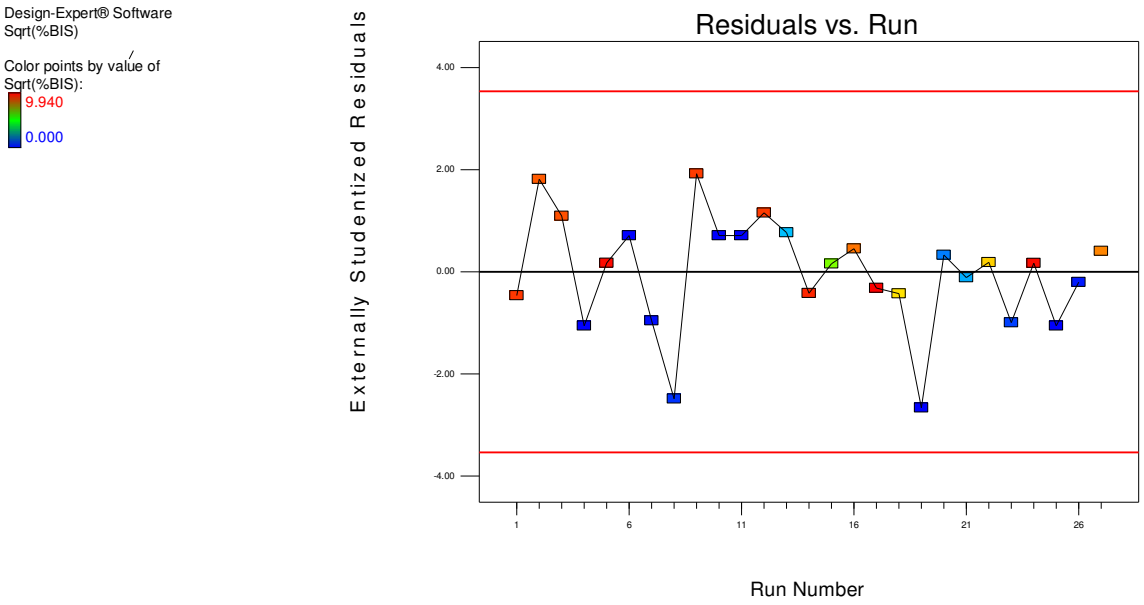

Figure F. 10: Residual vs. Run – Second Approach

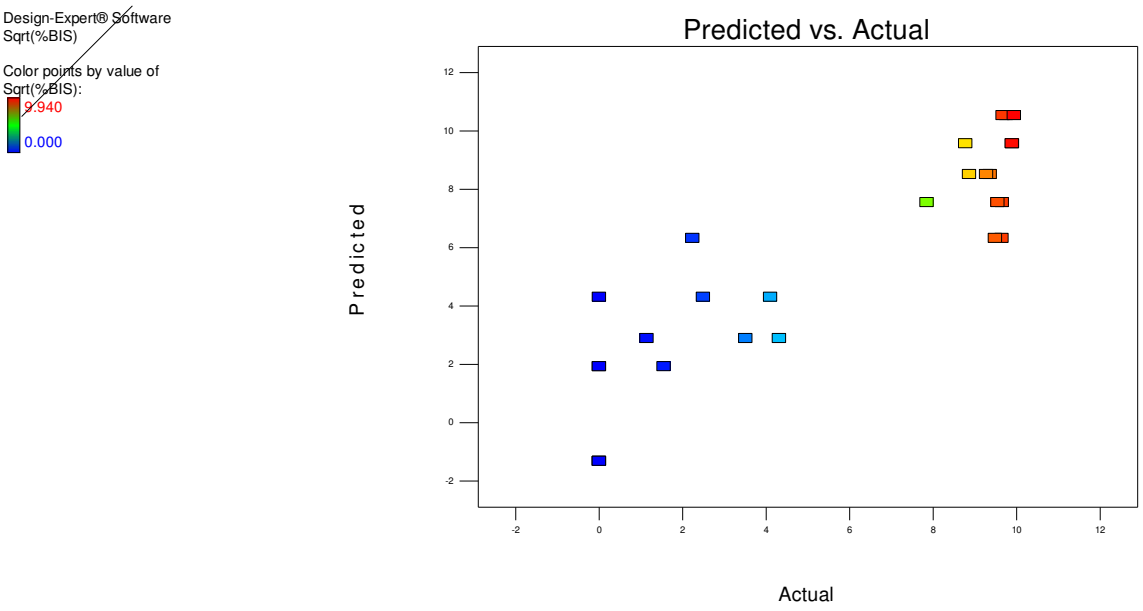

Figure F. 11: Predicted vs. Actual – Second Approach

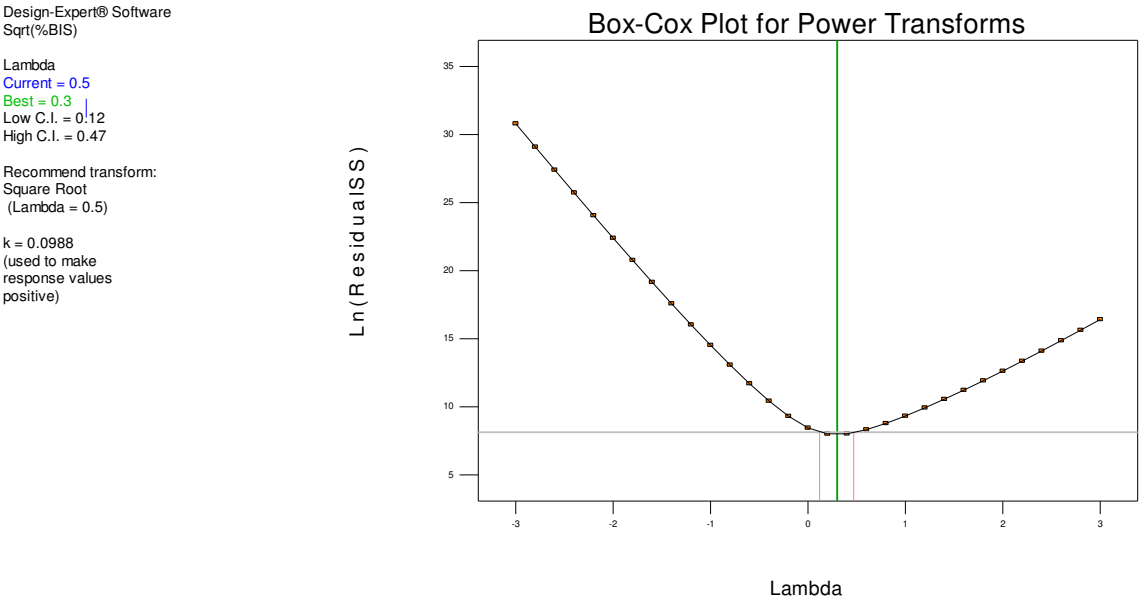

Figure F. 12: Box-Cox Plot – Second Approach

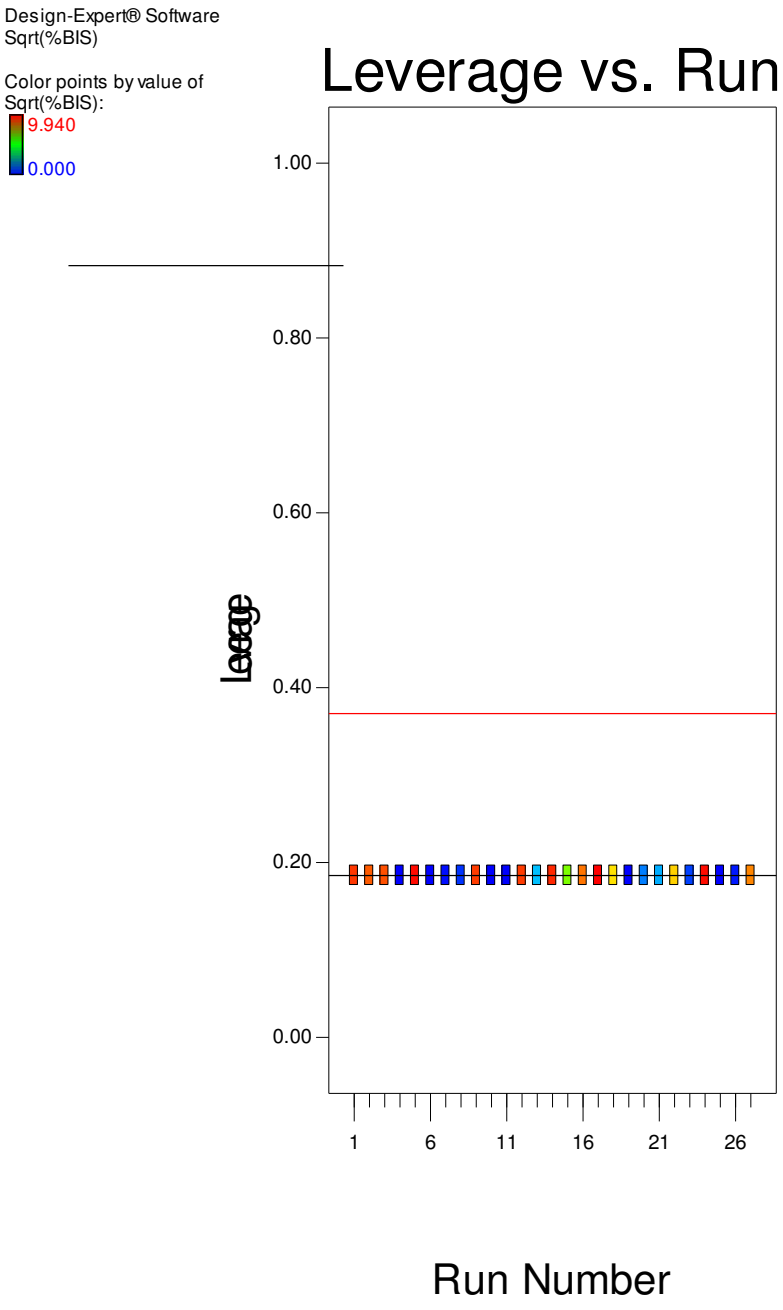

Figure F. 13: Leverage vs. Run – Second Approach

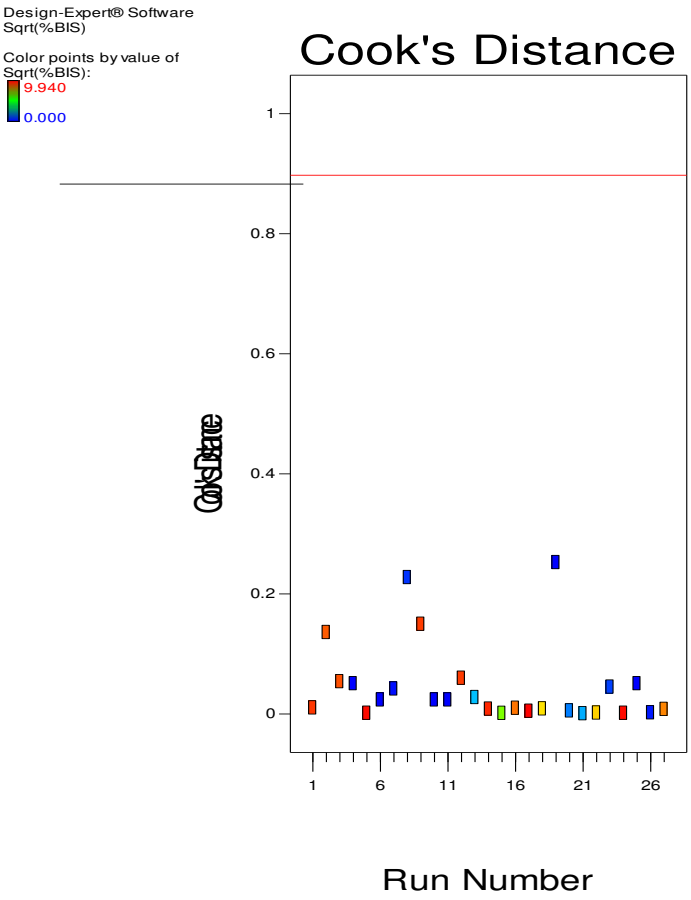

Figure F. 14: Cook's Distance – Second Approach

APPENDIX G: QEMSCAN DATA

Appendix G. 1: QEMSCAN image for test 43

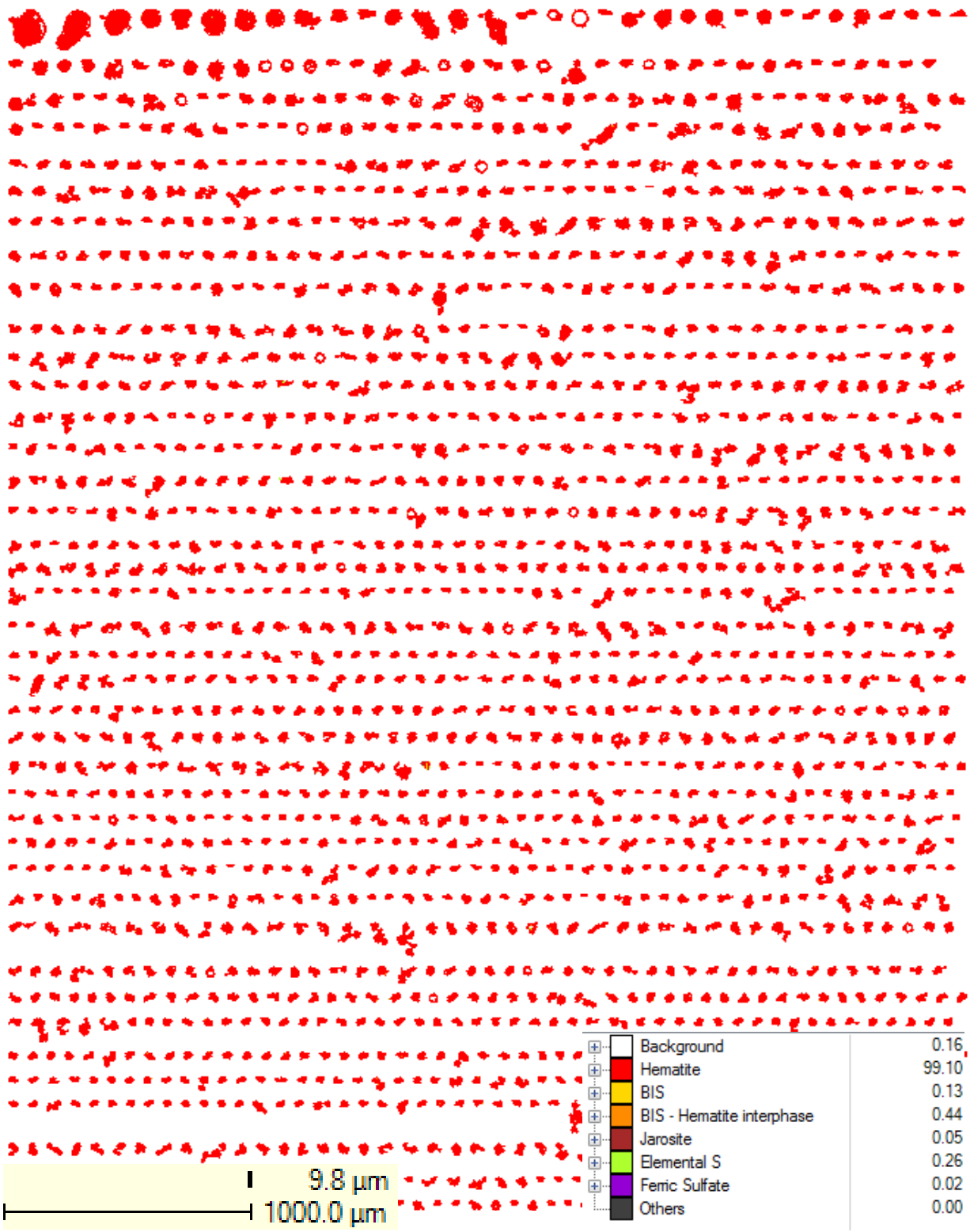

Appendix G. 2: QEMSCAN image for test 44

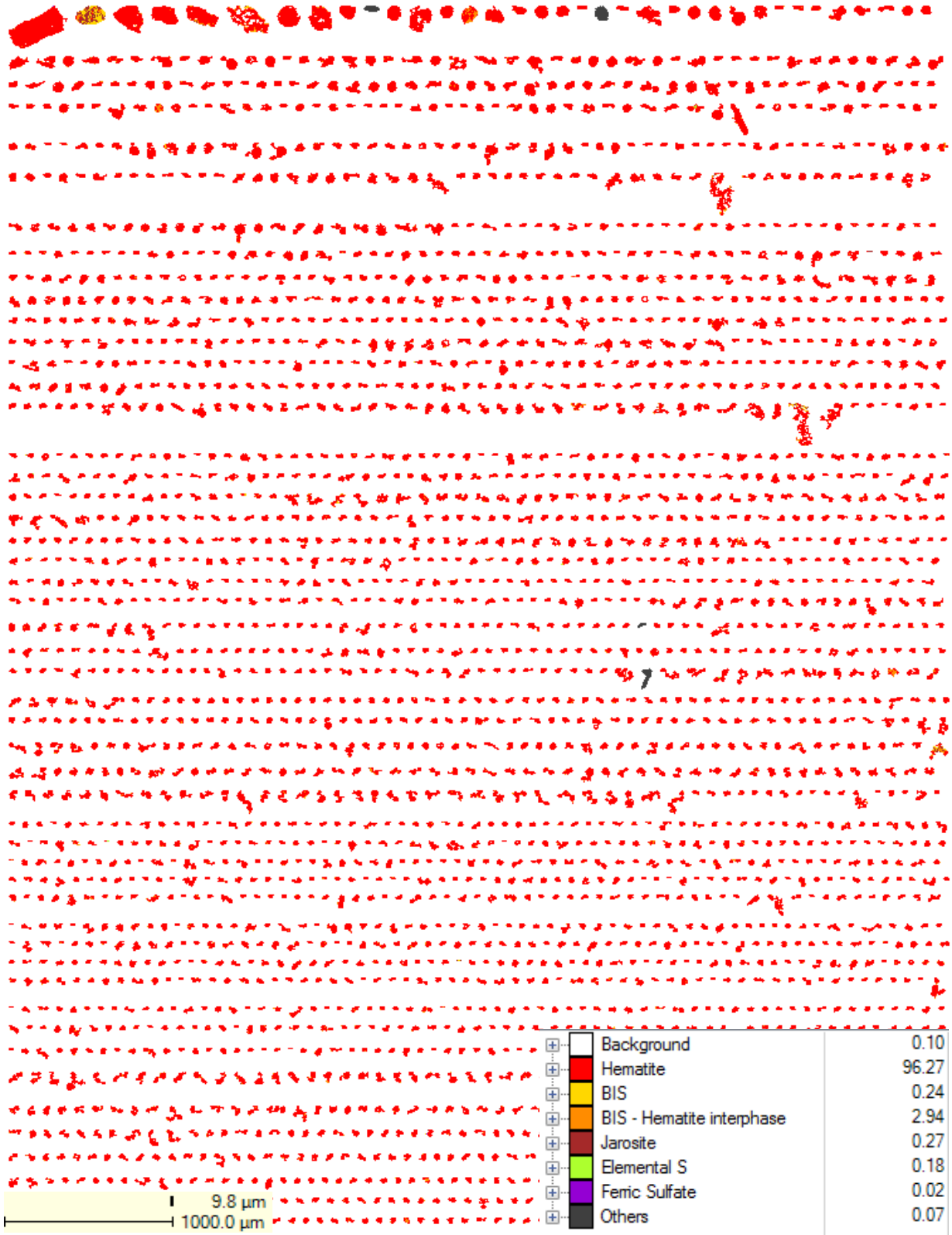

Appendix G. 3: QEMSCAN image for test 45

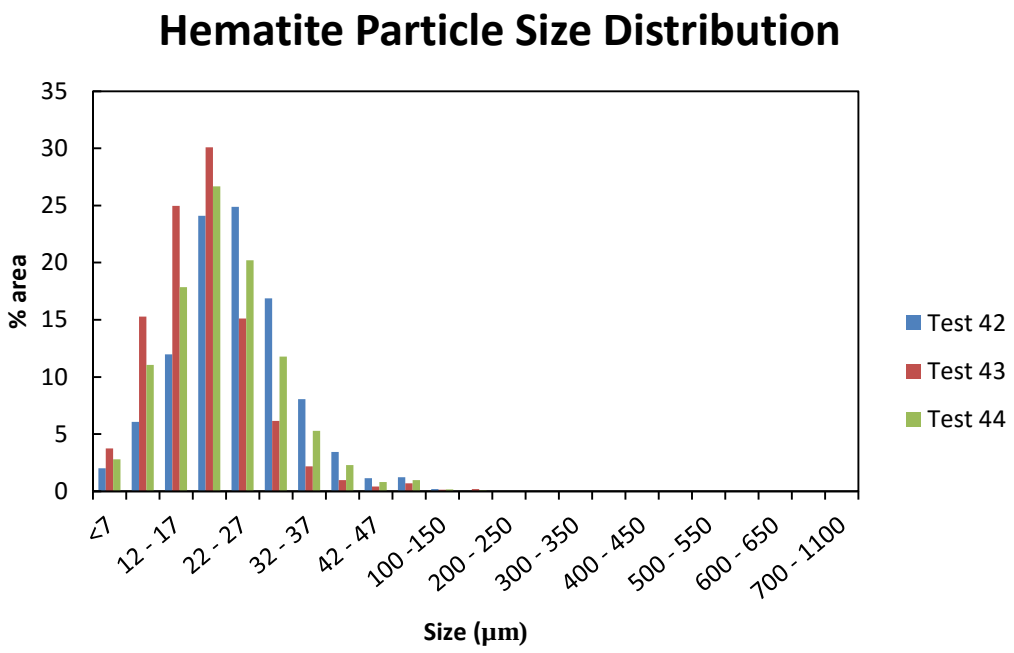

Appendix G. 4: Hematite PSD

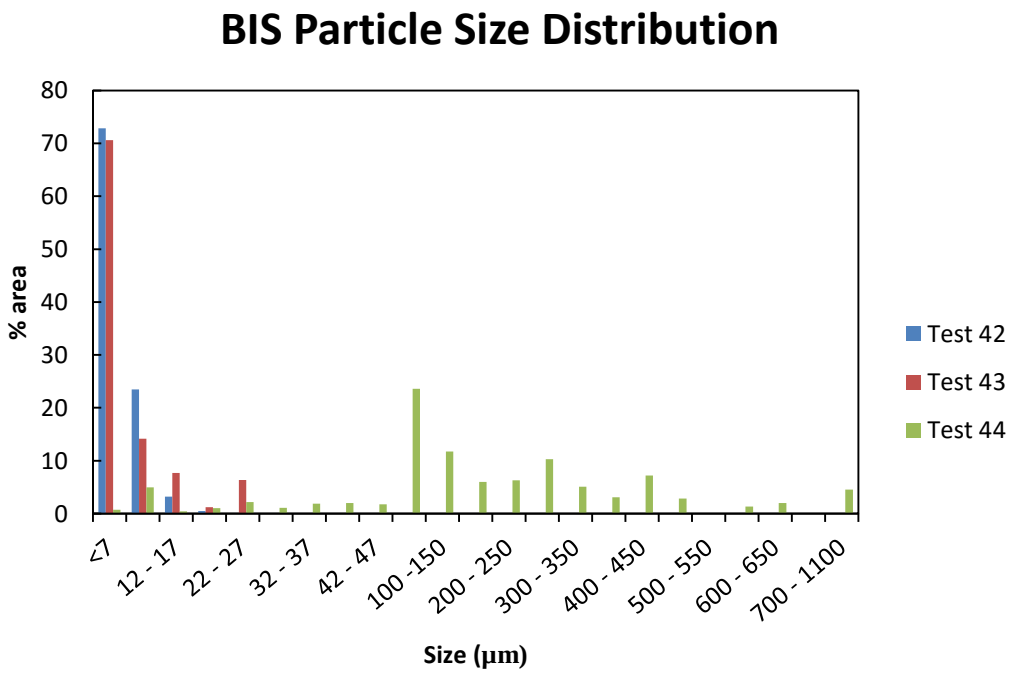

Appendix G. 5: BIS PDS

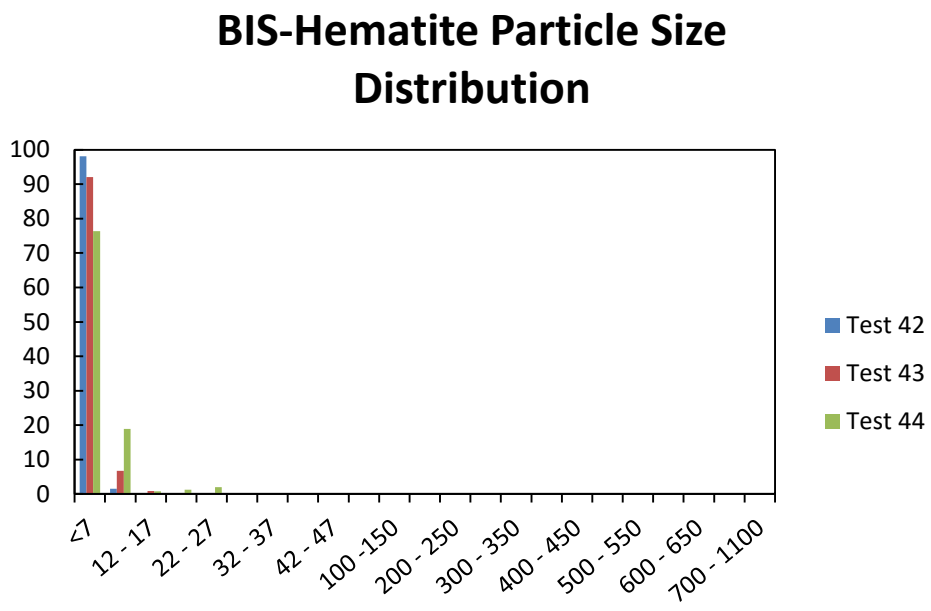

Appendix G. 6: BIS-Hematite PSD

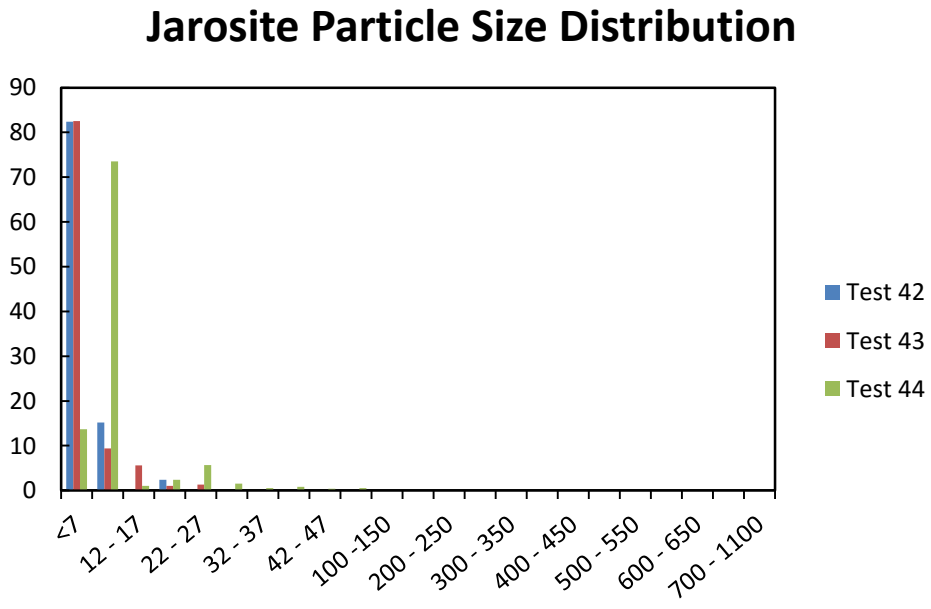

Appendix G. 7: Jarosite PSD

APPENDIX H: ECONOMIC ANALYSIS DATA

Table H. 1: Pressure Oxidation operating costs

Tonnes of concentrate feed per annum	560,660
Tonnes of concentrate feed per day	1,725
Tonnes of sulfur per annum	196,231
Regrinding of Concentrate Feed	
(15 kW.h/t of concentrate)	
12 cents/kW.h	1.8
Cost of grinding concentrate (M$/a)	1.01
Autoclave Agitation and Pumping Power	
400 kW.h/t S autoclaved	
6.25 cts/kW.h power cost	
Cost of agitation power (M$/a)	4,91
Oxygen t S/an	
t O2/t S = t O2/an	431,708
500 kW.h/t of O2	
6.25 cts/kW.h power cost	
Cost of oxygen (M$/a)	13.50
Maintenance 50$/t of S (M$/a)	9.81
Salaries and labour (M$/a)	0.8
Supplies	
M$/a based on a 1.3 $/t of concentrate	0.73
Total operating costs for POX assuming acid is used for heap leach (M$/a)	30.75

Table H. 2: Direct Operating Costs for production and marketing of cathode copper from the autoclave POX solution in M$/a

SX/EW	30.86
Value of Cu lost in the POX residue	10.58
Environment and tailing disposal	4.41
Cathode freight and marketing	6.61
Cost of producing and marketing copper cathode from AC oxide solution	52.47

Table H. 3: Capital Costs for production and marketing of cathode copper from the autoclave POX solution in M$/a

Direct Costs		
Oxygen Plant		
	Capital cost of installed O_2 plant, M$	39.14
Autoclave		
	# of claves (5m diam by 30m long, based on 5tonnes S per operating hour per clave)	4
	Capital costs for autoclave installed, M$ (including feed tanks, flash tanks etc)	36
Thickeners, neutralization tanks		12
SX		28
Tank farm, cap cost		9
EW cap cost		40
Tailing disposal capital		4
Environmental base line study		2
Total, $M		170.14
Indirect costs		
Construction overheads		10
Operations overheads		8
Project management		12
Design and engineering		12
Feasability study		5
Warehouse inventory		6
Freight and duty		12
Total indirect costs, M$		65
Total, M$		235.14

Table H. 4: Capital and Operating costs for flotation mill and grinding circuit

		2,000 tpd	1,000 tpd	2,460 tpd
OPEX				
	Supplies and Materials	8.32	9.29	7.87
	Labor	4.28	6.54	3.23
	Administration	1.84	2.66	1.46
	Sundry Items	1.44	1.85	1.25
Total OPEX per tonne of feed		15.88	20.34	13.81
Total OPEX per annum				11,061,429.93
CAPEX		$per annum	$ per annum	$ per annum
	Equipment	9,061,700.00	6,644,300.00	10,183,373.60
	Installation Labor	5,928,300.00	4,391,300.00	6,641,468.00
	Concrete	766,700.00	567,700.00	859,036.00
	Piping	2,361,100.00	1,697,800.00	2,668,871.20
	Structural Steel	861,800.00	649,200.00	960,446.40
	Instrumentation	570,500.00	423,700.00	638,615.20
	Insulation	270,400.00	195,100.00	305,339.20
	Electrical	1,124,400.00	829,100.00	1,261,419.20
	Coatings & Sealants	100,100.00	75,400.00	111,560.80
	Mill Building	2,151,600.00	1,459,000.00	2,472,966.40
	Tailings Embankment	3,961,400.00	2,087,700.00	4,830,796.80
	Engineering Management	4,102,500.00	3,231,700.00	4,506,551.20
	Working Capital	1,849,600.00	1,184,900.00	2,158,020.80
Total CAPEX		33,110,100.00	23,436,900.00	37,598,464.80